PREDICTION OF ACCOMMODATIVE OPTICAL RESPONSE IN YOUNG AND PRE-PRESBYOPIC HUMAN EYES USING ULTRASOUND BIOMICROSCOPY

By

Viswanathan Ramasubramanian
B.S.Optometry

DISSERTATION

In partial satisfaction of the requirements for the degree of

DOCTOR OF PHILOSOPHY

in

PHYSIOLOGICAL OPTICS

Presented to the Graduate Faculty of the

College of Optometry
University of Houston

December 2014

Approved:

_____

Adrian Glasser, Ph.D. (Chair)

_____

Jason Porter, Ph.D.

_____

Scott Stevenson, Ph.D.

_____

Heather Anderson, O.D., Ph.D.

_____

Jim Schwiegerling, Ph.D.

Committee in Charge

Dedication

This work is dedicated to my advisor Dr. Adrian Glasser.

Acknowledgements

First and foremost, I would like to thank my advisor Dr. Adrian Glasser. I feel so lucky and blessed to have you as my mentor. You have taught me how to go about answering questions in science. You have helped me, guided me, critiqued me, motivated me and supported me for the past five years. I feel so privileged to be your graduate student. Every time I stumbled in my research path, you were there to encourage me and you taught me how to overcome hurdles. Whenever I felt hopeless, I always make it a point to meet with you because I felt so better and energized. I'd like thank you for supporting and encouraging me to present my research at ARVO. Before I came to Houston, I did not have a role-model, but now I have you as my role-model. You have patiently gone over my manuscripts lot of times and gave useful comments, which made me a better writer. I will always remember what you have taught me and I should say that I felt you as my second parent. Thanks again for supporting me during these years.

I would like to thank my committee members for gladly accepting to serve in the committee for my oral qualifier and dissertation defense. I would like to thank Dr. Scott Stevenson and Dr. Glasser for giving me the opportunity to work as a clinical study coordinator in a clinical trial sponsored by Alcon. It was a good experience for me and I learnt a lot from it. Dr. Stevenson, it was very nice to work with you during the clinical trial and thanks for believing in me and giving that responsibility. Special thanks to Dr. Jason Porter for sitting with me regularly and listening to the updates on my schematic

eye analysis. Dr. Porter, your suggestions on the schematic eye analysis were valuable and constructive. I would like to thank Dr. Anderson, Dr. Porter and Dr. Stevenson for their useful comments on my grant proposal and making my oral qualifier a pleasant one. Many thanks to Dr. Jim Schwiegerling for gladly accepting to serve as the external committee member and for flying to Houston from Tucson, AZ for my dissertation defense. Thank you all for your valuable suggestions on my dissertation research proposal and on my dissertation.

Special thanks to Dr. Laura Frishman for keeping track of my progress and motivating me at each and every step of my graduate program. Dr. Frishman, you supported me a lot during these years and I have to say that you took care of me just like my mother. Thanks again for your help. Many thanks to Michele Stafford and Diana Davis in the graduate office for taking care of the administrative aspects of the graduate program. You make life of every graduate student smooth and easy here at UHCO.

My thanks to Drs. Alan Burns, Jason Porter and Vallabh Das for their valuable comments on my graduate seminar, abstract and bio sketch. Your reviews have improved my presentations skills here and at ARVO. I would also like to thank all UHCO faculty for their teaching in the 1st year core course. The core course at UHCO gave me exposure in other areas of research and it was an enriching experience.

I want to convey my wishes and thanks to my fellow graduate students for supporting each other during this journey. All your comments and reviews on my graduate seminar motivated me to improve my skills. Thanks for sharing your knowledge and experiences.

Special thanks to Drs. Glasser and McDermott lab alumni and members: Mark, Jonathan, Dorothy, Alireza, Andreu Coret, Misae Ito, Satya Kolar, Joseph Manarang and Hasna Baidouri. I had a good time with you all and thanks for the wonderful time spent these years. Thanks Satya for motivating me whenever I felt hopeless and I am fortunate to have you as my officemate.

Thanks to Chris Kuether, John and Charles Neff for their assistance with the technical aspects of my study and for some machine shop experience. Chris, I will miss your conversations in units of inches/pounds/other units which I am not familiar with. Thanks to Dr. Jason Marsack, Jim Elswick for cutting contact lenses for my study. Thanks to the staff at the contact lens clinic who readily gave me sample contact lenses for my study. Big thanks to all my subjects for believing in me and participating in my research that involved invasive procedures.

I would like to thank my wife and parents for supporting me during this journey. I owe a lot for the sacrifices they have made for me to achieve this degree. Thanks for all

your prayers and blessings. I thank God almighty for giving me the strength to complete my graduate program.

PREDICTION OF ACCOMMODATIVE OPTICAL RESPONSE IN YOUNG AND

PRE-PRESBYOPIC HUMAN EYES USING ULTRASOUND BIOMICROSCOPY

By

Viswanathan Ramasubramanian
B.S.Optometry

DISSERTATION

In partial satisfaction of the requirements for the degree of

DOCTOR OF PHILOSOPHY
in
PHYSIOLOGICAL OPTICS

Presented to the Graduate Faculty of the

College of Optometry
University of Houston

December 2014

General Abstract

Purpose: Clinical accommodation testing involves measuring either the accommodative optical response (AOR) or the accommodative biometric changes in the ocular anterior segment. Currently, it is not possible to measure both with a single instrument. Measuring the AOR and the accommodative biometric changes are important for evaluating accommodation restoration concepts. The specific goals of this research are: 1) to perform automated, objective measurements of accommodative biometric changes from ultrasound biomicroscopy (UBM) images in young phakic eyes; 2) to measure the static AOR using a Grand Seiko (GS) autorefractor and infra-red photorefraction (PR) in young eyes and to predict the AOR from UBM measured biometric changes; 3) to measure the AOR using GS and PR and the biometric changes using UBM in pre-presbyopes to predict the AOR; 4) to calculate and correct the spatial and optical distortion in Visante optical coherence tomography corneal images; 5) to construct accommodative schematic eye models for individual eyes for each of the young and pre-presbyopic subjects and calculate refraction and AOR from the schematic eye models.

Methods: *Experiments were 1)* Accommodative anterior segment biometric changes were measured in response to 0 D to 6 D accommodative stimuli in 1 D steps in 26 young human subjects using a 35 MHz UBM and an A-scan ultrasound. *2)* Static AOR to the same stimulus demand were measured with GS and PR in the same group of young subjects. AOR was predicted from UBM measured biometry parameters using linear

regression, 95% confidence intervals and 95% prediction intervals. *3)* Static AOR to 0 D to maximal stimulus demand in at least 0.25 D steps was measured with GS and PR in 25 pre-presbyopic human subjects. Accommodative anterior segment biometric changes were measured using UBM and A-scan ultrasound. AOR was predicted from UBM measured biometry parameters as described in experiment 2. *4)* Five contact lenses of known front and back surface radii of curvature and central thicknesses were imaged using the Visante to calculate spatial and optical distortion corrections which were then applied to corneal images captured from the young and pre-presbyopic subjects. *5)* Ocular biometry parameters (Visante, A-scan and UBM) from Experiments 1, 3 and 4 in young and pre-presbyopic subjects were used to construct paraxial schematic eye models for each individual subject for each accommodative stimulus demand.

Results: 1) Standard deviations of UBM measured parameters were smaller than A-scan measures. 2) Mean prediction errors of AOR using linear regression in young subjects for various biometry parameters ranged from 0.56 D to 0.91 D. 3) Mean prediction errors of AOR using linear regression in pre-presbyopic eyes ranged from 0.41 D to 0.62 D. 4) Root mean square (RMS) error of the power of the contact lens surfaces after distortion correction was 0.18 D for the front and 0.11 D for the back surfaces, respectively. 5) Mean ± SD of prediction errors of AOR from individual schematic eyes for the young and pre-presbyopic subjects were 0.50 ± 0.39 D and 0.50 ± 0.37 D, respectively.

Conclusions: The results show: 1) the utility of automated image analysis to get accurate, rapid and objective measurements of anterior segment biometry from UBM images; 2)

how spatial distortion in UBM images can be corrected to get accurate measurements and the ability of each UBM measured biometry parameter to predict the AOR; 3) how UBM, despite having low axial resolution, can predict AOR in pre-presbyopic eyes with low accommodative amplitudes; 4) how spatial and optical distortions in Visante images can be corrected to get accurate corneal biometry that can be used for schematic eye modeling; 5) how individual schematic eye predictions of the AOR are better than predictions using LR from individual UBM measured biometry parameters.

Table of Contents

List of Figures

List of Tables

List of Publications

Accepted for publication

Ramasubramanian, V. & Glasser, A. (2014). Objective Measurement of Accommodative Biometric Changes Using Ultrasound Biomicroscopy. *Journal of Cataract and Refractive Surgery.* (Chapter 2)

Submitted for publication

Ramasubramanian, V. & Glasser, A. (2014). Can Ultrasound Biomicroscopy (UBM) be Used to Predict Accommodation Accurately? *Journal of Refractive Surgery.* (Chapter 3)

Ramasubramanian, V. & Glasser, A. (2014). Prediction of Accommodative Optical Response in Pre-presbyopes using Ultrasound Biomicroscopy. *Journal of Cataract and Refractive Surgery.* (Chapter 4)

Ramasubramanian, V. & Glasser, A. (2014). Correction of Corneal Distortions from Visante Anterior Segment Optical Coherence Tomography Images. *Journal of Refractive Surgery.* (Chapter 5)

List of Abbreviations

Abbreviations	Expansion
AAD	Angle to angle distance
ACD	Anterior chamber depth
AL	Axial length
ALRC	Anterior lens radius of curvature
AOR	Accommodative optical response
ARC	Anterior corneal radius of curvature
ASL	Anterior segment length
CL	Contact lens
CT	Corneal thickness
D	Diopter
GS	Grand Seiko autorefractor
IR	Infrared
LACA	Left anterior chamber angle
LED	Light emitting diode
LT	Lens thickness
MRI	Magnetic resonance imaging
OCT	Optical coherence tomography
PCI	Partial coherence interferometry
PLRC	Posterior lens radius of curvature
PMMA	Poly (methyl methacrylate)
PRC	Posterior corneal radius of curvature
RACA	Right anterior chamber angle
RMS	Root mean square
SD	Standard deviation
UBM	Ultrasound biomicroscopy
VCD	Vitreous chamber depth

Chapter 1 – General Introduction

Accommodation is the physiological process by which a young distance corrected eye increases its optical power to focus on near targets (Gullstrand, 1909). During accommodation, in response to ciliary muscle contraction, anterior chamber depth (ACD) decreases, lens thickness (LT) increases, anterior and posterior lens radius of curvature (ALRC and PLRC) decreases and the posterior lens surface moves posteriorly (Bolz, Prinz, Drexler et al., 2007; Ostrin, Kasthurirangan, Win-Hall et al., 2006). These accommodative changes in the anterior segment biometry (accommodative biometric changes) result in an increase in the optical power of the eye. The ability to accommodate gradually declines with increasing age and is completely lost around 50 years of age in the condition called presbyopia. Emmetropic individuals over 40 years of age typically begin to report symptoms such as blurred near vision and often require near vision correction to perform near tasks. While conventional near vision correction in the form of bifocals, progressive addition lenses, monovision, multifocal contact lenses and multifocal intraocular lenses provide functional far and near vision, they do not render the true, dynamic, continuous range of focusing ability present as accommodation in young eyes. There is considerable interest in understanding if it is possible to restore accommodation in presbyopes and attempts have been made using various accommodation restoration procedures (Sheppard, Bashir, Wolffsohn et al., 2010; Glasser, 2008). However, none of the approaches have been able to reliably restore accommodation in all presbyopic eyes. Understanding the mechanism of accommodation

and presbyopia and using objective methods for accommodation measurement are important for the design and evaluation of accommodation restoration strategies.

Clinically, accommodation is measured objectively either as an accommodative change in the optical power (accommodative optical response; AOR) of the eye or as accommodative biometric changes in the ocular anterior segment. While measuring the AOR using an autorefractor or an aberrometer provides objective information on how much the eye accommodated, it does not allow for visualization or quantification of the biometric changes that produced the accommodative optical change (Win-Hall, Ostrin, Kasthurirangan et al., 2007). On the other hand, using biometric imaging instruments such as ultrasound biomicroscopy (UBM) or optical coherence tomography (OCT) to measure accommodation do allow understanding on how the eye undergoes accommodative changes, but they do not provide a measure of the dioptric change in accommodation (Sun, Fan, Zheng et al., 2013; Marchini, Pedrotti, Sartori et al., 2004). Visualizing and quantifying the accommodative biometric changes and measuring the AOR are important to fully evaluate the accommodative ability of an eye or of an accommodative restoration concept. Clinical studies are being undertaken towards achieving United States Food and Drug Administration (US-FDA) or *Communauté Européenne* (European CE) mark approval for various accommodation restoration concepts. For these procedures to achieve regulatory approval with a claim for accommodation will require objective demonstration of the AOR of the eye or objective measurements of accommodative biometric changes from which the AOR can be calculated. Ideally, both the AOR and the accommodative biometric changes would be

measured in clinical studies. However, currently, it is not possible to measure the accommodative optical and biometric changes with a single clinical instrument. Therefore, to do this requires doing accommodation testing while first measuring the accommodative refractive change and then repeating the testing while doing accommodative biometry measurements. This is laborious, time consuming, costly and can cause fatigue in the patients, thereby compromising the data obtained. The following studies were undertaken to establish if a single clinical instrument can be used to accurately measure accommodative biometric changes and then use the measured results to predict the AOR.

Prior studies have measured accommodative anterior segment biometric changes using A-scan ultrasound, UBM, OCT, Scheimpflug, partial coherence interferometry (PCI) and magnetic resonance imaging (MRI) (Ostrin et al., 2006; Marchini et al., 2004; Bolz et al., 2007; Dubbelman, van der Heijde, & Weeber, 2005; Kasthurirangan, Markwell, Atchison et al., 2011). While A-scan and PCI allow quantitative measurements of anterior segment biometry, since they are not imaging methods, they do not allow for visualization of the accommodative changes. Methods that do provide images such as Scheimpflug and OCT suffer from optical distortions and require distortion correction to extract accurate biometric measurements. In addition, OCT does not allow for visualization of structures posterior to the iris. Limitations of using MRI for accommodation studies include the constraints imposed by having to have the subject in an MRI instrument, longer imaging times and limited image resolution (Kasthurirangan et al., 2011). Ultrasound biomicroscopy is a clinical instrument commonly used to image

the ocular anterior segment and is used for diagnosis and management of anterior segment disorders. Compared to high resolution OCT, UBM has a deeper signal penetration and, since it uses ultrasound, has the ability to image structures up to the anterior vitreous with no optical distortion. Prior studies have used UBM to perform quantitative anterior segment biometry measurements during accommodation (Modesti, Pasqualitto, Appolloni et al., 2011; Marchini et al., 2004). However, these studies have limitations in that only manual, subjective measurements were performed on limited numbers of images which have the potential for introducing measurement bias. The question addressed in Chapter 2 is: can accommodative biometric changes be measured accurately using automated image analysis of UBM images during accommodation? To answer this question, UBM images of the anterior segment were captured in 26 young subjects, while accommodating to various stimulus demands. Axial accommodative biometric changes were measured using A-scan for the same stimulus demands. Automated Matlab image analysis software was developed to perform objective analysis of UBM images. Standard deviation and repeatability parameters were calculated for UBM measured parameters and comparisons were made between UBM and A-scan measurements.

Prior studies in humans and monkeys have shown that the AOR and the accommodative biometric changes are linearly correlated (Bolz et al., 2007; Ostrin et al., 2006; Vilupuru & Glasser, 2005). Therefore, it might be possible to use these linear relationships to predict the AOR if the accommodative biometric changes are measured. No prior publications have attempted to estimate the AOR from measurements of

accommodative biometric changes. The question addressed in Chapter 3 is: how well can UBM measured accommodative biometric changes predict the accommodative optical response? To answer this question, in the same subjects that had UBM accommodation measurements from Chapter 2, static AORs were measured using a Grand Seiko autorefractor and an infra-red photorefraction system for the same accommodative stimulus demands. To observe optical and biometric relationships, each of the UBM measured biometry parameters were plotted with the measured AOR. These comparisons yielded linear relationships. Using each of the UBM measured parameters, AOR was predicted independently using linear regressions, 95% confidence intervals and 95% prediction intervals.

It is of interest to know if objective UBM measurements could be used to estimate the AOR in accommodation restoration concepts. However, before attempting to do this kind of prediction with accommodation restoration concepts, it is important to first establish the standard deviations of UBM biometric measurements and the accuracy of AOR predictions in older phakic eyes with lower accommodative amplitudes. Pre-presbyopic subjects are a more appropriate study population because they have lower accommodative amplitudes, they are closer representative subjects to presbyopes in terms of age and ocular health and they form part of the target patient population for accommodation restoration concepts. The question addressed in Chapter 4 is: what are the standard deviations of UBM measured accommodative biometric changes in a pre-presbyopic population and how accurate are the accommodative optical response predictions in pre-presbyopic subjects compared to young subjects? To answer this

question, static AORs were measured using the Grand Seiko autorefractor and an infra-red photorefraction system in 25 pre-presbyopic subjects for various accommodative demands. In addition, UBM was used to measure anterior segment biometric changes during accommodation for the same stimulus demands. Axial accommodative biometric changes were also measured with A-scan ultrasound. The accommodative optical and biometric changes were linearly correlated. Accommodative optical response was predicted from UBM measured biometry parameters from the linear regressions as described for the young subjects in Chapter 3.

Prediction of AOR from linear regressions as mentioned in Chapters 3 and 4 involve the use of a single UBM measured anterior segment biometry parameter. Since all the accommodative anterior segment biometric changes occur simultaneously during accommodation and are strongly linearly related to each other (Bolz et al., 2007; Ostrin et al., 2006), using all the biometric parameters that change together with accommodation collectively might strengthen predictions of the AOR. One approach to using all the parameters together might be to use a multiple regression model. However, because of the strong linear correlations among the individual biometry parameters, a multiple regression model is unstable and unsuitable to use. Another approach might be to use schematic eye models. Schematic eye models generally include calculation of surface and equivalent powers of cornea, lens and the eye and other optical parameters, such as cardinal points and entrance and exit pupil positions. Schematic eyes provide information on the optical properties of the eye and may be useful in understanding optical image quality (Li, Zwick, Stuck et al., 2000), in the design of intraocular implants

(Preussner, Wahl, & Weitzel, 2005) and for customized refractive surgery (MacRae, Schwiegerling, & Snyder, 1999). In addition, of particular interest for these studies, the schematic eyes can be used to calculate the refraction and the AOR based on measurements of the accommodative biometric changes.

Schematic eyes are constructed using corneal surface radii of curvature, corneal thickness, ACD, LT, ALRC, PLRC, axial length and the refractive indices of the various optical media. All the required schematic eye parameters except for the corneal thickness and corneal surface curvatures were measured from UBM images and A-scan ultrasound for the studies mentioned above in young and in pre-presbyopic subjects (Chapters 2 and 4). Visante anterior segment OCT (AS-OCT) is a high resolution clinical instrument that is used for corneal biometry measurements. Visante images suffer from spatial and optical distortions (Dunne, Davies, & Wolffsohn, 2007; Westphal, Rollins, Radhakrishnan et al., 2002) and require that these distortions be corrected for accurate measurements. Wolffsohn and colleagues previously described a distortion correction for the Visante AS-OCT (Dunne et al., 2007). There are a number of uncertainties in the methods used and when the distortion correction equations from their paper were applied to Visante images of rigid contact lenses of known parameters they did not yield correct values. The question addressed in Chapter 5 is: If optical and spatial distortions are present in Visante OCT images, what corrections need to be applied to get accurate corneal measurements to be able to use the measurements in schematic eye calculations? To answer this question, five contact lenses of known front and back radii of curvature and central thickness were imaged using the Visante AS-OCT to calculate spatial and

optical distortion corrections. The accuracy of the applied corrections was evaluated and the distortion corrections were then applied to Visante corneal images captured from the same young and pre-presbyopic subjects used in Chapters 3 and 4.

Prior accommodation dependent schematic eye models have biometric measurements and optical parameters for just a few accommodative states (Bennett & Rabbetts, 2007; Navarro, Santamaria, & Bescos, 1985). No prior accommodation dependent schematic eye models have been used to calculate refraction and AOR from biometry measurements. Furthermore, there are no accommodation dependent schematic eye models for older eyes with low accommodative amplitudes. Since many of the ocular biometric parameters are known to change with age, age-dependent schematic eyes would be needed to attempt to make predictions for specific age-groups. The question addressed in Chapter 6 is: can schematic eyes constructed from UBM biometry parameters measured during accommodation be used to yield more accurate predictions of objectively measured AOR in the young and pre-presbyopic eyes? To answer this question, ocular biometry parameters from Visante, A-scan and UBM measurements (Chapters 2, 3, 4 and 5) in young and pre-presbyopic subjects were used to construct paraxial schematic eye models for each individual subject for each accommodative stimulus demand. Schematic eye calculated refractions and AORs were compared with Grand Seiko measured refractions and AORs in both age groups. The accuracy of the prediction between schematic eyes and individual linear regressions (Chapters 3 and 4) were compared.

Chapter 2 – Objective Measurement of Accommodative Biometric Changes Using Ultrasound Biomicroscopy

2.1   Introduction

Accommodation is the ocular dioptric change in refraction in response to ciliary muscle contraction that allows the young distance corrected eye to focus on near objects (Helmholtz von, 1962). This change in refraction, the accommodative optical response, is brought about by changes in the ocular anterior segment structures. During accommodation, anterior chamber depth (ACD) decreases (Vilupuru and Glasser, 2005; Ostrin et al., 2006; Bolz et al., 2007), lens thickness (LT) increases (Ostrin et al., 2006; Bolz et al., 2007; Richdale, Bullimore, & Zadnik, 2008), lens equatorial diameter decreases (Glasser, Wendt, & Ostrin, 2006; Jones, Atchison, & Pope, 2007), anterior and posterior lens surface radii of curvature (ALRC and PLRC) decrease (Kasthurirangan et al., 2011; Dubbelman et al., 2005) and the posterior lens surface moves posteriorly (posterior lens movement: PLM). The ocular accommodative biometric changes have been extensively studied in humans (Bolz et al., 2007; Jones et al., 2007; Sheppard, Evans, Singh et al., 2011; Kasthurirangan et al., 2011) and monkeys (Glasser & Kaufman, 1999; Vilupuru and Glasser, 2005) and most studies are in agreement with the accommodative biometric changes described above, except with regards to the accommodative movements of the posterior lens surface. Studies report anterior movement (Koretz, Cook, & Kaufman, 1997; Koeppl, Findl, Kriechbaum et al., 2005),

23

posterior movement (Tsorbatzoglou, Nemeth, Szell et al., 2007; Ostrin et al., 2006; Vilupuru and Glasser, 2005; Dubbelman et al., 2005) or no movement (Koretz, Bertasso, Neider et al., 1987; Kasthurirangan et al., 2011) of the posterior lens surface during accommodation.

Anterior segment biometric changes during accommodation have been measured using A-scan ultrasound (Ostrin et al., 2006; Garner & Yap, 1997; Shum, Ko, Ng et al., 1993; Beauchamp & Mitchell, 1985), ultrasound biomicroscopy (UBM) (Modesti et al., 2011; Marchini et al., 2004), optical coherence tomography (OCT) (Sun et al., 2013; Richdale et al., 2008), partial coherence interferometry (PCI) (Bolz et al., 2007; Tsorbatzoglou et al., 2007), Scheimpflug photography (Dubbelman et al., 2005) and magnetic resonance imaging (MRI) (Sheppard et al., 2011; Kasthurirangan et al., 2011; Jones et al., 2007). A-scan and PCI provide quantitative information on axial biometry, but without allowing visualization of the anterior segment. On the other hand, MRI, UBM, OCT and Scheimpflug capture images of the anterior segment and allow both visualization of the anterior segment structures and quantitative measurements to be performed. Although MRI has been used to measure accommodative changes in the ocular anterior segment (Kasthurirangan et al., 2011; Jones et al., 2007), imaging times are long (seconds to minutes) and the image resolution is limited (0.156 mm) (Kasthurirangan et al., 2011). OCT has the capability to capture images more rapidly (micro to milliseconds) and with a resolution of a few microns (Sun et al., 2013). While optical imaging methods such as OCT and Scheimpflug may offer higher resolution than MRI and UBM, they suffer from the disadvantage that optical interfaces preceding the

24

surfaces being measured create optical distortions which require correction for accurate measurements to be made (Dubbelman et al., 2005; Siedlecki, de Castro, Gambra et al., 2012). While optical correction of the posterior corneal surface and the anterior lens surface from refraction by the preceding optical surfaces may be relatively straightforward, accurate optical correction of the crystalline lens posterior surface requires detailed knowledge of the lens gradient refractive index (Siedlecki et al., 2012).

UBM is a clinical method widely used to image the anterior segment of the eye in the diagnosis and management of conditions such as glaucoma and uveal tumors (Ishikawa, Liebmann, & Ritch, 2000). The advantages of UBM over other current commercial available clinical anterior segment imaging instruments such as OCT include deeper signal penetration, the ability to image structures covered by the iris and absence of optical distortions inherent in optical ocular imaging methods. UBM also acquires images as video sequences from which multiple measurements can be performed. Disadvantages of UBM include limited image resolution and that it is relatively more invasive requiring topical anesthesia, a scleral cup and a fluid interface on the eye.

Visualizing and measuring ocular accommodative biometric changes is important for understanding how the eye undergoes accommodation and for understanding design and evaluation of accommodative restoration strategies. While ocular imaging methods allow visualization of the accommodative structures, their true strength becomes evident when objective measurements can be made from the images. Accurate objective measurements of biometry are useful to evaluate accommodation in pseudophakes with

accommodative IOLs and for assessment of accommodative IOL design, performance and limitations. In addition, since accommodative biometric changes and the accommodative optical response (AOR) have been shown to be linearly correlated (Vilupuru and Glasser, 2005; Ostrin et al., 2006; Glasser et al., 2006; Bolz et al., 2007), objective measures of biometry can be used to provide a prediction of the AOR. Prior UBM studies have reported measurements of various anterior segment parameters (distances and angles), which might change during accommodation (Marchini et al., 2004; Modesti et al., 2011). However, none of the prior studies have used objective image analysis methods on the UBM images. Manual measurements were performed by one or more examiners by using software calipers. Moreover, measurements were made only on one (Marchini et al., 2004) or two (Modesti et al., 2011) individual UBM images.

In the current study, accommodative changes in the ocular anterior segment were imaged using UBM in young phakic human subjects. An automated Matlab image analysis program was developed to perform objective measurements on sequences of captured UBM images. The UBM parameters measured were compared with similar measures from A-scan ultrasound. Slopes of the accommodative stimulus-response functions of different anterior segment parameters in the current study were compared with existing values from prior anterior segment imaging studies.

2.2   Methods

Subjects

Twenty six subjects (8 males and 18 females), aged 21 to 36 years (mean ± standard deviation (SD): 24.15 ± 3.03 years) participated. The study followed the tenets of Declaration of Helsinki and was performed in accordance with an institutionally approved human subjects protocol. All subjects signed an informed consent document and completed a visual history questionnaire. Exclusion criteria included spherical refractive errors greater than ± 6 D, astigmatism greater than 2 D, prior ocular surgeries, ocular disease and known sensitivities or contraindications to topical anesthetic (Proparacaine hydrochloride). Preliminary screening was performed, which included measurement of uncorrected, objective baseline refraction, subjective refraction and anterior segment evaluation using slit-lamp biomicroscopy. Cycloplegic refraction with 1% tropicamide was performed in hyperopes (baseline refraction greater than +0.50 D). Subjects with refractive error were corrected with spherical or toric soft contact lenses. Accommodative stimulus demands from 0 D to 8 D was used to measure the accommodative amplitude of subjects using a Grand Seiko autorefractor (WR-5100 K).

Ultrasound Biomicroscopy (UBM)

Because subjects were required to lie on their back and look upward for the UBM imaging, an aluminum frame was constructed (ITEM, Akron, OH) to hold a mirror for viewing a far target and a beam splitter for viewing a near target (Figure 2.1 A). The frame was adjustable to allow the correct positioning of these components. A projected far letter target was viewed at 6 m reflected off a plane mirror inclined at 45^0. The near target was a custom designed, illuminated near-letter chart which was viewed by the subjects' right eye as reflected off a beam splitter. The near target could be moved on a meter stick to change the target vergence from 1 D to 6 D in 1 D steps. In addition, the meter stick could be rotated around a pivot point to alter the angle of gaze of the two eyes. Anterior segment accommodative changes in the left eye were imaged using UBM (VuMax, Sonomed-Escalon, Lake Success, NY). The subject lay supine on a reclining clinic exam chair with his/her head stabilized with a gel head rest (Figure 2.1 B). Prior to imaging, contact lenses were removed from the left eye. Two drops of 0.5% proparacaine hydrochloride (Eye Caine, Bausch & Lomb, Tampa, FL) were instilled in the left eye and a scleral eye cup was inserted under the eyelids and filled with warmed saline solution (BSS, Alcon, Fort Worth, TX). All UBM imaging was performed in dim room illumination. Three sequences each of 50 well aligned anterior segment UBM images of the left eye were captured over 8 seconds using a 35 MHz transducer, as the subjects accommodated to each stimulus amplitude from 0 D to 6 D in 1 D steps. All UBM scans were of the horizontal ocular meridian (3-9 O'clock). For each stimulus amplitude, the subject adjusted the angle of the near target on the meter stick such that the right eye took

up all of the accommodative convergence as determined by the examiner and the left eye remained in the primary gaze posture. Alignment of the UBM transducer was achieved by ensuring an absence of tilt of the iris plane in the UBM image as well as imaging a plane of the eye that provided the largest possible pupil diameter (Figure 2.1 C). Adequate distance of the anterior corneal surface from the top of the UBM scan window was maintained to ensure that UBM corneal distortion artifacts were avoided.

Figure 2.1

(A) Illustration of the aluminum frame designed to hold various optical components and to stimulate accommodation. (B) Experimental setup for ultrasound biomicroscopy (UBM) on the left eye while the right eye views the near target. (C) A raw UBM image in the unaccommodated state from a subject. (D) UBM image of the acrylic calibration block with red points marked. Yellow arrows indicate the distances measured from the images. H: horizontal; V: vertical.

Figure 2.1
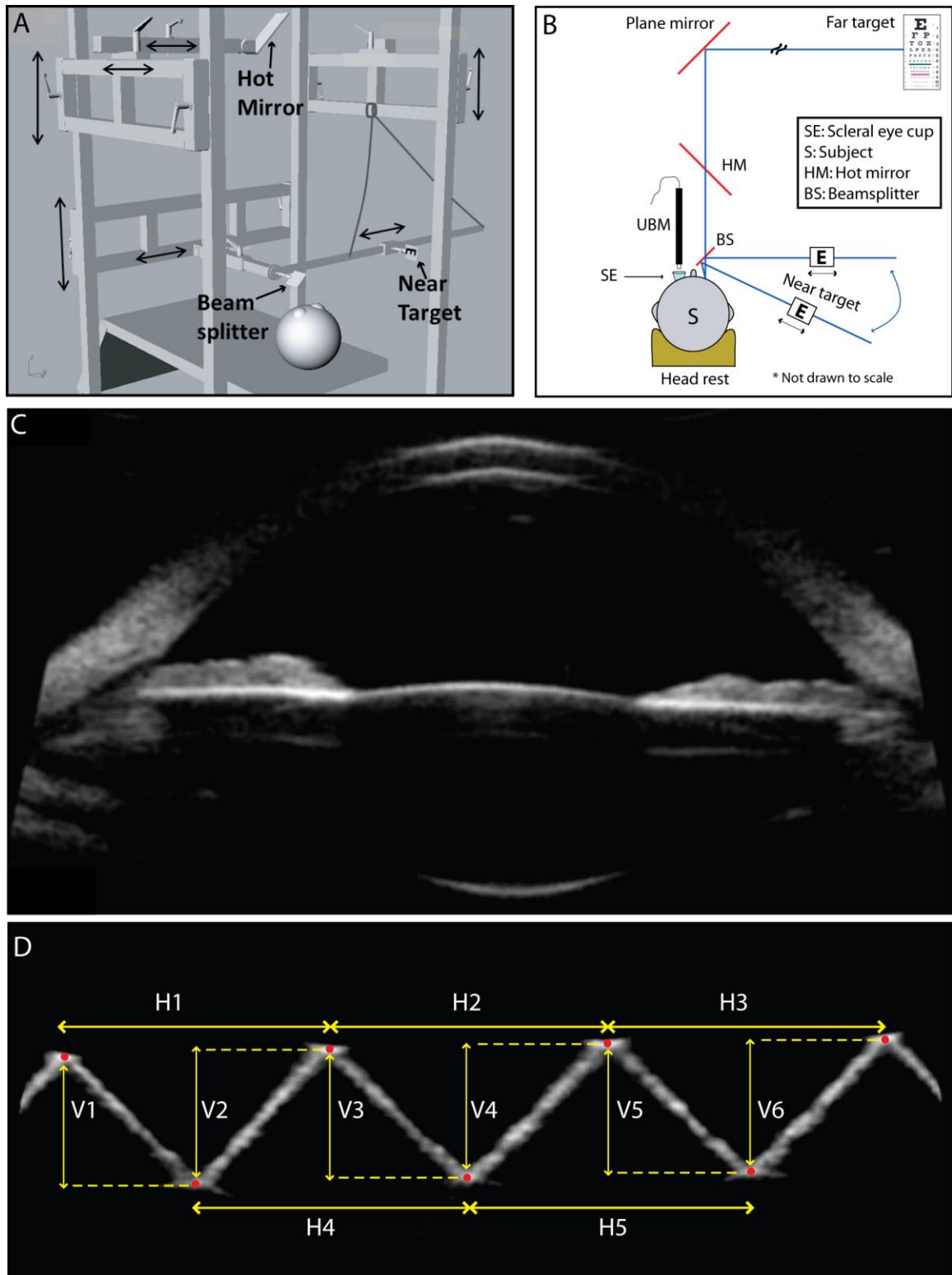
Image Analysis

Horizontal and vertical spatial pixel-to-mm calibration factors for the UBM images were calculated by imaging a saw-tooth acrylic calibration block of known dimensions. The peaks and valleys of the saw-tooth block were manually marked on the UBM images and distances were measured as shown in Figure 2.1 D. The mean ± standard deviations (SD) of horizontal and vertical pixel-to-mm conversion factors calculated from 20 images were 54.60 ± 1.38 pixels/mm and 51.20 ± 1.02 pixels/mm, respectively.

All captured UBM images were analyzed offline using a custom developed automated Matlab (The MathWorks, Natick, MA) image analysis program. The program loaded the first of a sequence of 50 UBM video images and required the user to make two mouse clicks, one in the vicinity of each of the vertices of the anterior chamber angles in this first image. This was the only user input required and all further analysis on the 50 images was performed automatically by the software as follows: The gray-scale UBM image was converted to a black and white binary image using an automatically determined threshold. A 20 x 20 pixel region of interest around each of the marked points was used to find the left and right anterior chamber angle vertices. The distance between the two anterior chamber angle vertices was calculated as the angle to angle distance (AAD). The two angle x, y coordinate vertices served as the starting points to trace up to a maximum of 80 boundary pixels along the anterior surface of the iris and a maximum of 80 pixels along the posterior corneal surface. The number of boundary pixels from

each trace was automatically determined by finding the smallest mean square deviation of the pixels from a segmented linear regression progressively increasing in length. The left and the right anterior chamber angles (LACA and RACA) were determined as the angle between the two resulting linear regression lines (Figure 2.2 A and Figure 2.2 B). If the left and right angle y-coordinates were different, the angle of the line connecting them was determined and the gray-scale UBM image was rotated by this angle to correct for tilt in the image. All further analysis was performed on the rotated gray-scale image. The midpoint of the x-coordinates of the two angle vertices was considered as the axis of symmetry of the eye. All axial biometry measurements were made vertically along this axis. The luminance profile along this axis was extracted and the maxima of each of the four peaks corresponding to the vertex positions of the anterior and posterior surfaces of the cornea and the lens were determined. Corneal thickness (CT), anterior chamber depth (ACD), lens thickness (LT) was calculated from the distances between the peaks (Figure 2.2 C).

The x- and y-coordinates of the vertex of the anterior lens surface served as the starting point to trace up to a maximum of 200 pixels along the anterior surface of the lens and the iris on either side of the vertex. The pupil diameter (PD) was identified as the distance between the two x-coordinates with the largest y-coordinates of the two traced contours (Figure 2.2 D). To identify the anterior lens surface, a region of interest containing the anterior lens surface was automatically extracted. The region of interest had a width equal to 10 pixels less than the identified pupil diameter and a height of 40 pixels. Another 200 x 40 pixel region of interest was extracted around the posterior lens

surface vertex. The anterior and posterior lens surface coordinates were determined as the maxima of the peaks of the luminance profiles along each vertical line of pixels within the regions of interest. The number of luminance lines was equal to the width of the regions of interest. A subset of these luminance lines with the maxima are shown in Figure 2.2 E. All of the lens anterior and independently the posterior surface coordinates were fit with circles to get the radii of curvatures. These represent the radii of curvature of the anterior and posterior lens surfaces (ALRC and PLRC). The complete analysis of a single UBM image with all the measured parameters is shown in Figure 2.2 F.

Figure 2.2

(A) Left and (B) right anterior chamber angles (LACA & RACA) were calculated from individual regression lines (yellow) fitted to the traced corneal and iris edge points (red, green, cyan and magenta). Asterisks (*) represent the vertices of the left and right anterior chamber angles. (C) Axial biometric distances were calculated from the peaks of the luminance profiles (yellow and green). (D) Pupil diameter (PD) is represented by the distance between the x-coordinates with the largest y-coordinates of the two contour traces (yellow arrows on red and green boundaries). (E) Lens surface points (yellow) were detected from the peak of luminance profiles along each vertical red line within the two red search regions of interest. For clarity, only subsets of the vertical lines (red) are shown. (F) A UBM image with all analyzed measurements shown. CT: corneal thickness; ACD: anterior chamber depth; LT: lens thickness; AAD: angle to angle distance; ALRC: anterior lens radius of curvature; PLRC: posterior lens radius of curvature; PD: pupil diameter; LACA: left anterior chamber angle; RACA: right anterior chamber angle.

Figure 2.2
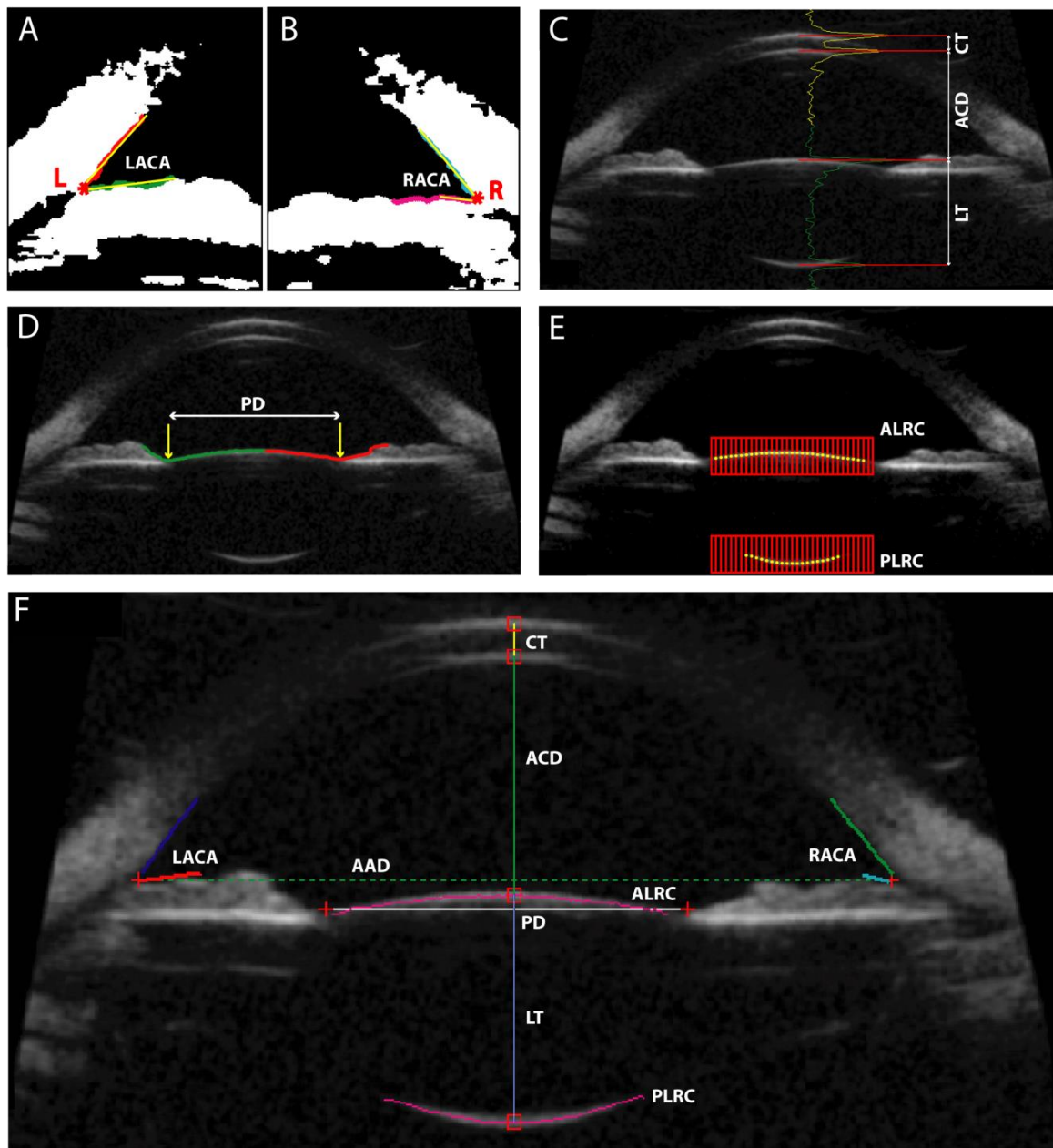
The angle coordinate points found in the first image of the sequence of 50 UBM images served as the starting point for angle coordinate search regions of interest in the second UBM image and the automated analysis proceeded as described above on the remaining 49 images without further user intervention. Anterior segment length (ASL) was calculated as the distance from the first corneal vertex to the posterior lens vertex (ASL = CT + ACD + LT). Anterior lens surface movement was defined as the accommodative change in anterior chamber depth and posterior lens surface movement was defined as the accommodative change in anterior segment length (anterior cornea to posterior lens). The mean ± SD of the measured parameters was calculated from all 150 analyzed images for each accommodative stimulus amplitude.

Calibration of UBM Images

The lens surface radii of curvature (ALRC and PLRC) measured as described above were found to be outside of the range expected for lens anterior and posterior surfaces (Dubbelman et al., 2005). It was determined that the measured radius of curvature was dependent on the y-position of the surface in the UBM image due to image distortion. To correct for this distortion, convex and concave calibration surfaces of known radii of curvature approximating the range of lens surface curvatures expected (Table 2.1) were imaged at various distances from the UBM transducer. The transducer was clamped to a miniature optical rail (M-MRL-6M; Newport Corporation, Irvine, CA) which allowed precise vertical positioning of the transducer. For each calibration surface and at each position with respect to the transducer, 50 images were captured. Each UBM

image measured 1024 x 512 pixels and a pixel position of (x = 1, y = 1) represented the top left corner of an image. In each image, the calibration surface coordinates were identified using a custom written automated Matlab image analysis program (Figure 2.3 A and Figure 2.3 B). Circles were fit to 174 and 138 pixel coordinates for the convex and concave surface, respectively and radius of curvature was calculated. The y-vertex position of the surface in the image was determined and marked by a yellow 'x'. The range of y-vertex positions of the convex and concave surfaces in the images were 210 to 329 pixels and 390 to 509 pixels, respectively. This range corresponded to the range over which the positions of anterior and posterior crystalline lens surfaces from the imaged subjects were located in uncalibrated UBM images. Figure 2.3 C and Figure 2.3 D show the calibration functions for the convex and concave surface, respectively, of a single contact lens imaged at various distances from the transducer. The y-vertex position that corresponded to the actual radius of curvature was calculated from the calibration functions for each calibration surface. The slopes of the convex and concave surface calibration functions were similar for all the calibration surfaces. From the graphs, the mean ± SD of the y-vertex image position from each calibration surface that yielded the actual radius of curvature for the convex and the concave surface was 288.50 ± 4.74 pixels and 383.14 ± 8.79 pixels, respectively.

Table 2.1

Parameters of the calibration surfaces. CL: contact lenses; AB: acrylic ball.

Table 2.1

Convex Surface		Concave Surface	
Calibration Surface	**Radius of Curvature (mm)**	**Calibration Surface**	**Radius of Curvature (mm)**
AB 01	9.51	CL 01	7.50
CL 01	8.30	CL 02	7.00
CL 02	7.80	CL 03	6.52
CL 03	7.50	CL 04	6.30
CL 04	7.30	CL 05	6.13

Figure 2.3

UBM image analysis of a convex (A) and concave (B) calibration surface. The y-axis tick marks superimposed on the images represent the y-axis pixel positions in the UBM images. Comparison of the measured radius of curvature of the convex (C) and concave (D) surfaces as a function of vertex distance. The circled points represent the two corresponding images shown in A & B above. The actual radii for the convex and concave surfaces were calculated at vertex y-pixel positions of 287.39 and 386.04, respectively (green dashed lines). Calibration functions for the convex (E) and concave (F) calibration surfaces. Note that (E) includes one acrylic ball (AB) and 4 contact lenses (CL).

Figure 2.3

Panel C — Actual radius = 7.80 mm
$y = 0.0223 + 1.376$
$r^2 = 0.9833$
Actual Radius at 287.39 pixels
Measured Convex Surface Radius of Curvature (mm)
Vertex Position of Convex Surface (pixels)

Panel D — Actual radius = 7.50 mm
$y = -0.0237 + 16.657$
$r^2 = 0.996$
Actual Radius at 386.04 pixels
Measured Concave Surface Radius of Curvature (mm)
Vertex Position of Concave Surface (pixels)

Panel E
$y = -0.0209x - 6.041$
$r^2 = 0.9811$
Delta Convex Surface Radius of Curvature (mm)
Vertex Position (pixels)
AB 01, CL 01, CL 02, CL 03, CL 04

Panel F
$y = -0.0232x + 8.890$
$r^2 = 0.9800$
Delta Concave Surface Radius of Curvature (mm)
Vertex Position (pixels)
CL 01, CL 02, CL 03, CL 04, CL 05

42

Calibration functions for the convex and concave calibration surfaces fit with cumulative linear regressions are shown in Figure 2.3 E and Figure 2.3 F, respectively. These calibration graphs show that the radius of curvature of any surface is accurate in the UBM image if the surface is imaged at a particular y-position in the UBM image – i.e., the focus. If any surface is imaged above or below the focus, then the radius of curvature of the surface must be corrected by some amount (delta radius) which is directly proportional to the distance in pixels that the surface is from the focus (delta y-vertex position). For each surface imaged, the delta radius (i.e., the correction factor) was calculated from the calibration function (Figure 2.3 E and Figure 2.3 F) using the delta y-vertex position of the surface from the focus. Convex and concave calibration surface radii of curvature were corrected with the calculated correction factors. The y-vertex foci positions calculated from the cumulative linear regression lines (Figure 2.3 E and Figure 2.3 F) for the convex (288.14) and the concave (384.68) surfaces were similar to the mean calculated y-vertex positions mentioned above. The subjects' lens anterior and posterior radii of curvature (ALRC and PLRC) were also corrected in the same way and all data shown is corrected as described here.

A-scan Ultrasound

Axial biometric changes during accommodation were also independently measured in 24 subjects using A-scan ultrasound (A-5500; Sonomed, Lake Success, NY) in the left eye as the subjects remained supine to provide a comparison for the measurements obtained from the automated UBM image analysis. Two drops of

proparacaine were instilled in the left eye. Calibration of the A-scan transducer was performed prior to each experiment according to the manufacturer's instructions. Five A-scan measurements each were performed by touching the transducer to the cornea independently for each accommodative stimulus amplitude from 0 D to 6 D in 1 D steps. Angular adjustment of the near target to compensate for convergence was performed by the subjects as described above for the UBM measurements. ACD, LT, vitreous chamber depth (VCD) and axial length (AL) were measured and corrected for the appropriate sound velocities (Jansson & Sundmark, 1961).

Data Management and Analysis

All the UBM image analysis data and A-scan data were stored in Matlab structures and saved as Matlab '.mat' files for later analysis. From the UBM analysis, CT, ACD, LT, ASL, ALRC, PLRC, AAD, PD, LACA, RACA, accommodative stimulus amplitude, the image frame number, and the image rotation angle were all stored. In addition, all the identified pixel x- and y-coordinate positions for the lens anterior and posterior surfaces were stored in the Matlab structures. This provided the opportunity to later independently calculate lens anterior and posterior radii of curvature for different entrance pupil diameters. This may be necessary because more pixels (representing a larger diameter) were always found for the lens anterior than posterior surface and more pixels are found in the unaccommodated compared to the accommodated state due to accommodative pupil constriction. For each subject, a single '.mat' file was created to store all the data for the above 15 analyzed parameters from each experiment from all

44

stimulus amplitudes representing all the analyzed data from 1050 images (7 stimulus amplitudes x 3 trials x 50 images per video). From the A-scan ultrasound measurements, ACD, LT, VCD and AL were stored as a separate '.mat' file. An independent Matlab program was written to read in these UBM and A-scan '.mat' files for the data analysis. The default sound velocities used by the UBM and A-scan instrument were 1540 m/s and 1548 m/s, respectively. Sound velocity correction was applied to all measured parameters in accordance with accepted sound velocities for the ocular media (cornea: 1660 m/s; aqueous and vitreous humors: 1532 m/s; crystalline lens: 1641 m/s) (Jansson and Sundmark, 1961). Accommodative biometric stimulus-response functions for UBM measured parameters were fit with linear regressions and second order functions and tested for statistical significance. UBM measured accommodative biometry changes and the standard deviation were compared with A-scan values. Intra-session repeatability analysis of the UBM measured parameters (ACD, LT, ALRC, PLRC and ASL) from three video sequences from all young subjects for the 0 D stimulus demand was performed. To calculate the inter-session repeatability, 8 out of 26 subjects had UBM and A-scan procedures repeated twice and 10 out of 26 subjects had these two procedures repeated three times on different days. Repeatability analysis was performed in SPSS (version 20.0; SPSS Inc., Chicago, IL). Each repeat was performed on a different day at least 5 days apart.

2.3   Results

Because of the relatively low image resolution of UBM, an analysis of the standard deviations (SD) of the measured parameters was undertaken. The range of SDs (min to max) of the measured convex and concave surface radii of curvature from a set of 50 images for all transducer distances for all of the calibration surfaces were 0.02 mm to 0.12 mm and 0.01 mm to 0.12 mm, respectively. Table 2.2 shows the mean ± SD root mean square error of the convex and concave calibration surfaces after the UBM image calibration.

Table 2.2

Mean ± SD of root mean square error of radius (mm) and power (D) after UBM image calibration of the convex and concave calibration surfaces radii of curvature. Power for each surface was calculated using the respective refractive index of each of the calibration surfaces.

Table 2.2

Convex Calibration Surface		Concave Calibration Surface	
Radius (mm)	**Power (D)**	**Radius (mm)**	**Power (D)**
0.21 ± 0.07	1.59 ± 0.38	0.16 ± 0.07	1.92 ± 1.05

Of the twenty six subjects, 16 subjects had myopia (spherical refraction greater than - 0.50D) and 3 had hyperopia (spherical refraction > + 0.50 D) with refractive errors ranging from - 5.50 D to + 2.75 D (mean ± SD, - 1.31 ± 2.03 D).

Three separate stimulus-response functions of UBM measured anterior chamber depth and lens thickness from one subject is shown in Figure 2.4 A & Figure 2.4 B.

Figure 2.4

UBM measured (A) anterior chamber depth and (B) lens thickness stimulus-response curves from a 24 year old subject from three separate trials together with the mean. Error bars represent ± 1 standard deviation from 150 (3 sequences of 50 images) measurements.

Figure 2.4
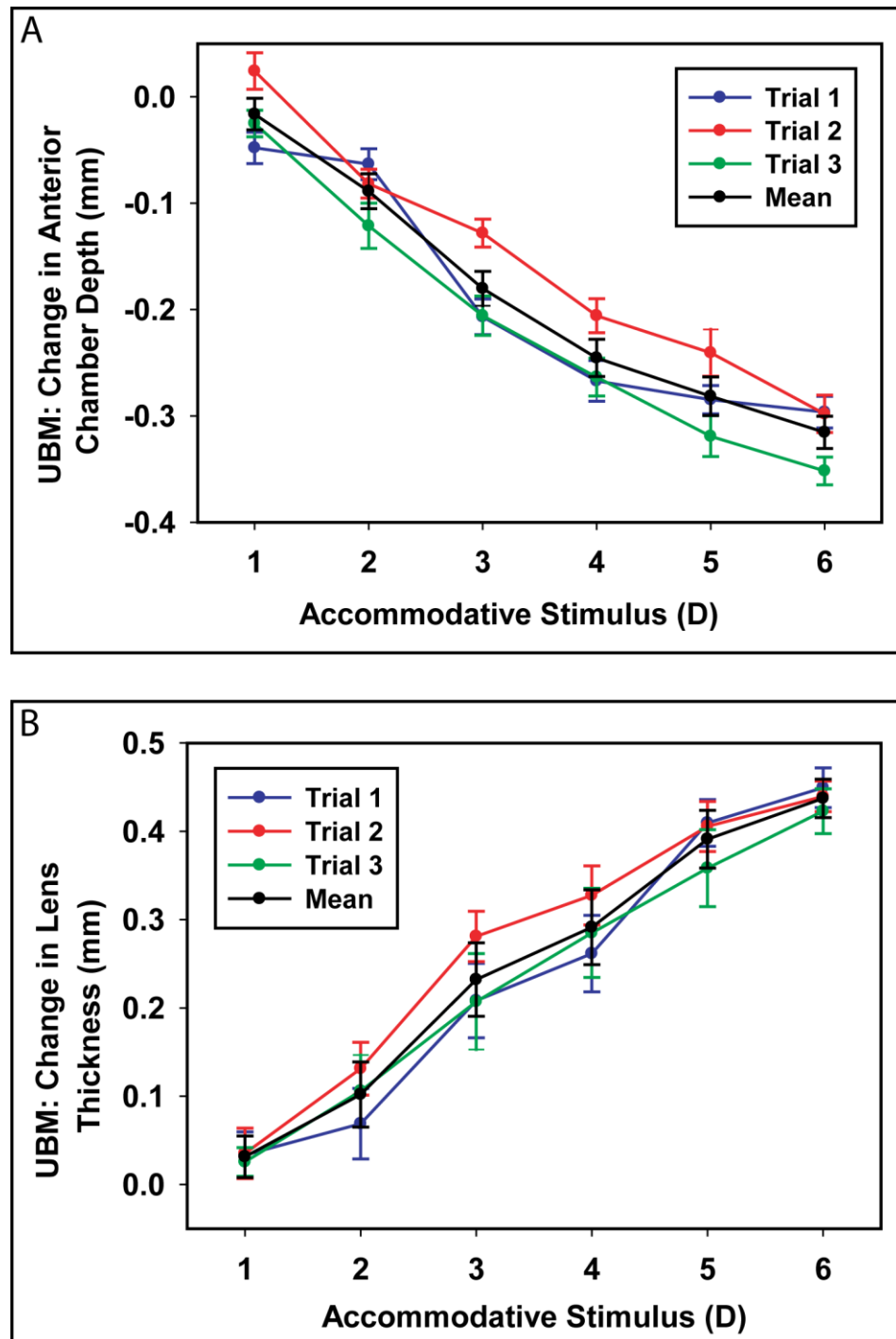
Although objective accommodative optical changes were also independently measured in these subjects, because of the extensive data available, that data will be presented separately. Here, data will be presented as a function of the accommodative stimulus demands. Because all subjects had accommodative amplitudes greater than the maximum stimulus demand (6 D), linear stimulus response relationships were expected for the parameters that change with accommodation (Wold, Hu, Chen et al., 2003). The number of subjects with statistically significant linear relationships between accommodative stimulus amplitude and each anterior segment biometry parameter were ACD: n = 25, LT: n = 26, ALRC: n = 26, PLRC: n = 25 and ASL: n = 13. Only data from subjects with statistically significant linear relationships between the accommodative stimulus and changes in biometry were included in the subsequent population plots. Figure 2.5 shows the change in each UBM measured anterior segment biometry parameter with the accommodative stimulus demands for this subject population. The population plots for these five biometry parameters (ACD, LT, ALRC, PLRC and ASL) were all statistically significant fit with linear regression lines and with second order fits (p < 0.0001), with only small improvements in the r^2 values for the second order equations.

Figure 2.5

Stimulus-response relationships of UBM measured biometry parameters of (A) anterior chamber depth, (B) lens thickness, (C) anterior lens radius of curvature, (D) posterior lens radius of curvature, (E) anterior segment length from all subjects who individually showed statistically significant linear stimulus-response functions for each parameter. Both linear (black lines) and second order fits (blue lines) are shown. The n's identify the number of subjects shown for each graph.

Figure 2.5

A

y = 0.0082x^2 - 0.1063x + 0.0653
r^2 = 0.786, p < 0.0001

n = 25

y = - 0.0489x - 0.011
r^2 = 0.742, p < 0.0001

Change in Anterior Chamber Depth (mm)

Accommodative Stimulus (D)

B

y = 0.065x + 0.019
r^2 = 0.738, p < 0.0001

n = 26

y = - 0.0069x^2 + 0.1132x - 0.0443
r^2 = 0.7563, p < 0.0001

Change in Lens Thickness (mm)

Accommodative Stimulus (D)

C

y = - 0.756x - 0.122
r^2 = 0.637, p < 0.0001

n = 26

y = 0.1058x^2 - 1.4953x + 0.8607
r^2 = 0.6639, p < 0.0001

Change in Anterior Lens Radius of Curvature (mm)

Accommodative Stimulus (D)

D

y = - 0.187x + 0.023
r^2 = 0.562, p < 0.0001

n = 25

y = 0.0157x^2 - 0.2971x + 0.1694
r^2 = 0.5704, p < 0.0001

Change in Posterior Lens Radius of Curvature (mm)

Accommodative Stimulus (D)

E

y = 0.0032x^2 + 0.0053x + 0.0020
r^2 = 0.6269, p < 0.0001

n = 13

y = 0.027x - 0.027
r^2 = 0.609, p < 0.0001

Change in Anterior Segment Length (mm)

Accommodative Stimulus (D)

The slopes of the linear regression lines represent the per-diopter of stimulus amplitude biometric changes. When per-diopter changes in biometry are calculated from stimulus amplitudes as opposed to measured accommodative optical response amplitudes, the resulting per-diopter biometry changes underestimate the actual per-diopter biometry changes because the actual accommodative response lags behind the stimulus amplitude (Nakatsuka, Hasebe, Nonaka et al., 2004; Vilupuru and Glasser, 2005). However, since per-diopter of stimulus amplitude values are reported in prior accommodation biometry studies (Dubbelman et al., 2005; Tsorbatzoglou et al., 2007; Shum et al., 1993; Beauchamp and Mitchell, 1985), the per-diopter of stimulus values together with those from prior studies are reported here for comparison (Table 2.3).

Table 2.3

Per-diopter of stimulus changes in biometry during voluntary accommodation from various human studies. N/A: not available; PCI: partial coherence interferometry; OCT: optical coherence tomography; MRI: magnetic resonance imaging; ACD: anterior chamber depth; LT: lens thickness; ALRC: anterior lens radius of curvature; PLRC: posterior lens radius of curvature; ASL: anterior segment length.

Table 2.3

Study	Method Used To Measure Biometry	Per-diopter Changes in Biometry (mm/D)				
		ACD	LT	ALRC	PLRC	ASL
Current study	UBM	-0.049	+0.065	-0.756	-0.187	+0.027
(Shum et al., 1993)	A-scan	-0.035	+0.053	N/A	N/A	N/A
(Beauchamp and Mitchell, 1985)	A-scan	-0.037	+0.056	N/A	N/A	+0.022
(Garner and Yap, 1997)	A-scan	-0.033	+0.040	N/A	N/A	+0.007
(Brown, 1973)	Photography	-0.030	+0.045	-0.545	-0.371	+0.015
(Tsorbatzoglou et al., 2007)	PCI	-0.027	+0.036	N/A	N/A	N/A
(Richdale et al., 2008)	OCT	N/A	+0.051	N/A	N/A	N/A
(Jones et al., 2007)	MRI	N/A	+0.050	N/A	N/A	N/A
(Dubbelman et al., 2005)	Scheimpflug	-0.038	+0.045	-0.620	-0.130	+0.008

Since various biometry parameters show statistically significant linear relationships with accommodative stimulus amplitudes, they are expected to also be linearly related to each other. Figure 2.6 shows correlations among several of the anterior segment biometry parameters that were found to change with accommodation. All of the correlations are tabulated in Table 2.4.

Figure 2.6

Linear relationships of change in (A) anterior chamber depth versus lens thickness (n = 25), (B) anterior lens radius of curvature versus posterior lens radius of curvature (n = 25), (C) anterior chamber depth versus anterior lens radius of curvature (n = 25), and (D) posterior lens radius of curvature versus posterior lens surface movement (n = 13) (p < 0.0001). Linear regression parameters for other statistically significant biometry relationships are shown in Table 2.4 [red lines: linear regression, blue lines: 95% confidence interval].

Figure 2.6

Table 2.4

Linear regression parameters (slope, intercept and r^2 values) for comparison between UBM measured anterior segment biometry parameters during accommodation. All regressions shown had statistically significant linear correlations ($p < 0.0001$). ACD: anterior chamber depth; LT: lens thickness; ALRC: anterior lens radius of curvature; PLRC: posterior lens radius of curvature; ASL: anterior segment length. **Data plotted in Figure 2.6.
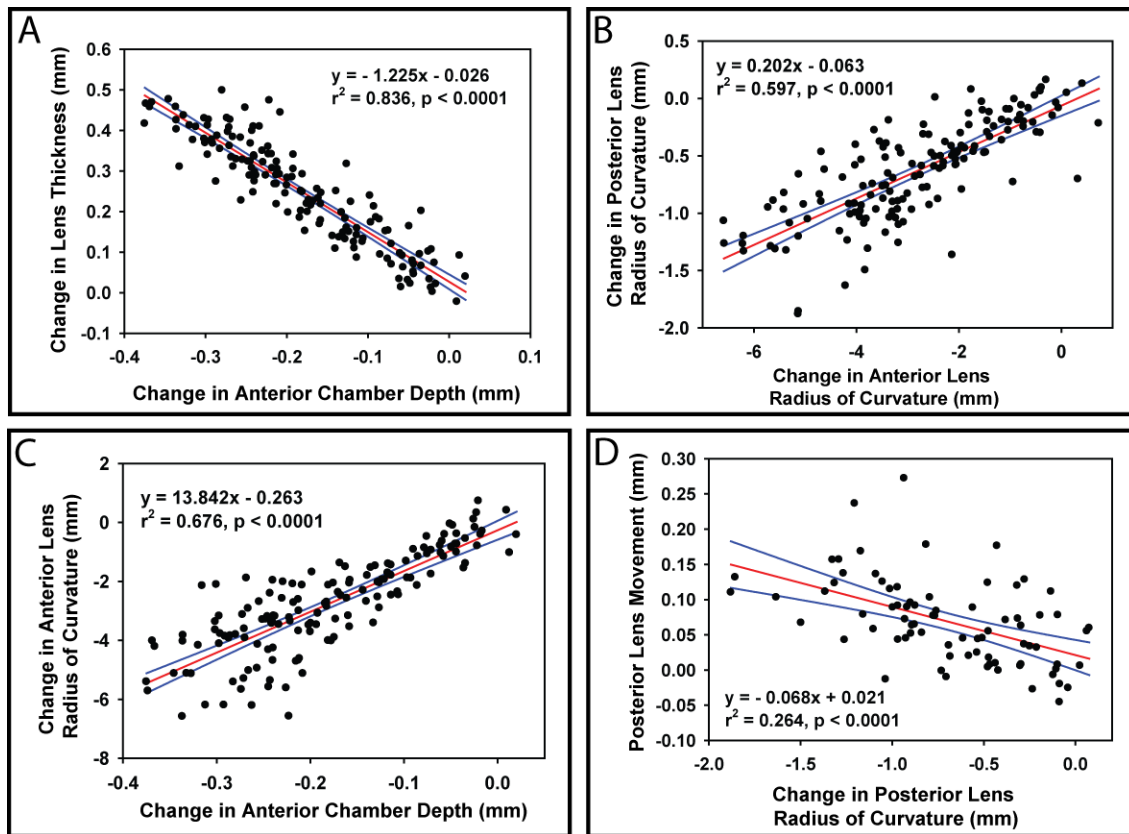
Table 2.4

Change in Biometry		Horizontal Axis			
		ACD	LT	ALRC	PLRC
Vertical Axis	LT	-1.225, - 0.026, 0.836**			
	ALRC	13.842, - 0.263, 0.676	- 9.925, - 0.307, 0.633		
	PLRC	3.471, - 0.012, 0.613	- 2.571, 0.000, 0.621	0.202, - 0.063, 0.597**	
	ASL	- 0.330, 0.001, 0.316	0.339, - 0.016, 0.569	- 0.023, 0.002, 0.383	- 0.068, 0.021, 0.264**

The standard deviation of the individual UBM parameters determined from the automated image analysis is indicative of the variance and resolution of the methods described. Standard deviation of each of the measured biometry parameters was found from 50 UBM images for each subject for each stimulus demand. None of the measured parameter SDs showed statistically significant relationships with stimulus demand in any individual subject, therefore, mean SD was calculated by taking the average SD of measured biometry parameters for all stimulus amplitudes, for all trials, from all subjects (Table 2.5). Mean SD of ACD, LT and ASL for the population are smaller than 0.050 mm. ALRC, PLRC and PD have larger mean SDs. Anterior segment parameters CT, LACA, RACA and AAD did not change significantly during accommodation.

Table 2.5

Mean standard deviation (SD) of the UBM measurements of biometry in this subject population.

Table 2.5

Biometry	Mean SD ± SD
Parameters that change during accommodation	
Anterior chamber depth (mm)	0.017 ± 0.003
Lens thickness (mm)	0.029 ± 0.007
Anterior lens radius of curvature (mm)	0.335 ± 0.138
Posterior lens radius of curvature (mm)	0.158 ± 0.038
Anterior segment length (mm)	0.034 ± 0.009
Pupil diameter (mm)	0.265 ± 0.130
Parameters that did not change during accommodation	
Corneal thickness (mm)	0.012 ± 0.003
Angle to angle distance (mm)	0.081 ± 0.022
Left anterior chamber angle (deg)	4.3 ± 1.7
Right anterior chamber angle (deg)	4.7 ± 1.9

Pupil diameter was not included in the analysis as the automated image analysis algorithm consistently underestimated pupil diameters relative to visual inspection due to indistinct pupillary margins. The UBM image analysis was visually inspected to ensure that the identification of the anterior lens surface coordinates and calculation of the ALRC did not include pixels belonging to the edges of the iris.

Figure 2.7 A shows the anterior and posterior lens surface movement as a function of accommodative stimulus. With increasing accommodative stimulus demands, the anterior lens surface moves anteriorly linearly and the posterior lens surface moves posteriorly linearly ($p < 0.0001$). The lens center as determined by the difference between the lens anterior and posterior vertices moves anteriorly during accommodation. In this subject population, from the linear relationships shown, the anterior lens surface movement and posterior lens surface movement contributes 70% and 30% of the change in lens thickness, respectively. Figure 2.7 B shows a comparison of the anterior segment biometry changes from a single subject from the unaccommodated state and the maximally accommodated state.

Figure 2.7

(A) Lens surface movements as a function of accommodative stimulus ($p < 0.0001$ for both 1st and 2nd order fits). The lens anterior surface moves anteriorly and the lens posterior surface moves posteriorly with accommodation. Both first and second order fits to the data are shown for comparison. (B) Comparison of anterior segment biometry images from the unaccommodated state while viewing the far target (0 D: left side) and during the maximally accommodated state viewing a 6 D target (right side) from one subject. Only a subset of the pixels representing the lens surfaces are shown so the underlying image surfaces can be seen. ACD: anterior chamber depth; LT: lens thickness; ALRC: anterior lens radius of curvature; PLRC: posterior lens radius of curvature; ALM: anterior lens surface movement; PLM: posterior lens surface movement.

Figure 2.7

Figure 2.7

68
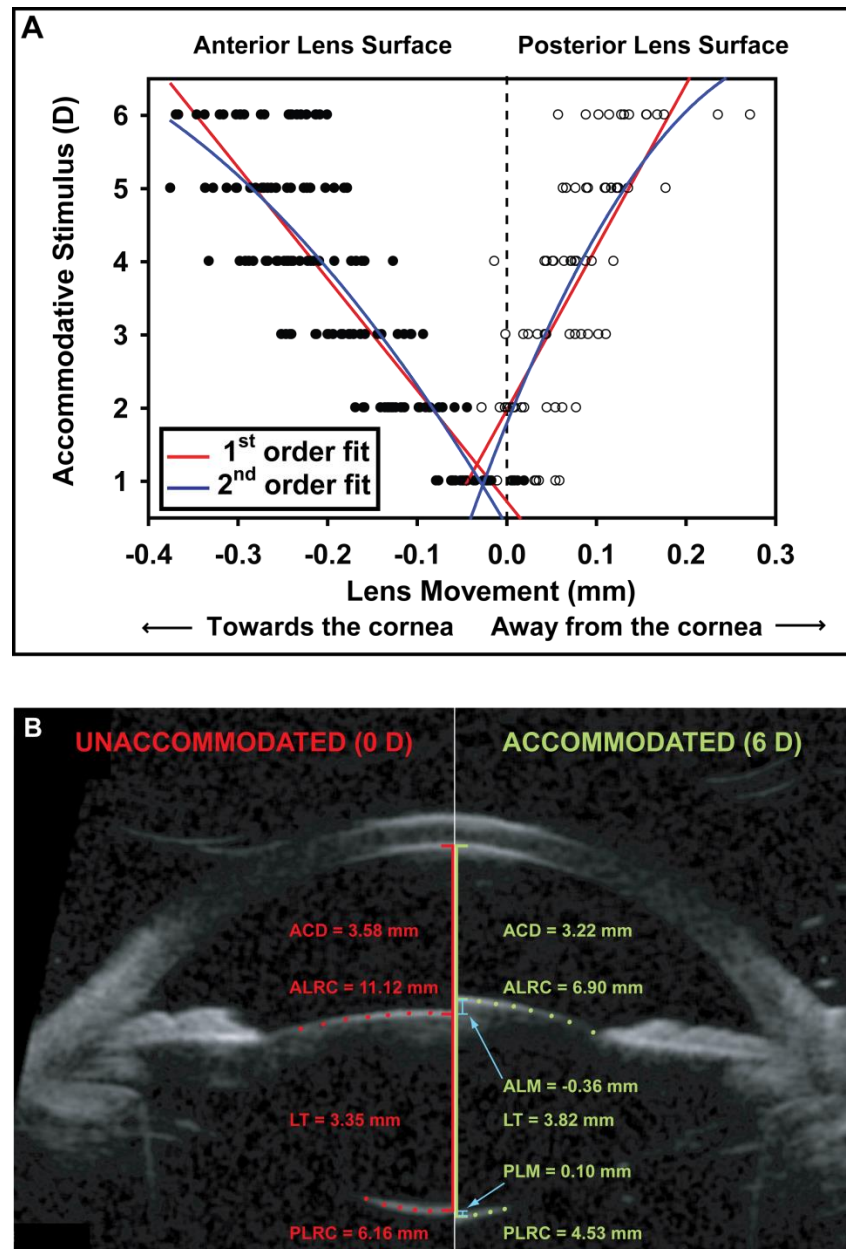
In the initial analysis of the images, anterior and posterior lens radii of curvature (ALRC and PLRC) were calculated by fitting circles to all the pixels available for each lens surface. However, since the pupil constricts during accommodation, less of the lens surface is visible when the eye is accommodated and, because of the nature of the UBM signal, there are fewer pixels available for the posterior lens surface (Figure 2.7 B). Therefore, using all the available pixels considers circle fits to more of the lens surface in the unaccommodated than in the accommodated state. Fitting a circle to fewer/more pixels could lead to an under/overestimate of the radius of curvature. Because all the available lens surface pixel coordinates were stored to the Matlab '.mat' files, this allowed a subsequent analysis to be performed in which ALRC and PLRC were recalculated for the smallest available diameter (from the higher stimulus demands with smaller pupil diameters). Decreasing the diameter and the number of pixels considered resulted in a decrease in the ALRC and PLRC (Figure 2.8).

Figure 2.8

(A) Anterior lens radius of curvature (ALRC) from one subject from a single trial for the full entrance pupil diameter available (the default analysis) (●), average minimum available lens zone diameter as determined from the maximally accommodated state pupil diameter for the anterior lens surface (ALS) (▲) and average minimum available lens zone diameter as determined from the posterior lens surface (PLS) (■) as a function of the accommodative stimulus. (B) Posterior lens radius of curvature (PLRC) from the same subject for the full lens zone diameter available (●) and average minimum available lens zone diameter from the maximally accommodated state as determined from the PLS (▲).

Figure 2.8
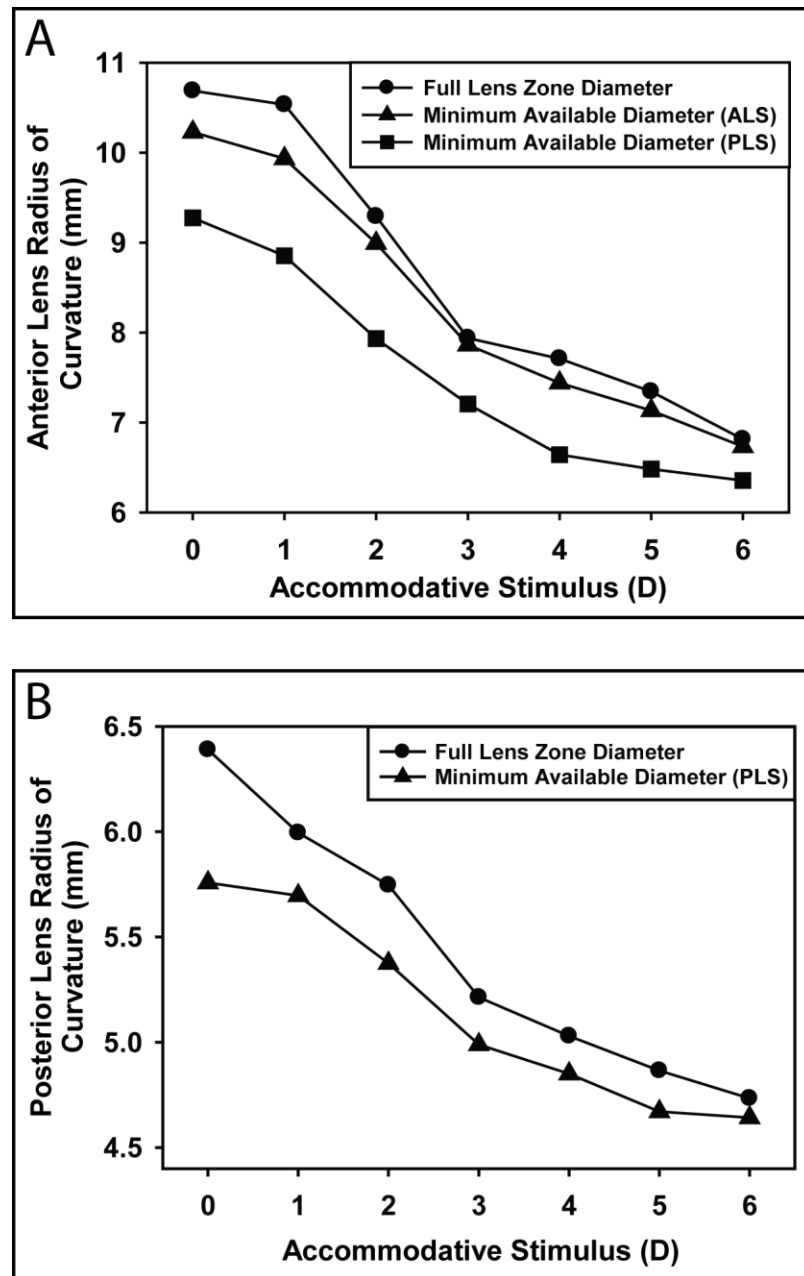
Intra-session repeatability analysis of the UBM measured parameters (ACD, LT, ALRC, PLRC, and ASL) from three video sequences from all the subjects for the 0 D stimulus demand was performed. Inter-session repeatability analysis was performed for the 0 D stimulus demand from 18 subjects who had at least two repeats of the experiment. Repeatability (intra- and inter-session) was evaluated in terms of a) coefficient of variation which is the ratio of the standard deviation of the measurements to the mean, b) mean standard deviation of the differences between the measurements, c) coefficient of repeatability (CoR) which is 2 times the mean standard deviation of the differences between the measurements, d) CoR (%) which is the ratio of CoR to the mean of the measurements multiplied by 100 and e) intraclass correlation coefficient (ICC). UBM parameters have a better within session than between session repeatability as shown by the ICC and other parameters in Table 2.6.

Table 2.6

Intra-session and inter-session repeatability parameters for various UBM measured parameters. ACD: anterior chamber depth; LT: lens thickness; ALRC: anterior lens radius of curvature; PLRC: posterior lens radius of curvature; ASL: anterior segment length; CT: central corneal thickness; CoV: coefficient of variation; SD: standard deviation; CoR: coefficient of repeatability; ICC: intraclass correlation coefficient.

Table 2.6

Repeatability parameters	Intra-session repeatability (n = 26)						Inter-session repeatability (n = 18)					
	ACD	LT	ALRC	PLRC	ASL	CT	ACD	LT	ALRC	PLRC	ASL	CT
CoV	0.005	0.008	0.032	0.026	0.006	0.022	0.005	0.008	0.032	0.026	0.006	0.022
Mean SD of differences (mm)	0.020	0.026	0.301	0.108	0.039	0.005	0.025	0.021	0.434	0.117	0.038	0.004
CoR	0.040	0.052	0.602	0.216	0.077	0.009	0.050	0.043	0.869	0.235	0.076	0.009
CoR (%)	1.183	1.433	5.193	3.860	1.034	1.711	1.486	1.164	7.126	4.101	1.004	1.627
ICC	0.994	0.985	0.949	0.960	0.975	0.984	0.989	0.987	0.828	0.939	0.957	0.985

Comparison between UBM and A-scan ultrasound for measurements of ACD and LT are shown in Figure 2.9 A and Figure 2.9 B, respectively. There is a statistically significant linear correlation between A-scan and UBM for both the measured biometry parameters. A-scan overestimated the UBM measured LT measurements by, on average, 0.166 mm and underestimated the UBM measured ACD by, on average, 0.070 mm as shown in the Bland-Altman plots (Figure 2.9 C and Figure 2.9 D).

Figure 2.9

(A & B) Linear correlation between A-scan ultrasound measured and ultrasound biomicroscopy measured lens thickness and anterior chamber depth, respectively. (C & D) Bland-Altman comparison between A-scan ultrasound measured and UBM measured lens thickness and anterior chamber depth, respectively. Appropriate corrections for sound velocity were applied for lens thickness and anterior chamber depth measurements. Data points circled in red are from a single subject who showed an unusual response. The data from this one subject is not included in the regression calculations/equations.

Figure 2.9
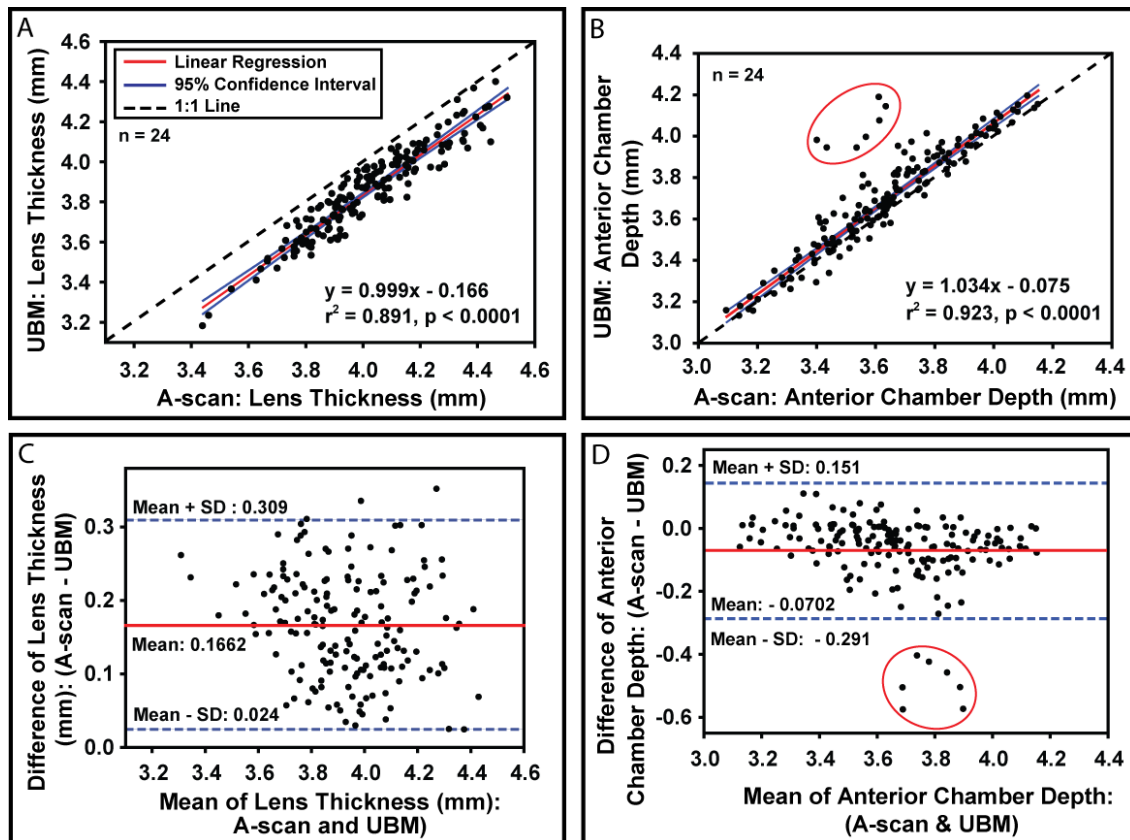
The mean SD of A-scan measured ACD and LT were calculated as previously described for the UBM images (Table 2.5). There was no significant relationship between the SD of the A-scan measurements and the stimulus demand in any individual subject. The mean SD of A-scan measurements of ACD and LT were calculated as the average SD of five measurements for all stimulus amplitudes, for all trials, from all subjects. Table 2.7 shows the comparison of the SD of the A-scan and UBM measurements in the current study with the A-scan measurements from a previous study (Ostrin et al., 2006).

Table 2.7

Standard deviation (SD) of anterior chamber depth (ACD) and lens thickness (LT) during accommodation measured with ultrasound biomicroscopy (UBM) and A-scan ultrasound in the current study (*) compared with the SD of A-scan ultrasound from a prior study (Ostrin et al., 2006).

Table 2.7

Biometry	UBM* Mean SD ± SD (mm)	A-scan* Mean SD ± SD (mm)	A-scan Mean SD (mm) (Ostrin et al., 2006)
ACD	0.017 ± 0.003	0.041 ± 0.024	0.135
LT	0.029 ± 0.007	0.039 ± 0.022	0.115

2.4   Discussion

Although objectively measured optical accommodative responses were also independently measured in this same subject population, because of the extensive data collected and analysis available, those results will be presented in Chapter 3. Ideally, measured accommodative biometric changes would be compared with measured accommodative optical refractive changes to know how the accommodative biometry changes relate to refractive changes. However, clinical accommodation testing can be demanding on patients, so most clinical protocols may only choose to do either accommodative optical measurements or accommodative biometric measurements. For this reason, the biometric accommodative changes measured here are only compared against the accommodative stimulus demands, rather than against the objectively measured accommodative optical responses. The latter comparison will be discussed in Chapter 3.

Per-diopter of stimulus demand changes in the anterior segment biometry in the current study were generally larger than per-diopter of stimulus demand from prior studies (Tsorbatzoglou et al., 2007; Dubbelman et al., 2005; Shum et al., 1993) (Table 2.3). The differences between the current study and previous studies might be due to several factors such as differences in the accommodative stimulus presentation, subject populations, sample size, different imaging techniques and difference in subject posture (erect vs. supine). Gravitational force due to patient posture during measurements might have an effect on how the lens moves during accommodation (Kasthurirangan et al.,

2011; Tromans & Storey, 1990). In the current study, the posterior accommodative movement of the posterior lens surface (PLM) is in agreement with several prior studies (Bolz et al., 2007; Vilupuru and Glasser, 2005; Beauchamp and Mitchell, 1985), but not with an MRI study (Kasthurirangan et al., 2011). It is possible this is not seen in MRI images due to limited MR image resolution of approximately 0.150 mm (Kasthurirangan et al., 2011). The percentage contribution of the lens surface movements to the overall increase in lens thickness is comparable to values reported from prior human (Tsorbatzoglou et al., 2007; Ostrin et al., 2006; Bolz et al., 2007; Beauchamp and Mitchell, 1985) and monkey studies (Vilupuru & Glasser, 2003; Vilupuru and Glasser, 2005).

The standard deviations of the measured UBM biometry parameters reported here are considerably smaller than in prior UBM (Modesti et al., 2011; Marchini et al., 2004), A-scan ultrasound (Ostrin et al., 2006), or OCT (Sun et al., 2013) studies or even than from a prior partial coherence interferometry study (which has considerably higher resolution than UBM) (Bolz et al., 2007). The standard deviation calculated from automated analysis of a sequence of 50 UBM images does not include variability due to multiple independent measurements where ocular alignment with the instrument may change with each repeated measure. However, the SD calculated here (Table 2.5) are from all stimulus amplitudes, from three repeats and from all subjects, and therefore these SD do include all possible sources of variability. Although the SD is calculated from many measurements, increasing the number of measurements does not reduce the SD, but rather results in a more robust estimate. Factors such as eye movements, UBM transducer

positioning and stability, position of the plane of best focus of the UBM, physiological variations of biometry between trials, tilt of the transducer and scanning location on the eye can affect the standard deviation of the biometry measurements. The standard deviations of the UBM measured anterior and posterior lens radii of curvatures are larger than for the other parameters. This is likely due to the limited number of lens surface pixels used to fit a circle which is limited by the pupil diameter. The anterior and posterior lens surfaces in the UBM images are indistinct which adds further variability. Dilation of the iris with phenylephrine could improve measurements of the lens surface curvatures without affecting accommodation (Richdale, Bailey, Sinnott et al., 2012). Of all the measured biometry parameters, most of the accommodative change in power of the phakic lens comes from the changes in lens surface curvatures during accommodation (Maceo, Manns, Borja et al., 2011). Moreover, the surfaces of the anterior and posterior lens are aspheric. Fitting the surface coordinates with a spherical equation might not represent the true geometry of the lens surface; however the resolution of the UBM images and the data available from the lens surfaces precludes meaningful analysis with aspheric fits.

In the current study, UBM and A-scan measurements were performed independently; therefore measurement differences are expected if subjects don't accommodate the same amount for both measurements (Figure 2.9). However, if on average both instruments measure the same accommodative changes, then the Bland-Altman plots should show an average difference of zero. The source of the systematic difference in lens thickness between UBM and A-scan is unclear. The standard deviation

83

of UBM measured ACD and LT are smaller than from A-scan. This might be due to the stable positioning and alignment of the UBM transducer that the user can achieve by viewing the live UBM image on the monitor. Factors contributing to the standard deviation from UBM measurements as described above also apply to A-scan.

Differences within the subject groups, a different examiner and the different subject postures might account for smaller A-scan standard deviation of ACD and LT in the current study compared to a previous study (Ostrin et al., 2006). Considering A-scan ultrasound as the gold-standard, the mean correction factor for the UBM measured ACD and LT to, on average, match the A-scan measures was calculated. Ratios of A-scan measures and UBM measures of ACD and LT were calculated for 24 subjects, for 7 stimulus demands (0 D to 6 D) to yield 168 correction factors. The mean $\pm$ SD of all these ratios is 0.982 ± 0.03 and 1.044 ± 0.02 respectively for ACD and LT. Multiplying the UBM measurements by the ratios would, on average, get the UBM measurements in agreement with the A-scan measurements.

The Matlab automated image analysis program used in the current study provides the ability to perform objective measurements on UBM image sequences. Image analysis programs such as this might be useful if they could be incorporated in the commercially available UBM software to perform real-time image analysis. Visualizing the accommodative anterior segment changes and performing real-time objective measurements of biometry might be useful for understanding the accommodative mechanism and in the design and evaluation of accommodative intraocular lenses.

Clinicians might also use real-time image analysis in the pre-operative assessment of presbyopic eyes and also to quantify movements of an accommodative IOL in pseudophakic eyes. If the correlations between ocular accommodative biometry changes and objectively measured optical accommodative response are strong, then it may also be possible to predict with some reasonable degree of accuracy the accommodative optical response of the eye simply from the measured accommodative biometry changes.

The results from this chapter have demonstrated the utility of automated image analysis to perform objective measurement of the accommodative biometric changes from UBM image sequences. The standard deviation of the UBM measured biometry parameters from automated image analysis is considerably smaller than reported in prior UBM and A-scan studies. UBM measured accommodative anterior segment biometry parameters have smaller standard deviation and good repeatability. Radius of curvature of intraocular structures calculated from UBM images requires distortion correction. With automated objective measurements, UBM can be a useful commercially available clinical tool for accommodation studies.

Chapter 3 - Can Ultrasound Biomicroscopy (UBM) be Used to Predict Accommodation Accurately?

3.1   Introduction

Clinical accommodation testing involves objectively measuring accommodative optical changes or anterior segment accommodative biometric changes. Objective instruments to measure the accommodative optical response (AOR) include autorefractors (Win-Hall, Houser, & Glasser, 2010; Wolffsohn, O'Donnell, Charman et al., 2004), refractometers (Win-Hall et al., 2007; Wold et al., 2003), infra-red photorefraction (Ostrin et al., 2006; Kasthurirangan & Glasser, 2005) or aberrometers (Win-Hall & Glasser, 2008; Lopez-Gil, Fernandez-Sanchez, Legras et al., 2008). Instruments that measure the AOR do not allow for visualization or quantification of the accommodative intraocular biometric changes that produce the AOR.

Accommodative biometric changes have been measured using A-scan ultrasound (Ostrin et al., 2006), ultrasound biomicroscopy (Marchini et al., 2004), optical coherence tomography (Gambra, Ortiz, Perez-Merino et al., 2013), partial coherence interferometry (Bolz et al., 2007), Scheimpflug imaging (Dubbelman et al., 2005) and magnetic resonance imaging (Richdale, Sinnott, Bullimore et al., 2013). Biometric measurements of the ocular anterior segment during accommodation demonstrate and quantify the intraocular movements that lead to accommodation, but do not directly provide information on the AOR.

86

Prior studies (Dubbelman et al., 2005; Drexler, Baumgartner, Findl et al., 1997; van der Heijde, Beers, & Dubbelman, 1996) have related accommodative biometric changes to accommodative stimulus demands. When the accommodative biometry response is expressed as per-diopter of stimulus demand, this underestimates the true per-diopter of accommodative response changes due to the accommodative lag resulting from the depth of focus of the eye (Nakatsuka et al., 2004). Hence, it is useful to measure both the AOR and the biometric changes to understand how the two are related. Currently, it is not possible to measure the accommodative optical and biometric changes with a single instrument. In a clinical setting, using two different instruments to measure the AOR and the biometric changes would be time consuming and costly.

Studies have measured accommodative biometric changes to demonstrate the mechanism of action and accommodative performance of an accommodation restoration strategy (Marcos, Ortiz, Perez-Merino et al., 2014). While measuring and showing biometric movements of an accommodation IOL, for example, can provide unequivocal objective evidence that the IOL accomplishes what is claimed of it, it can be difficult to relate the biometric measurements to how much accommodation this produces.

Several human (Bolz et al., 2007; Ostrin et al., 2006), monkey (Wendt, Croft, McDonald et al., 2008; Vilupuru and Glasser, 2005) and in vitro (de Castro, Birkenfeld, Maceo et al., 2013; Glasser & Campbell, 1999) studies have shown linear correlations between AOR and accommodative biometric changes. These linear relationships allow

the AOR to be estimated if the accommodative biometric changes are measured or known. If the AOR could be predicted from biometric measurements, then accommodation could be evaluated using only a single biometry instrument.

The current study was performed to determine how well ultrasound biomicroscopy can be used to predict the AOR from anterior segment accommodative changes in a population of young adult phakic human subjects.

3.2   Methods

Subjects

Twenty six subjects (8 males and 18 females), aged 21 to 36 years (mean ± standard deviation [SD]: 24.15 ± 3.03 years) participated. AOR was first measured with a Grand Seiko autorefractor, then again with infrared photorefraction and then the accommodative biometric changes were measured to the same stimulus demands with ultrasound biomicroscopy and with A-scan ultrasound as described previously (Ramasubramanian & Glasser, 2014c). The study followed the tenets of Declaration of Helsinki and was performed in accordance with an institutionally approved human subject protocol. Subjects were enrolled after passing a screening exam (Ramasubramanian & Glasser, 2014c). Subjects with refractive error were corrected with spherical or toric soft contact lenses.

Grand Seiko Autorefractor

Baseline refraction and static AOR were measured using a Grand Seiko (GS) autorefractor (WR-5100 K). The far target was a back illuminated Snellen chart (Precision Vision, La Salle, IL) at 6 meters from the subject. The near target was a custom designed back illuminated letter chart suspended on a calibrated near-point rod attached to the GS. The far and near targets were aligned to ensure on-axis measurements

in both conditions. Measurements were recorded in dim room illumination. Subjects viewed the far or near targets monocularly with the left eye through the GS open field beam splitter with their right eye occluded. Three refraction measurements were made for each stimulus demand from 0 D to 8 D in 1 D steps and the mean ± SD sphere at each stimulus demand was used for analysis.

To calculate the accuracy and noise of the Grand Seiko, trial lenses from -5 D to +2 D in 1 D steps were placed in front of the GS model eye and 10 refraction measurements were taken with the GS with each trial lens. The induced and measured model eye refractions were strongly correlated (Figure 3.1 A). Noise of the GS measurements calculated as the average standard deviations of all refraction measurements with all trial lenses was 0.009 D. Bland-Altman analysis showed a mean difference of +0.072 D (Figure 3.1 B).

Figure 3.1

(A) Comparison of the induced and measured model eye refraction using a Grand Seiko (GS) autorefractor. Standard deviations of GS measurements are small; hence the error bars plotted cannot be seen. (B) Bland-Altman plot shows a mean difference of 0.072 D between induced and measured model eye refraction.

Figure 3.1
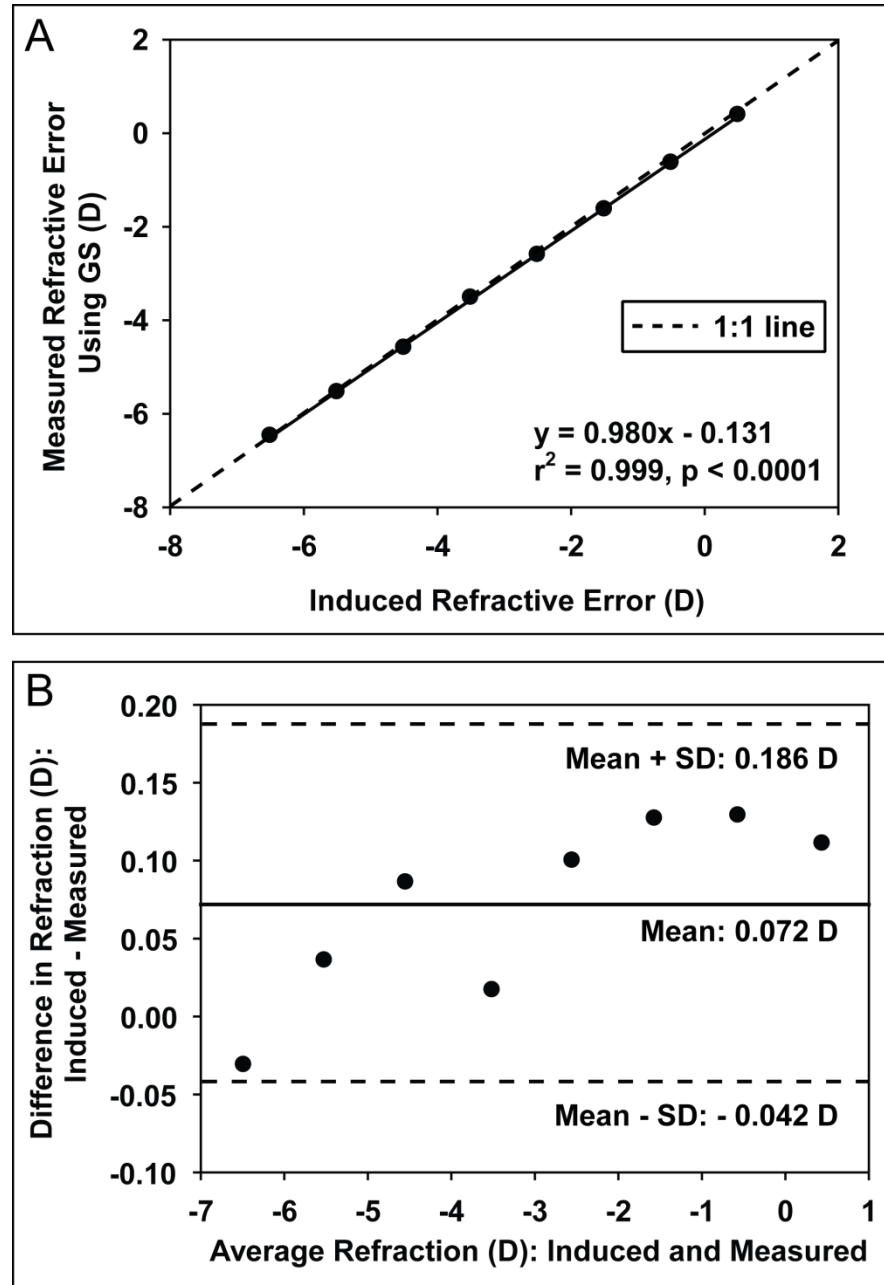
Infra-red Photorefraction

An aluminum frame was constructed (ITEM, Akron, OH) to perform photorefraction and ultrasound biomicroscopy measurements during accommodation on supine subjects as described previously (Ramasubramanian & Glasser, 2014c). The adjustable frame held a mirror (for viewing a far target), a near target, a beam splitter, a photorefractor camera and a hot mirror for the refraction measurements (Figure 3.2 A). The photorefractor camera was positioned at 1 meter from the subjects' eye. The subject lay supine with the head stabilized with a gel head rest and viewed a projected far letter target reflected off a plane mirror inclined at 45° (Figure 3.2 B). A custom designed illuminated near letter target was viewed reflected off a beam splitter. The near target could be moved on a meter stick to change the target vergence. A custom developed photorefractor (inset in Figure 3.2 B) was used to measure refraction of the left eye via a hot mirror (Tabernero & Schaeffel, 2009). All measurements with photorefraction were performed in dim room illumination.

A photorefraction trial lens calibration was performed on each subject at a working distance of 1 meter. Photorefraction video sequences of the left eye were recorded at 30 Hz for 8 seconds for each trial lens (+8 D to 0 D) in 1 D steps using a custom developed Matlab software (Mathworks, Natick, MA). During the trial lens calibration, subjects were asked to fixate on the far target using their right eye and to ignore the blur from the left eye produced by the trial lens.

Figure 3.2

(A) An aluminum frame designed to hold various optical components for the study performed. (B) Experimental setup for infra-red photorefraction on the left eye. (C) An example of a trial lens calibration curve from a single subject. Inset is a Matlab analyzed (colored overlay) photorefraction image. The pixel intensity profiles are extracted along the red and green vertical lines. A circle fit to the pupil edge is shown in yellow. The blue and red crosses represent the positions of pupil center and the first Purkinje image. (D) Calibration function to calculate the pixel-to-mm conversion factor for photorefraction images. Inset shows the images of fixed pupil diameters used for this analysis.

Figure 3.2
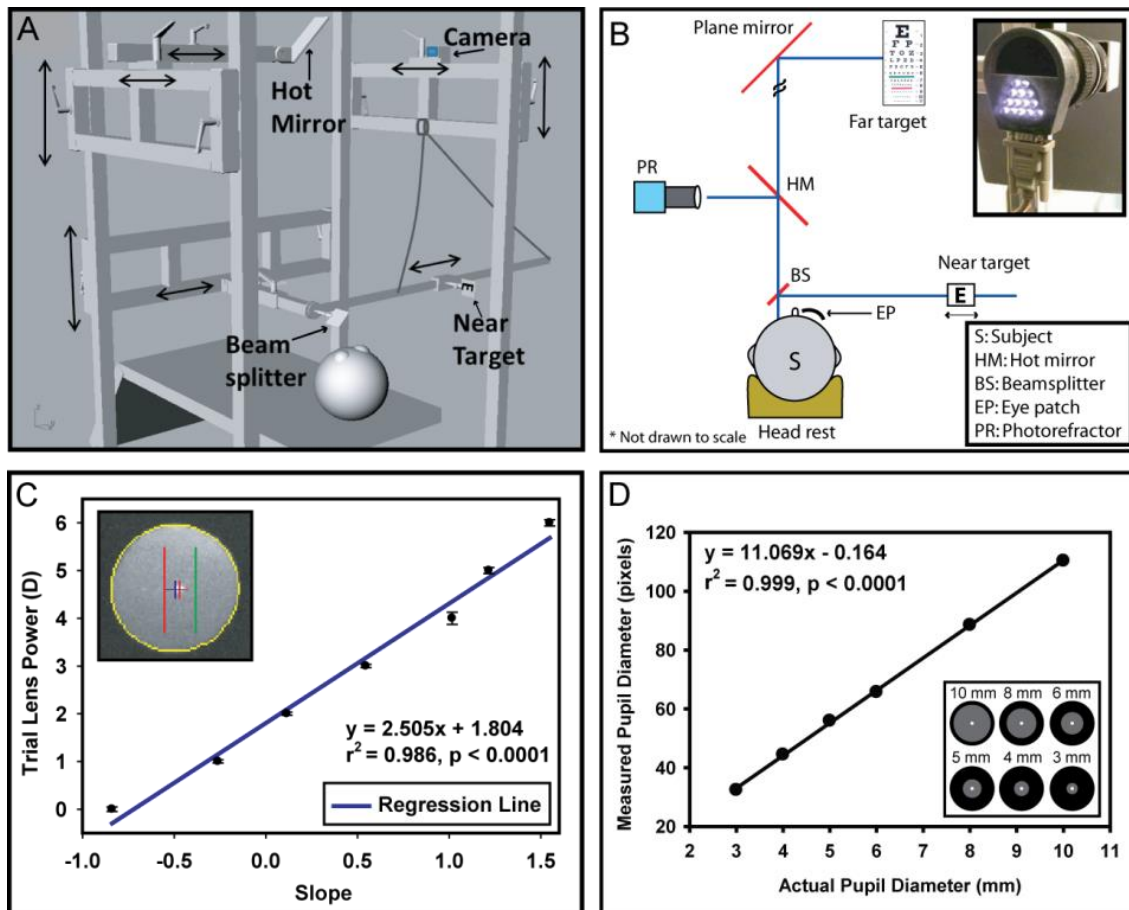
For the photorefraction AOR measurement, the right eye was patched. The far and the near targets were superimposed to ensure on-axis refraction of the left eye. Three, eight-second photorefraction video sequences (each video containing 240 images) were recorded for each stimulus demand from 0 D to +6 D in 1 D steps. All photorefraction videos were analyzed offline using custom developed Matlab software. The software extracts pixel intensity values along the vertical pupil meridian (equal to 75% of the measured pupil diameter) (Figure 3.2 C inset) and computes the slope of the linear regression fit to these intensity values (Schaeffel, Wilhelm, & Zrenner, 1993; Roorda, Campbell, & Bobier, 1997). The mean slope values for each trial lens were plotted against the trial lens power to obtain individual calibration curves (Figure 3.2 C). The calibration curve was fit with a linear regression, 2nd order or a 3rd order polynomial based on the r^2 value and goodness of fit to the data. The best fitting curve was used for the calibrations. The mean slope calculated from the videos during accommodation measurements was converted to refraction using the calibration function and subtracting 1 D to account for the camera working distance (1 meter).

Pupil diameter was measured from the photorefraction images for all stimulus demands. Pixel-to-mm conversion factor for photorefraction images was calculated by imaging a series of printed pupils of known diameter (inset in Figure 3.2 D). The slope of the linear regression equation was the pixel-to-mm conversion (1 mm = 11.069 pixels) factor (Figure 3.2 D). To compute the noise of the photorefraction system, trial lenses ranging from -1 D to +5 D in 1 D steps were placed in front of a Heine ophthalmoscope trainer (Heine USA, Dover, NH) to get a calibration function (not shown) similar to the

trial lens calibration described above. Mean SD of the slope was calculated as the average SD of all slope values from all trial lens powers. From the calibration function, the range of refraction corresponding to 1 SD (a given x-value ± 0.5 × mean SD) of slope was calculated to represent noise of 0.022 D.

After the photorefraction measurements, UBM images of the left eye were captured while the subjects accommodated to a visual target with their right eye (Ramasubramanian & Glasser, 2014c). Accommodative changes in anterior chamber depth (ACD), lens thickness (LT), anterior and posterior lens radii of curvature (ALRC and PLRC) and anterior segment length (ASL) were measured from UBM images using custom developed Matlab software (Ramasubramanian & Glasser, 2014c).

3.3   Results

Mean ± standard deviation (SD) of objectively measured maximum accommodative amplitude using the GS was 5.86 ± 0.42 D (range: 4.93 D to 7.10 D). Data from a single subject shows a linear and reproducible stimulus-response function (Figure 3.3 A). Photorefraction measured stimulus-response functions from this subject plateaued at higher stimulus demands and had larger standard deviations than the GS (Figure 3.3 B).

Figure 3.3

(A) Grand Seiko (GS) accommodative stimulus-response function from one subject from three separate trials. (B) Photorefraction (PR) accommodative stimulus-response function from the same subject for the three separate trials. Each trial represents measurements made on a separate day. Error bars represent ± 1 standard deviation from three measurements.

Figure 3.3
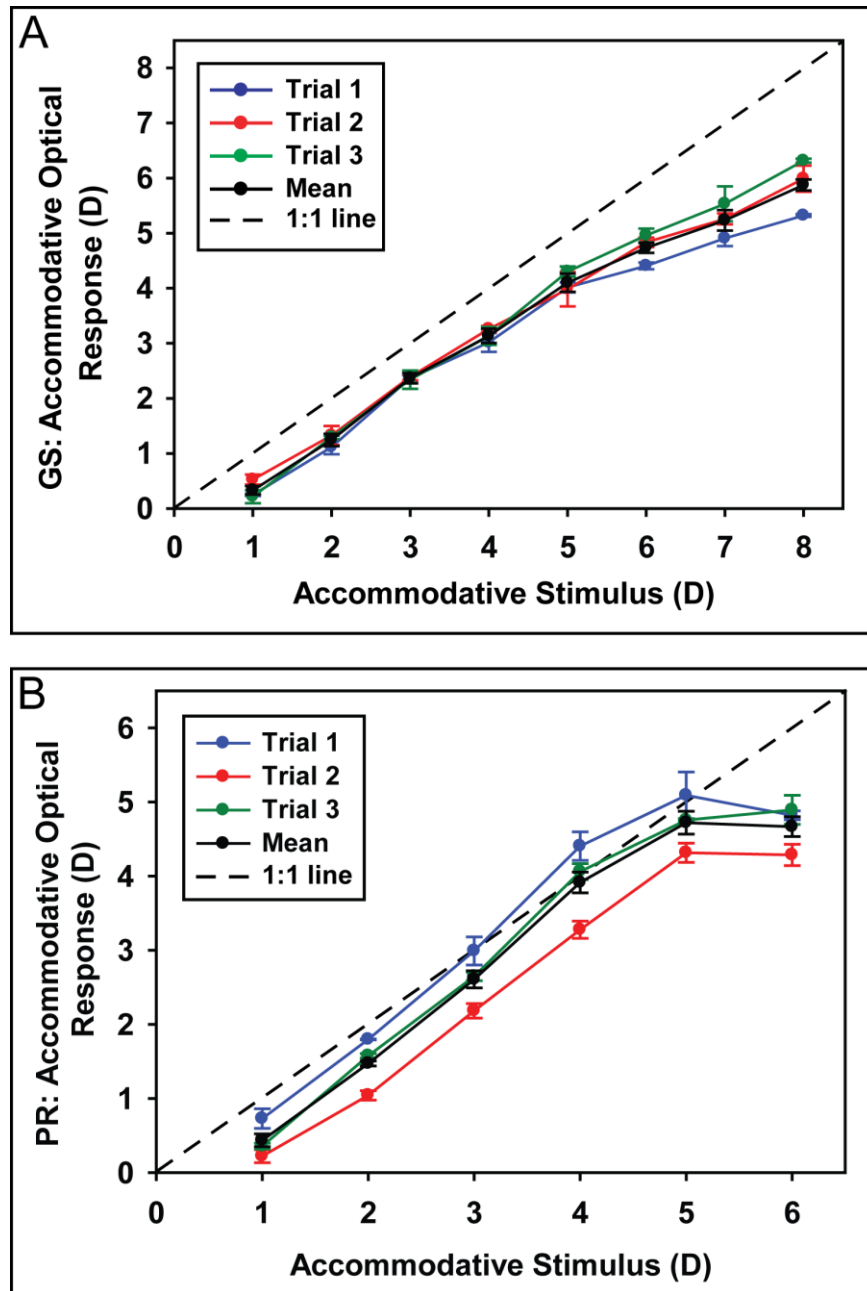
The population plots of GS and photorefraction measured AOR showed a non-linear relationship and saturation of photorefraction at higher stimulus demands (Figure 3.4 A and Figure 3.4 B). One subject had impossibly high photorefraction measured AOR due to smaller pupil diameters (around 3 mm) and darker pupil luminance, so the data from that subject was excluded. Analysis of the data for all subjects showed linear stimulus-response functions with the GS but slopes greater than 1.0 for photorefraction in some subjects. As a consequence of the discrepancy between the GS and photorefraction, the GS measured AOR was used for all subsequent analyses. Pupil diameter decreased as a function of AOR measured with the GS (-0.487 mm/D) and photorefraction (-0.393 mm/D), respectively (Figure 3.4 C and Figure 3.4 D).

Figure 3.4

(A) Comparison of accommodative optical responses (AOR) measured with Grand Seiko (GS) and photorefraction (PR) from all subjects. (B) Bland-Altman comparison between GS and PR measured AOR with PR overestimating the GS measured AOR at higher stimulus demands. Comparison of PR measured pupil diameter as a function of GS measured AOR (C) and PR measured AOR (D).

Figure 3.4
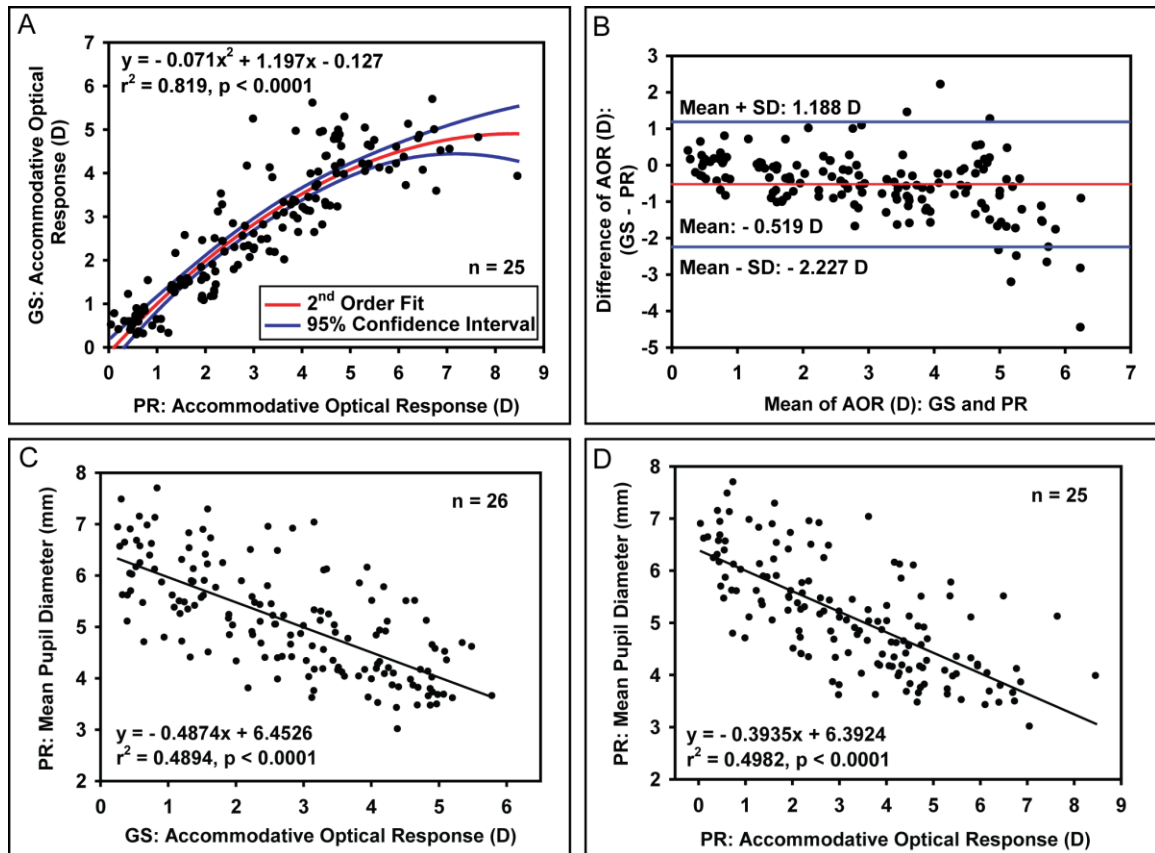
UBM measured accommodative biometric changes as a function of GS measured AOR for each subject were fitted with linear regressions. Only data from subjects with statistically significant linear relationships were included in the population plots. The number of subjects with statistically significant linear relationships between AOR and UBM measured biometry were ACD (n = 25), LT (n = 26), ALRC (n = 26), PLRC (n = 25), and ASL (n = 14). All the population plots for the five biometry parameters (ACD, LT, ALRC, PLRC and ASL) had statistically significant linear correlations ($p < 0.0001$) (Figure 3.5). The mm/per-diopter slopes were ACD: -0.055 mm/D, LT: +0.076 mm/D, ALRC: -0.854 mm/D, PLRC: -0.222 mm/D and ASL: +0.030 mm/D.

Figure 3.5

UBM measured ocular accommodative biometric changes as a function of Grand Seiko (GS) measured accommodative optical response (AOR). With accommodation, (A) anterior chamber depth decreases, (B) lens thickness increases, (C) anterior lens radius of curvature decreases, (D) posterior lens radius of curvature decreases, (E) posterior lens surface moves posteriorly. Each data point represents an average of all trials from each subject. 95% confidence intervals for the regression lines are shown. (F) Anterior (filled circles) and posterior (open circles) lens surface movement as a function of AOR ($p < 0.0001$).

Figure 3.5
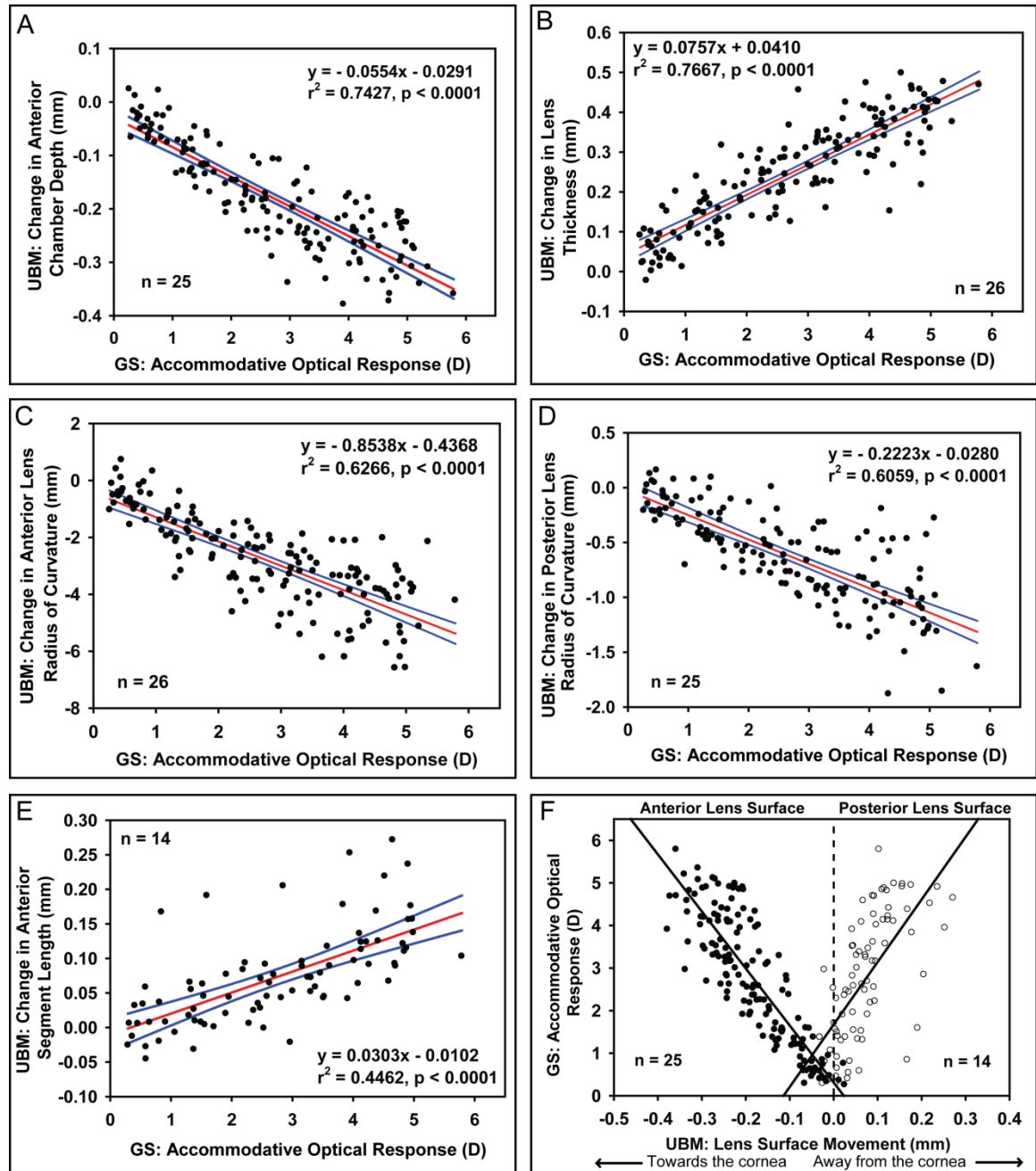
With accommodation, the anterior lens surface moves anteriorly linearly and the posterior lens surface moves posteriorly linearly ($p < 0.0001$) (Figure 3.5 F). The anterior and posterior lens surface movements contribute 63% and 37% of the change in lens thickness, on average respectively.

Accommodative optical response was predicted from each of the UBM measured anterior segment biometry parameters for the population and for individual subjects using three methods; i) directly from the linear regression lines, ii) using the 95% confidence intervals and iii) using the 95% prediction intervals. The axes of each graph in Figure 3.5 were flipped so that biometry became the independent variable on the horizontal axis and AOR the dependent or predicted variable on the vertical axis such as shown for ACD in Figure 3.6 A. Standard deviation of each of the UBM measured biometry parameters for the young subject population was calculated from 50 UBM images for each subject for each stimulus demand. None of the measured parameter SD's showed statistically significant relationships with stimulus demand in any individual subject, therefore, mean SD was calculated by taking the average SD of measured biometry parameters for all stimulus demands, for all trials, from all subjects. Mean SD's of UBM measured parameters were: ACD: 17.6 μm, LT: 29.4 μm, ALRC: 335 μm, PLRC: 158 μm, ASL: 34 μm as reported previously (Ramasubramanian & Glasser, 2014c).

From the linear regressions, the range of y-values (AOR) corresponding to 1 SD (a given x-value ± 0.5 × mean SD) of each UBM measured biometry parameter (for example, ACD) was calculated.

To predict the AOR from the 95% confidence interval, the equations of the upper and lower confidence intervals were computed. Because the 95% confidence interval lines separate towards the extremes, the range of AOR was calculated as the mean difference between the y-values from the upper and lower 95% confidence interval equations for all corresponding x-values. Matlab code was written to run a loop from the minimum to the maximum x-value in fixed steps (ACD, LT, ASL: 0.0001 mm; ALRC, PLRC: 0.001 mm) to calculate the range of AOR for each x-value. Smaller step sizes were used for the ALRC and PLRC because the range of x-values was about 10 times larger than for the other biometry parameters. Mean, SD, maximum, minimum and median of the range was calculated for each biometry parameter. A similar calculation of the range of AOR was performed using the equations for the 95% prediction intervals. The mean ranges of AOR from all three methods for the population data together with the standard deviations from the GS and photorefraction measurements of AOR are shown in Table 3.1. These standard deviations were calculated as the mean SD of AOR for all stimulus demands, for all trials, from all subjects.

Figure 3.6

The range of accommodative optical response (AOR) for the study population as a whole (A) and for a single individual subject (B). AOR was predicted from the linear regression (red solid line) and from the 95% confidence and prediction intervals (solid blue and green lines) from the biometry measurements. For each value on the horizontal axis, the range of AOR was calculated using the equations for the upper and lower 95% confidence (blue dashed line) and prediction intervals (not shown). Using the linear regression equation, the range of AOR was calculated using the standard deviation of the biometry measurements (red dashed line).

Figure 3.6
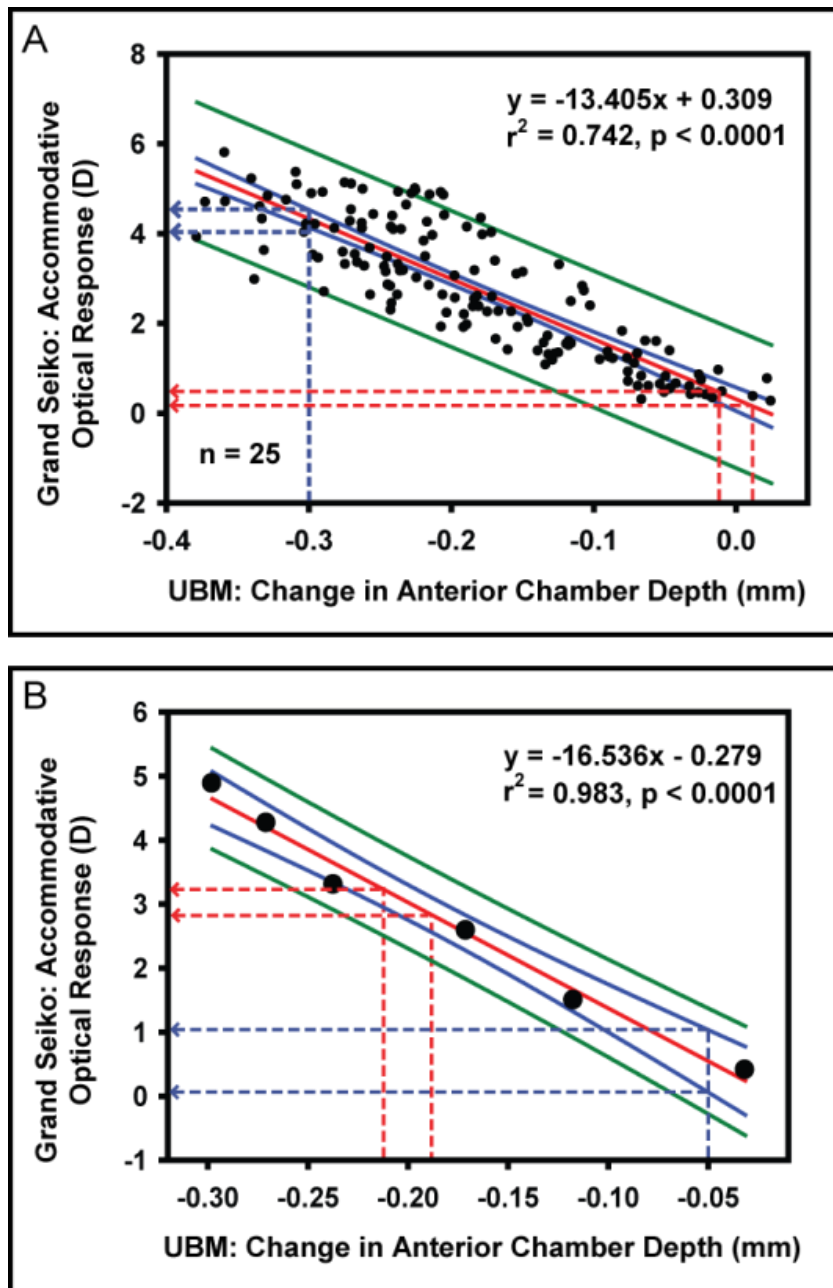
Table 3.1

Standard deviation of predicted accommodative optical response (AOR) from the young subject population as a whole. GS: Grand Seiko, PR: photorefraction, SD: standard deviation, ACD: anterior chamber depth, LT: lens thickness, ALRC: anterior lens radius of curvature, PLRC: posterior lens radius of curvature, ASL: anterior segment length.

Table 3.1

Biometry	Standard deviation of Predicted AOR (D)			GS: SD of AOR
	Linear Regression	95% Confidence Interval	95% Prediction Interval	
ACD (n = 25)	0.24	0.37	3.05	0.14
LT (n = 26)	0.30	0.34	2.89	
ALRC (n = 26)	0.24	0.46	3.66	
PLRC (n = 25)	0.43	0.52	3.77	
ASL (n = 14)	0.50	0.82	4.55	

For individual subjects with significant linear relationships between biometry changes and AOR, the mean SD of each UBM measured biometry parameter from all stimulus demands was calculated. The range of AOR was predicted from each subjects' linear regression line for each measured biometry parameter (Figure 3.6 B). Table 3.2 shows the mean ± SD of the predicted range of AOR from linear regressions from each measured biometry parameter from individual subjects. Root mean square error of AOR (predicted minus measured) was calculated from linear regressions for each subject for all UBM measured biometry parameters. Mean ± SD of RMS error of predicted AOR from each UBM measured biometry parameter was: ACD: 0.41 ± 0.19 D, LT: 0.29 ± 0.12 D, ALRC: 0.36 ± 0.15 D, PLRC: 0.40 ± 0.20 D and ASL: 0.55 ± 0.20 D. Mean ± SD of the mean range of predicted AOR from the 95% confidence and 95% prediction intervals from each subject for all UBM measured biometry parameters are shown in Table 3.2.

Linear regression equations used to calculate AOR independently from each of the UBM measured biometry parameters for the young subject population are shown in Table 3.3. AOR was calculated for each biometry parameter for each subject using the linear regression equations and the differences between the calculated and measured AOR is shown in Table 3.3.

Table 3.2

Mean ± standard deviation (SD) of the standard deviation of predicted accommodative optical response (AOR) from individual subjects. ACD: anterior chamber depth, LT: lens thickness, ALRC: anterior lens radius of curvature, PLRC: posterior lens radius of curvature, ASL: anterior segment length.

Table 3.2

Biometry	Standard deviation of Predicted AOR (D): Mean ± SD		
	Linear Regression	95% Confidence Interval	95% Prediction Interval
ACD (n = 25)	0.29 ± 0.05	1.51 ± 0.75	3.20 ± 1.54
LT (n = 26)	0.36 ± 0.10	1.06 ± 0.46	2.25 ± 0.94
ALRC (n = 26)	0.37 ± 0.11	1.34 ± 0.58	2.85 ± 1.19
PLRC (n = 25)	0.79 ± 0.49	1.45 ± 0.74	3.12 ± 1.57
ASL (n = 14)	1.04 ± 0.43	2.15 ± 0.95	4.40 ± 1.77

Table 3.3

Accommodative optical response (AOR) predictions using linear regression equations from biometry. Δ: accommodative change in, ACD: anterior chamber depth, LT: lens thickness, ALRC: anterior lens radius of curvature, PLRC: posterior lens radius of curvature, ASL: anterior segment length, SD: standard deviation.

Table 3.3

Biometry	Population Linear Regression Equations To Predict AOR from Biometry	Absolute Difference between Measured AOR and Predicted AOR (D)			
		Mean	SD	Minimum	Maximum
ACD	$AOR = -13.405 \times \Delta ACD + 0.309$	0.62	0.44	0.02	1.87
LT	$AOR = +10.121 \times \Delta LT + 0.219$	0.56	0.46	0.00	2.57
ALRC	$AOR = -0.733 \times \Delta ALRC + 0.694$	0.74	0.54	0.00	3.08
PLRC	$AOR = -2.725 \times \Delta PLRC + 0.991$	0.75	0.56	0.01	3.33
ASL	$AOR = +14.678 \times \Delta ASL + 1.675$	0.91	0.65	0.00	3.29

3.4 Discussion

Here, photorefraction overestimated the AOR compared to the GS measurements. This might be due to small pupils (approximately 3 mm) and therefore darker photorefraction reflexes in some subjects while accommodating to higher demands. A small pupil diameter allows only a limited number of pixels to be extracted from the pupil for the slope determination which might account for a greater standard deviation in the refraction measurement. The photorefractor camera used in this study has a linear operating range of ± 6 D. Hence, accommodative optical responses for higher stimulus demands outside this operating range might have inaccuracies and larger standard deviations. The overestimation of AORs might also be due to the differences in the entrance pupil diameters used by these two instruments. The GS measurement is performed through a fixed 2.3 mm aperture regardless of the actual pupil diameter, whereas photorefraction as employed here always used 75% of the available pupil diameter.

Per-diopter of accommodative response changes in biometry from the current study are comparable to values reported in prior human and monkey accommodation studies (Table 3.4). The percentage contribution of posterior lens surface movement to the accommodative increase in lens thickness in this current study is higher than reported from prior human (Ostrin et al., 2006; Bolz et al., 2007) and monkey studies (Vilupuru and Glasser, 2003; Vilupuru and Glasser, 2005). The per-diopter of stimulus amplitude changes in biometry (Table 2.3) are larger than per-diopter of accommodative response

changes (Table 3.4) because, the measured accommodative responses are smaller than the accommodative stimulus amplitudes due to lag of accommodation.

Table 3.4

Comparison of per-diopter of accommodative response changes in anterior segment biometry from prior studies. ACD: anterior chamber depth, LT: lens thickness, ALRC: anterior lens radius of curvature, PLRC: posterior lens radius of curvature, ASL: anterior segment length, UBM: ultrasound biomicroscopy, OCT: optical coherence tomography, MRI: magnetic resonance imaging, PCI: partial coherence interferometry, CUB: continuous ultrasound biometry, N/A: not available.

Table 3.4

Study	Subjects	Method Used To Measure Biometry	Per-diopter Changes in Biometry (mm/D)				
			ACD	LT	ALRC	PLRC	ASL
Current study	Human	UBM	-0.055	+0.076	-0.853	-0.222	+0.030
(Richdale et al., 2013)	Human	OCT	N/A	+0.064	N/A	N/A	N/A
(Sheppard et al., 2011)	Human	3D MRI	N/A	+0.080	-0.630	-0.150	N/A
(Hermans, Pouwels, Dubbelman et al., 2009)	Human	3D MRI	N/A	+0.061	-0.510	-0.140	N/A
(Bolz et al., 2007)	Human	PCI	-0.057	+0.072	N/A	N/A	+0.025
(Ostrin et al., 2006)	Human	A-scan	-0.051	+0.067	N/A	N/A	+0.017
(Vilupuru and Glasser, 2005)	Monkey	CUB	-0.046	+0.063	N/A	N/A	+0.017

The primary goal of this study was to determine how accurately the AOR can be predicted in a population from UBM biometry measurements. Prior accommodation studies have reported linear correlations between refraction and biometry (Bolz et al., 2007; Vilupuru and Glasser, 2005; Ostrin et al., 2006), but have not attempted to predict the AOR from the measured biometry. In the current study, the linear regression method used the SD of the biometry measurements to predict the corresponding range of AOR. The range of the predicted AOR is smaller when the slope of the regression line is flatter and/or the mean SD of biometry is smaller. Using the 95% confidence interval to estimate the range of AOR takes account of the variability in the subject population. When the spread in the population data is smaller, the confidence interval is smaller and so the predicted range of AOR becomes smaller. The 95% prediction interval is wider than the confidence interval since it predicts 95% of the position of future data if the measurements were to be repeated. Accommodative optical response predictions from averaging the data from individual subjects (Table 3.2) are slightly worse than predictions from the population as a whole (Table 3.1) for all UBM measured biometry parameters. This might be due to the relatively stronger influence of a small number of data points on the slopes of the linear regressions in individual subjects and on the width of the 95% confidence and prediction intervals in individual subjects compared to the population plots.

Here, AOR was predicted independently from each UBM measured biometry parameter. An effort to predict the AOR using a multiple linear regression model fails because the strong linear correlations among all the UBM measured accommodative

biometry parameters (Ramasubramanian & Glasser, 2014c) causes the multiple linear regression model to be unstable and therefore unsuitable to use.

Here, the AOR and biometric changes were not measured simultaneously. Hence, subjects could have accommodated to different degrees during sequential optical and biometric measurements. The consequence of this is that the linear relationship between AOR and biometry might not be as strongly correlated as they actually are. Also, UBM has limited axial resolution which might have contributed to increased standard deviation of biometry measurements. Factors affecting the standard deviation of UBM measurements (Ramasubramanian & Glasser, 2014c) in turn affect the AOR predictions. Simultaneous measurements of AOR and biometric changes using higher resolution imaging techniques such as anterior segment OCT might offer better predictions.

Based on the current study, if accommodative changes in anterior segment biometry were measured, the linear regression equations provided (Table 3.3) could be used to calculate AOR in a young phakic subject population. On average, prediction errors from the linear regressions are less than 1 D for all biometry parameters with LT being the best predictor. However, when predicting the AOR in this way, errors might occur due to the differences between the individual subjects' AOR and biometric response with that of the population. In the current study, although only data from subjects who had statistically significant linear relationship between optical and biometric changes were used for AOR prediction, almost all of the subjects had statistically

significant linear relationship for all UBM measured biometry parameters except ASL. Hence, it would be better to use ACD, LT, ALRC or PLRC for AOR predictions and to not use ASL.

Predicting the AOR could be useful in instances where accommodative optical measurements may prove difficult or impossible due to the inability of an autorefractor or an aberrometer to measure a pseudophakic eye, for example because of spurious light reflections from the IOL and/or miotic pupils (Glasser, 2008; Win-Hall & Glasser, 2009). Further investigation is required to test the validity of this prediction in pre-presbyopic subjects with lower accommodative amplitudes. Application of this method may be important for evaluating accommodative ability in patients with accommodative IOLs where evaluating and understanding the accommodative movements of IOLs may be as important as measuring the AOR of the eye. However, the relationships between biometric movements and AOR in pseudophakic eyes would likely be very different from the relationships shown here in young phakic eyes. Therefore, the relationships in eyes with specific types of IOLs would first have to be established for the predictions to be made.

Chapter 4 - Prediction of Accommodative Optical Response in Pre-presbyopes using Ultrasound Biomicroscopy

4.1   Introduction

The ability to accommodate decreases progressively with age and is completely lost around 50 years resulting in the condition called presbyopia. Corrective options for presbyopia such as bifocals, progressive addition lenses, monovision, multifocal contact lenses and multifocal intraocular lenses provide functional far and near vision. However, these corrections do not provide the true, dynamic, continuous range of focusing ability present in young eyes. There is considerable interest in restoring accommodation to the presbyopic eye (Sheppard et al., 2010; Glasser, 2008; Dick, 2005). Prior studies demonstrate that presbyopia is due to age-related stiffening of the lens (Glasser and Campbell, 1999; Heys, Cram, & Truscott, 2004) and that the ciliary muscle continues to contract in the presbyopic eye (He, Donnelly, III, Stevenson et al., 2010). Attempts have been made to utilize the functional ciliary muscle activity to increase the optical power of the eye by producing forward shift of an intraocular lens (IOL) (Dick & Dell, 2006), increasing the separation of dual optic IOLs (McLeod, Vargas, Portney et al., 2007; Ossma, Galvis, Vargas et al., 2007) or by increasing the curvature of the IOL surfaces (Nichamin & Scholl, 2008). However, so far, these strategies have not reliably restored accommodation in presbyopic patients.

To establish if accommodation has been restored to the presbyopic eye, it is essential to employ objective methods that provide a true measure of the accommodative ability of an eye. Clinically, accommodation is either measured as an optical change in power of the eye or as biometric changes in the ocular anterior segment. Although commercially available autorefractors and aberrometers provide objective measurement of the accommodative optical changes in an eye, they do not allow for visualization and quantification of the anterior segment biometric changes that produce the optical change (Win-Hall et al., 2010). Visualizing and measuring accommodative biometric changes using imaging methods such as UBM or OCT enables the accommodative mechanism to be evaluated, but this does not provide a quantitative measure of the ocular refractive changes. It is important to measure both the accommodative optical and biometric changes to fully evaluate the accommodative ability of an eye or of an accommodation restoration concept *in vivo*. Currently, it is not possible to objectively measure the accommodative optical and biometric changes with a single clinical instrument. Prior studies have reported that the accommodative optical and biometric changes are linearly related (Ramasubramanian & Glasser, 2014a; Kasthurirangan et al., 2011; Atchison, Markwell, Kasthurirangan et al., 2008; Bolz et al., 2007). Using these linear relationships, a prior study in young human subjects showed that the accommodative optical response (AOR) could be predicted from ultrasound biomicroscopy (UBM) measured anterior segment biometry parameters with an error of less than 0.50 D (Ramasubramanian & Glasser, 2014a). This means that UBM can be used to visualize and quantify the accommodative changes in ocular anterior segment and to predict the AOR in young phakic individuals with high accommodative amplitudes.

126

It is of interest to know if objective UBM measurements could be used to estimate the AOR in accommodation restoration concepts. However, before attempting to use UBM on accommodation restoration concepts, it is important to first establish if UBM can estimate AOR in older phakic eyes within clinically acceptable limits of variance. Since older phakic eyes have lower accommodative amplitudes than young subjects and UBM has relatively low axial resolution, it is important to first establish the accuracy of UBM in measuring accommodative biometric changes in older phakic eyes and to then estimate the AOR from the measured biometry. While a prior study has done this in young subjects (Ramasubramanian & Glasser, 2014a), pre-presbyopic subjects are a more appropriate study population because they have lower accommodative amplitudes, they are closer representative subjects to presbyopes in terms of age and ocular health and they form part of the target patient population for accommodation restoration concepts.

The goal of this study is to establish the accuracy of UBM to objectively measure accommodative biometric changes and estimate the AOR from the measured biometric changes in phakic pre-presbyopic subjects with low accommodative amplitudes.

127

4.2   Methods

Subjects

Twenty five subjects (8 males and 17 females), aged 36 to 46 years (mean ± standard deviation (SD): 40.80 ± 3.08 years) participated. The study followed the tenets of the Declaration of Helsinki and was performed in accordance with an institutionally approved human subject protocol. Subjects were enrolled after passing a screening exam (Ramasubramanian & Glasser, 2014c). Subjects with less than 1 D of objectively measured accommodative amplitude were excluded. Refractive errors were corrected with spherical or toric soft contact lenses.

Grand Seiko Autorefractor

A Grand Seiko (GS) autorefractor (WR-5100 K) was used to perform objective measurement of the static accommodative optical response (AOR) as described previously (Ramasubramanian & Glasser, 2014a). Briefly, subjects viewed the illuminated near target monocularly with their left eye, with their right eye occluded. Plus 1 D was added to the subject's contact lens correction to facilitate near working distances. Emmetropic subjects wore a +1 D soft contact lens. Three refraction measurements were made for each stimulus demand from 0 D to 2 D in 0.25 D steps, 2 D to 4 D in 0.50 D steps and 4 D to 6 D in 1 D steps (a total of 15 stimulus demands). High

enough stimulus demands were used to ensure that the stimulus-response curve plateaued and the maximum accommodative response was measured. Measurements were recorded in dim room illumination to maintain pupil diameters as large as possible. The stimulus demand that achieved a subject's maximal objectively measured AOR was recorded and this served as the maximum demand to be presented for that subject for all subsequent procedures. Mean ± SD of the sphere component of the refraction measurements for all stimulus demands were used for the analysis. The WR-5100K did not have the ability to measure pupil diameters.

Infra-red Photorefraction

Accommodative optical response and pupil diameter was measured in the left eye with a custom built photorefraction system as described previously (Ramasubramanian & Glasser, 2014a). Plus 1 D was added to the subject's contact lens correction to facilitate near working distances. The far and the near targets were aligned to ensure on-axis measurements. A photorefraction trial lens calibration was performed prior to accommodation measurements (Ramasubramanian & Glasser, 2014a). Three eight-second photorefraction video sequences (each video containing 240 images) were recorded as the subjects accommodated to each stimulus demand from 0 D to the maximal demand determined previously, with the right eye occluded. Photorefraction videos were analyzed offline using custom Matlab (MathWorks, Natick, MA) automated image analysis software (Ramasubramanian & Glasser, 2014a).

Ultrasound Biomicroscopy

Accommodative anterior segment biometry changes were imaged using a 35 MHz UBM (VuMax, Sonomed-Escalon, Lake Success, NY) as described previously (Ramasubramanian & Glasser, 2014c). Briefly, the subject lay supine with their head stabilized with a gel head rest. Prior to imaging, contact lenses were removed from the left eye. Two drops of 0.5% proparacaine (Eye Caine, Bausch & Lomb, Tampa, FL) were instilled in the left eye and a scleral eye cup was inserted under the eyelids and filled with warmed saline solution (BSS, Alcon, Fort Worth, TX). All UBM imaging was performed in dim room illumination. Three sequences each of 50 well aligned UBM images of the left eye were captured over 8 seconds using a 35 MHz transducer, as the subjects accommodated to each stimulus demand from 0 D to the maximal stimulus demand determined previously. All scans were captured along the horizontal meridian (3-9 o'clock). UBM images were analyzed offline using custom automated Matlab image analysis software and were corrected for spatial distortion (Ramasubramanian & Glasser, 2014c). Anterior chamber depth (ACD), lens thickness (LT), corneal thickness (CT), anterior and posterior lens radius of curvature (ALRC and PLRC) and anterior segment length (ASL = CT + ACD + LT) were measured from UBM images.

A-scan Ultrasound

Axial accommodative biometric changes were measured in 24 of the 25 subjects using A-scan ultrasound (A-5500; Sonomed, Lake Success, NY) as described previously (Ramasubramanian & Glasser, 2014c). One subject declined to have A-scan measurements recorded. Five A-scan measurements each were recorded by touching the transducer to the cornea while subjects were accommodating to stimulus demands from 0 D to the maximal stimulus demand determined previously. Accommodative changes in ACD, LT, vitreous chamber depth (VCD) and axial length (AL) were measured.

Data Analysis

Data from each procedure were stored in Matlab arrays and saved as Matlab '.mat' files for data analysis. All UBM and A-scan measured biometric parameters were corrected for appropriate sound velocities (Ramasubramanian & Glasser, 2014c). Accommodative optical and biometric changes from the pre-presbyopic subjects in the current study were plotted with data from a prior study in young subjects (Ramasubramanian & Glasser, 2014a; Ramasubramanian & Glasser, 2014c) for comparison. To calculate repeatability (intra- and inter-session), three subjects had two repeats of the experiment at least 5 days apart. Repeatability of UBM measured parameters were calculated as previously described (Ramasubramanian & Glasser, 2014c). Other anterior segment parameters such as angle-to-angle distance, left and right

anterior chamber angles were measured from UBM images; however, these parameters are not discussed further since they did not change significantly with accommodation.

4.3   Results

Of the twenty five subjects, 13 had myopia and 3 had hyperopia with refractive errors ranging from -6 D to +0.50 D (mean ± SD, -1.40 ± 1.98 D). Mean ± SD of objectively measured accommodative amplitude using the GS was 2.56 ± 1.01 D (range: 1 D to 4.56 D). Representative data from two repeated trials in one subject are shown in Figure 4.1. Accommodative stimulus response functions recorded with GS and PR were both repeatable, but dissimilar from each other with photorefraction tending to plateau in 24 out of 25 subjects at higher stimulus demands (Figure 4.1 A and Figure 4.1 B). Grand Seiko measured accommodative optical response plotted against sequentially measured UBM biometry in the same subject, showed a decrease in ACD (Figure 4.1 C) and an increase in LT (Figure 4.1 D) with accommodation. The mean curves comparing biometry and GS measured AOR (black lines) for this subject (Figure 4.1 C and Figure 4.1 D) show statistically significant linear relationships [GS AOR vs. ACD: $r^2 = 0.9248$, $p < 0.0001$; GS AOR vs. LT: $r^2 = 0.9180$, $p < 0.0001$] (regression lines not shown), although 2nd order functions were better fits and improved the r^2 values [GS AOR vs. ACD: $r^2 = 0.9871$, $p < 0.0001$; GS AOR vs. LT: $r^2 = 0.9650$, $p < 0.0001$] (also not shown).

Figure 4.1

(A) Grand Seiko (GS) stimulus-response function from a 36 year old subject from two separate trials. (B) Photorefraction (PR) accommodation stimulus-response function from the same subject for the two separate trials. Comparison of UBM measured change in anterior chamber depth (C) and lens thickness (D) as a function of GS measured accommodative optical response from two separate trials from the same subject. Error bars represent $\pm$ 1 standard deviation from three measurements.

Figure 4.1
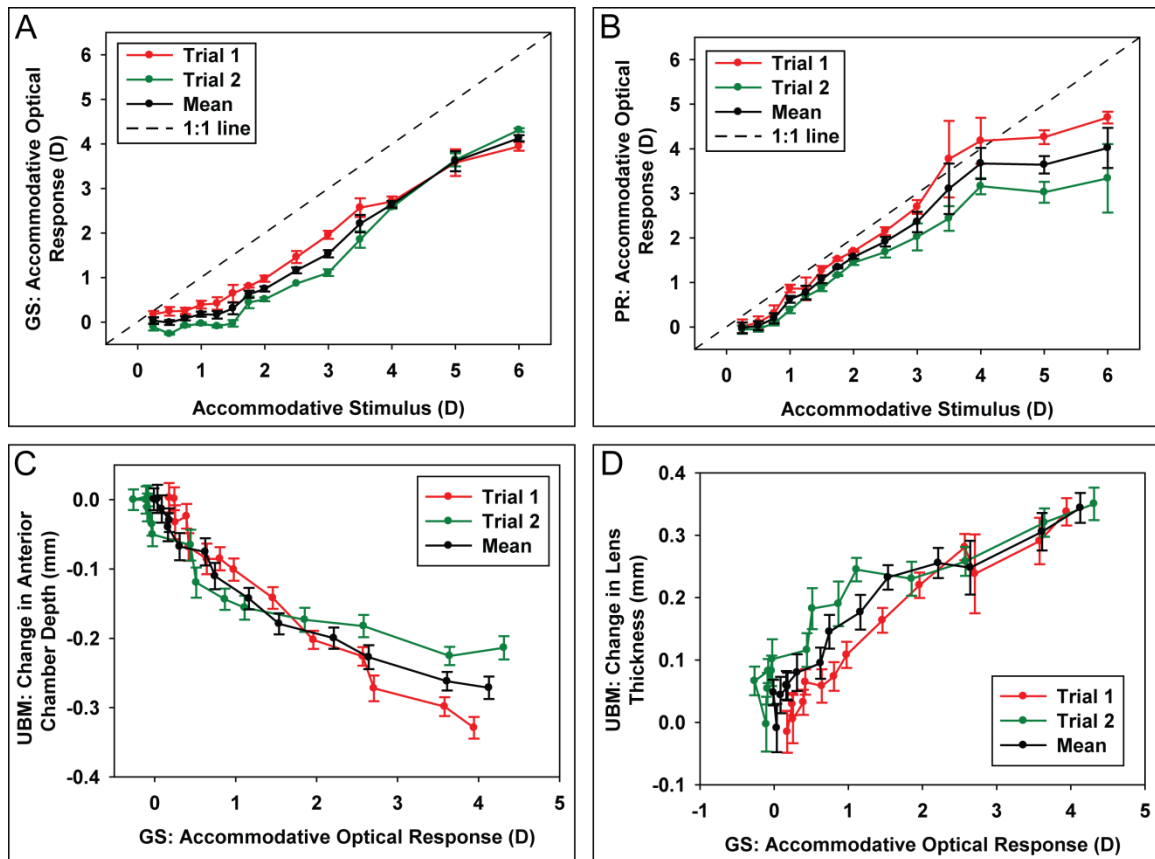
The relationship between the GS and photorefraction measured AOR in all subjects was linear (Figure 4.2 A) although a 2nd order fit to the data marginally improved the r^2 value. In the individual data from each subject, a second order function provided a better fit (as determined by a higher r^2 value) in most of the subjects (22 out of 25). Only one subject did not have a statistically significant relationship between AOR measured with GS and PR (data not shown). A Bland-Altman plot of the data from all subjects shows that photorefraction overestimated the GS measured AOR with a mean difference of -0.30 D and more so at higher stimulus demands (Figure 4.2 B). Due to this difference, the GS measured AOR was used for all subsequent analyses. Photorefraction measurements showed an accommodative decrease in pupil diameter as a function of GS measured AOR in pre-presbyopic (black symbols) and young subjects (blue symbols) (Figure 4.2 C). The per-diopter accommodative decrease in pupil diameter in pre-presbyopic and young subjects was -0.677 mm/D and -0.480 mm/D, respectively.

Figure 4.2

(A) Comparison of the accommodative optical responses (AOR) measured with the Grand Seiko (GS) and photorefraction (PR) from 24 subjects. One subject did not have a statistically significant relationship between GS and PR measured AOR, hence data from this subject is not plotted. (B) Bland-Altman comparison between GS and PR measured AOR. Blue lines represent 95% limits of agreement. (C) Comparison of PR measured accommodative change in pupil diameter as a function of GS measured AOR. Data from young subjects (blue symbols) are plotted for comparison.

Figure 4.2
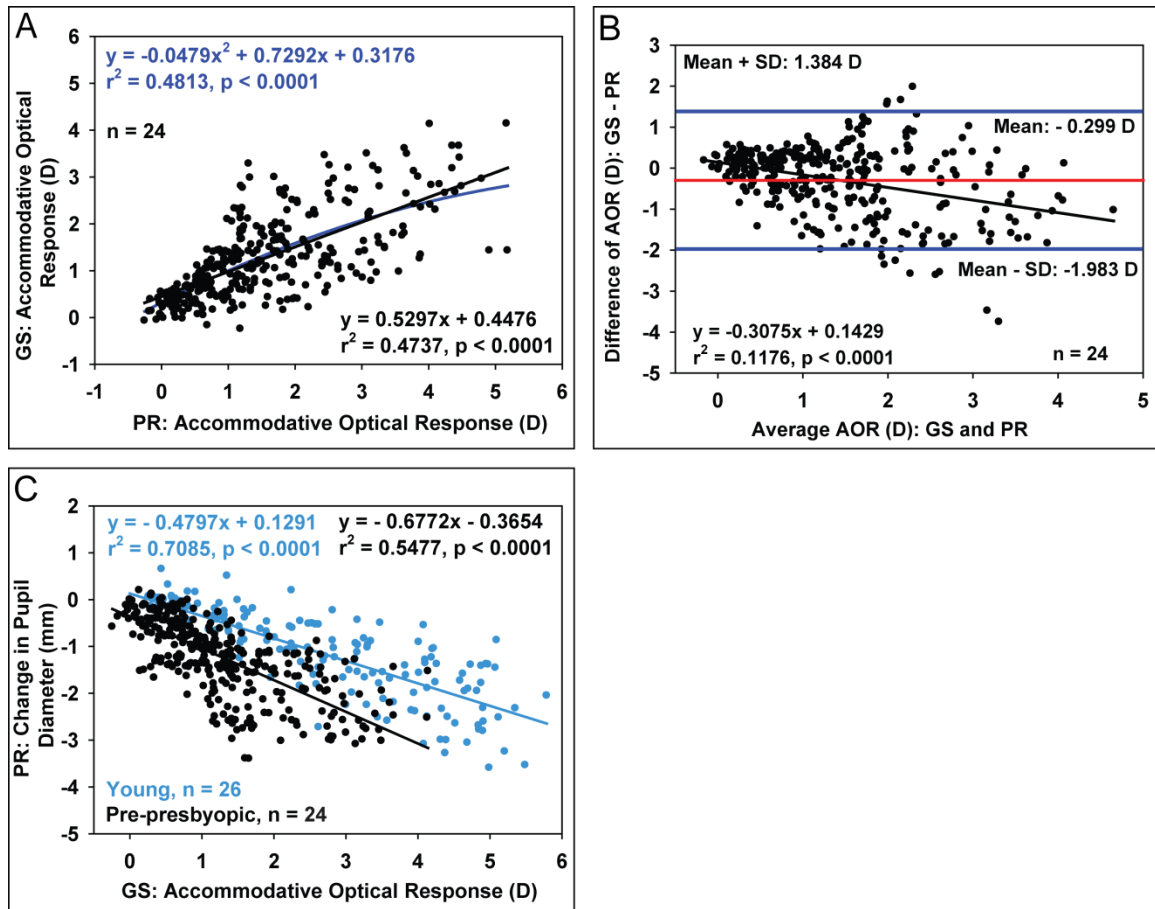
Accommodative changes in each UBM measured biometric parameter as a function of GS measured AOR for each subject were fitted with linear regressions and tested for statistical significance. Only data from individual subjects with statistically significant linear relationships were included in the population plots. The number of subjects with statistically significant linear relationships between AOR and each biometry parameter were ACD (n = 20), LT (n = 24), ALRC (n = 24), PLRC (n = 12), and ASL (n = 9). With accommodation, there was a decrease in ACD, an increase in LT, a decrease in the radii of curvature of the lens surfaces (ALRC and PLRC) and an increase in ASL in both the pre-presbyopic and young subjects (Figure 4.3 A to Figure 4.3 E). All five biometry parameters (ACD, LT, ALRC, PLRC, and ASL) had statistically significant linear correlations with AOR (p < 0.0001). The per-diopter accommodative response changes in biometry (indicated by the slope of the linear regression equations) for pre-presbyopic subjects were ACD: -0.053 mm/D, LT: +0.073 mm/D, ALRC: -0.938 mm/D, PLRC: -0.170 mm/D and ASL: +0.035 mm/D. The per-diopter changes were similar and not significantly different between the pre-presbyopic and the young subject population for all accommodative biometry parameters except for PLRC (t = -2.667, p = 0.011, independent sample t-test).

With accommodation, the anterior lens surface moves anteriorly linearly and the posterior lens surface moves posteriorly linearly in both the younger and older subjects (p < 0.0001) (Figure 4.3 F). The lens geometric center moves anteriorly during accommodation. In this pre-presbyopic population, the anterior and posterior lens surface movement contributed to 63% and 37% change in lens thickness, respectively. The

139

percentage contribution to change in lens thickness was similar between pre-presbyopic and young subjects (Ramasubramanian & Glasser, 2014a). UBM measured biometry parameters were statistically significantly linearly correlated with each other and four of the correlations are shown in Figure 4.4. All of the correlations are shown in Table 4.1.

Figure 4.3

UBM measured ocular accommodative biometric changes as a function of the Grand Seiko (GS) measured accommodative optical response (AOR) showing data from pre-presbyopic (black symbols) and young subjects (blue symbols). With accommodation, (A) anterior chamber depth decreases, (B) lens thickness increases, (C) anterior lens radius of curvature decreases, (D) posterior lens radius of curvature decreases, and (E) anterior segment length increases. (F) Accommodative movements of the anterior and posterior lens surfaces (i.e., changes in ACD and ASL) as a function of AOR in young and pre-presbyopic subjects. Each data point represents an average of all trials from each subject.

Figure 4.3
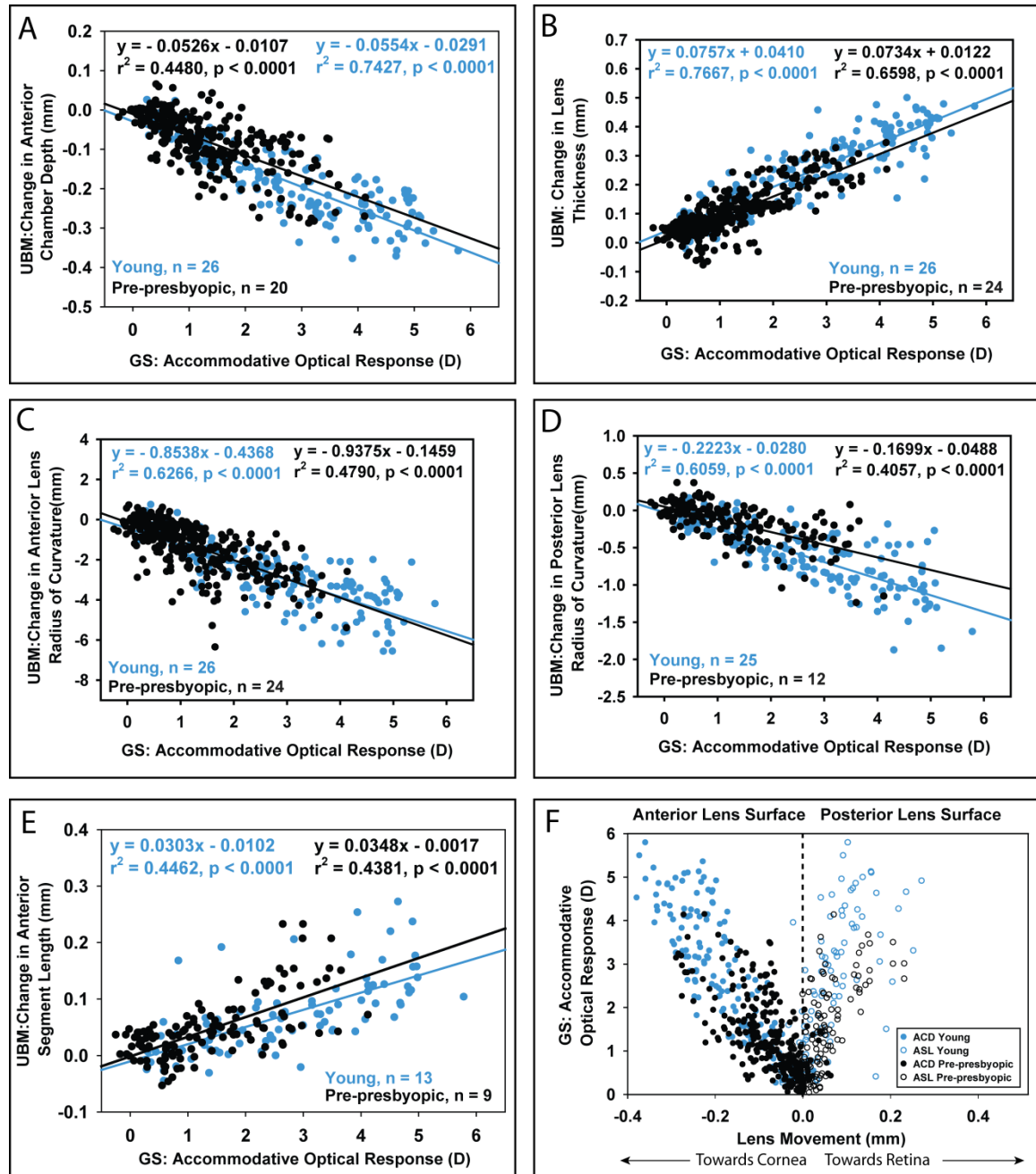
Figure 4.4

Linear relationships of change in (A) anterior chamber depth versus lens thickness (n = 20), (B) anterior lens radius of curvature versus posterior lens radius of curvature (n = 12), (C) anterior lens radius of curvature versus anterior chamber depth (n = 20) and (D) lens thickness versus anterior segment length (n = 9) in the pre-presbyopic subjects. Linear regression parameters for other statistically significant biometry relationships are shown in Table 4.1.

Figure 4.4
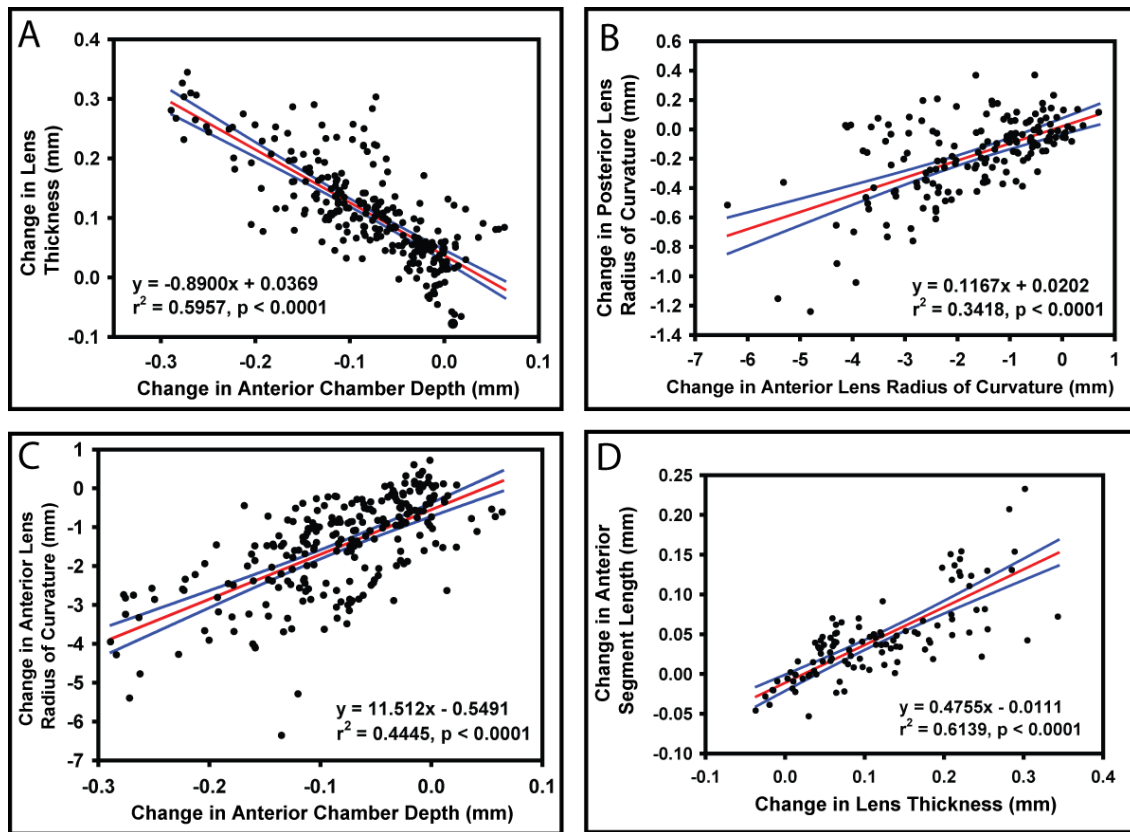
Table 4.1

Linear regression parameters (slope, intercept and r^2 values) for UBM measured anterior segment biometry parameters during accommodation. All regressions shown had statistically significant linear correlations (p < 0.0001, except for ACD vs ASL [p = 0.006] and PLRC vs ASL [p = 0.032]). ACD: anterior chamber depth; LT: lens thickness; ALRC: anterior lens radius of curvature; PLRC: posterior lens radius of curvature; ASL: anterior segment length. **Data plotted in Figure 4.4.

Table 4.1

Change in Biometry		Horizontal Axis			
		ACD	LT	ALRC	PLRC
Vertical Axis	LT	-0.890, 0.036, 0.596**			
	ALRC	11.512, -0.549, 0.444**	-11.30, -0.101, 0.510		
	PLRC	2.740, 0.117, 0.534	-2.074, 0.091, 0.435	0.117, 0.020, 0.342**	
	ASL	-0.2653, 0.024, 0.088	0.475, -0.011, 0.614**	-0.022, 0.019, 0.267	-0.055, 0.039, 0.065

The standard deviations (SD's) of the UBM measured biometry parameters were calculated from 50 UBM images for each subject for each stimulus demand from all trials. None of the measured parameter SD's showed significant relationships with stimulus demand in any individual subject, therefore, mean SD was calculated by taking the average SD of each measured biometry parameter for all stimulus demands, for all trials, from all subjects (Table 4.2). The SD's were similar between the two age groups and are smaller than SD's reported in prior studies (Rosales, Dubbelman, Marcos et al., 2006; Bolz et al., 2007).

Table 4.2

Mean standard deviation (SD) of UBM biometry measurements for the pre-presbyopic (current study) and young subjects (Ramasubramanian & Glasser, 2014a). Data from prior anterior segment biometry studies are shown for comparison. ACD: anterior chamber depth, LT: lens thickness, ALRC: anterior lens radius of curvature, PLRC: posterior lens radius of curvature, ASL: anterior segment length.

Table 4.2

Biometry	Mean SD ± SD		Mean SD from Prior Anterior Segment Biometry Studies
	Pre-presbyopic Subjects (n = 25)	Young Subjects (n = 26)	
ACD (mm)	0.018 ± 0.004	0.017 ± 0.003	0.148 (Bolz et al., 2007)
LT (mm)	0.028 ± 0.009	0.029 ± 0.008	0.224 (Bolz et al., 2007)
ALRC (mm)	0.351 ± 0.194	0.335 ± 0.138	1.100 (Rosales et al., 2006)
PLRC (mm)	0.154 ± 0.031	0.158 ± 0.038	0.550 (Rosales et al., 2006)
ASL (μm)	0.034 ± 0.011	0.034 ± 0.009	0.239 (Bolz et al., 2007)

Intra-session repeatability analysis of the UBM measured parameters (ACD, LT, ALRC, PLRC, ASL and CT) from three video sequences from all pre-presbyopic subjects for the 0 D stimulus demand was performed. Inter-session repeatability analysis was performed for the 0 D stimulus demand from 3 subjects who had two repeats of the experiment. Repeatability (intra- and inter-session) was evaluated in terms of a) coefficient of variation, b) mean standard deviation of the differences between the measurements, c) coefficient of repeatability (CoR), d) CoR (%) and e) intraclass correlation coefficient (ICC) as described previously (Ramasubramanian & Glasser, 2014c). UBM parameters have a better intra-session than inter-session repeatability (Table 4.3) and the repeatability estimates are comparable between the pre-presbyopic and young subjects (Ramasubramanian & Glasser, 2014c).

Table 4.3

Intra-session and inter-session repeatability for various UBM measured parameters. ACD: anterior chamber depth, LT: lens thickness, ALRC: anterior lens radius of curvature, PLRC: posterior lens radius of curvature, ASL: anterior segment length, CT: central corneal thickness, CoV: coefficient of variation, SD: standard deviation, CoR: coefficient of repeatability, ICC: intraclass correlation coefficient.

Table 4.3

Repeatability parameters	Intra-session repeatability (n = 25)						Inter-session repeatability (n = 3)					
	ACD	LT	ALRC	PLRC	ASL	CT	ACD	LT	ALRC	PLRC	ASL	CT
CoV	0.006	0.008	0.030	0.030	0.005	0.022	0.006	0.008	0.031	0.025	0.005	0.024
Mean SD of differences (mm)	0.014	0.018	0.199	0.122	0.025	0.004	0.011	0.102	0.688	0.093	0.089	0.018
CoR	0.028	0.037	0.397	0.243	0.049	0.007	0.022	0.204	1.376	0.186	0.178	0.036
CoR (%)	0.890	0.953	3.585	4.585	0.642	1.304	0.674	5.385	11.227	3.174	2.339	6.966
ICC	0.999	0.998	0.989	0.982	0.996	0.995	0.989	0.900	0.833	0.992	0.973	0.954

Accommodative optical response was predicted from each of the measured anterior segment biometry parameters for individual subjects (Figure 4.5 A) and for the pre-presbyopic population (Figure 4.5 B) using three methods; i) directly from the linear regression lines, ii) using the 95% confidence intervals and iii) using the 95% prediction intervals as described previously (Ramasubramanian & Glasser, 2014a). Standard deviations of predicted AOR were consistently smaller in the pre-presbyopes than in young subjects for predictions using the respective subject populations as a whole (Table 4.4) and from individual subjects (Table 4.5). Root mean square error of AOR was calculated from linear regressions for each pre-presbyopic subject for all UBM measured biometry parameters. Mean ± SD of RMS error of predicted AOR from each UBM measured biometry parameter was: ACD: 0.33 ± 0.22 D, LT: 0.28 ± 0.07 D, ALRC: 0.30 ± 0.14 D, PLRC: 0.53 ± 0.21 D and ASL: 0.56 ± 0.20 D.

Figure 4.5

The range of accommodative optical response (AOR) predicted for a single individual subject (A) and for the study population as a whole (B). AOR was predicted from the linear regression lines (red solid line) and from the 95% confidence and prediction intervals (solid blue and green lines) from the biometry measurements. For each value on the horizontal axis, the range of AOR was calculated using the linear regression line with the mean standard deviation of the UBM measurements (red dashed line), equations for the upper and lower 95% confidence (blue dashed line) and prediction intervals (not shown).

Figure 4.5
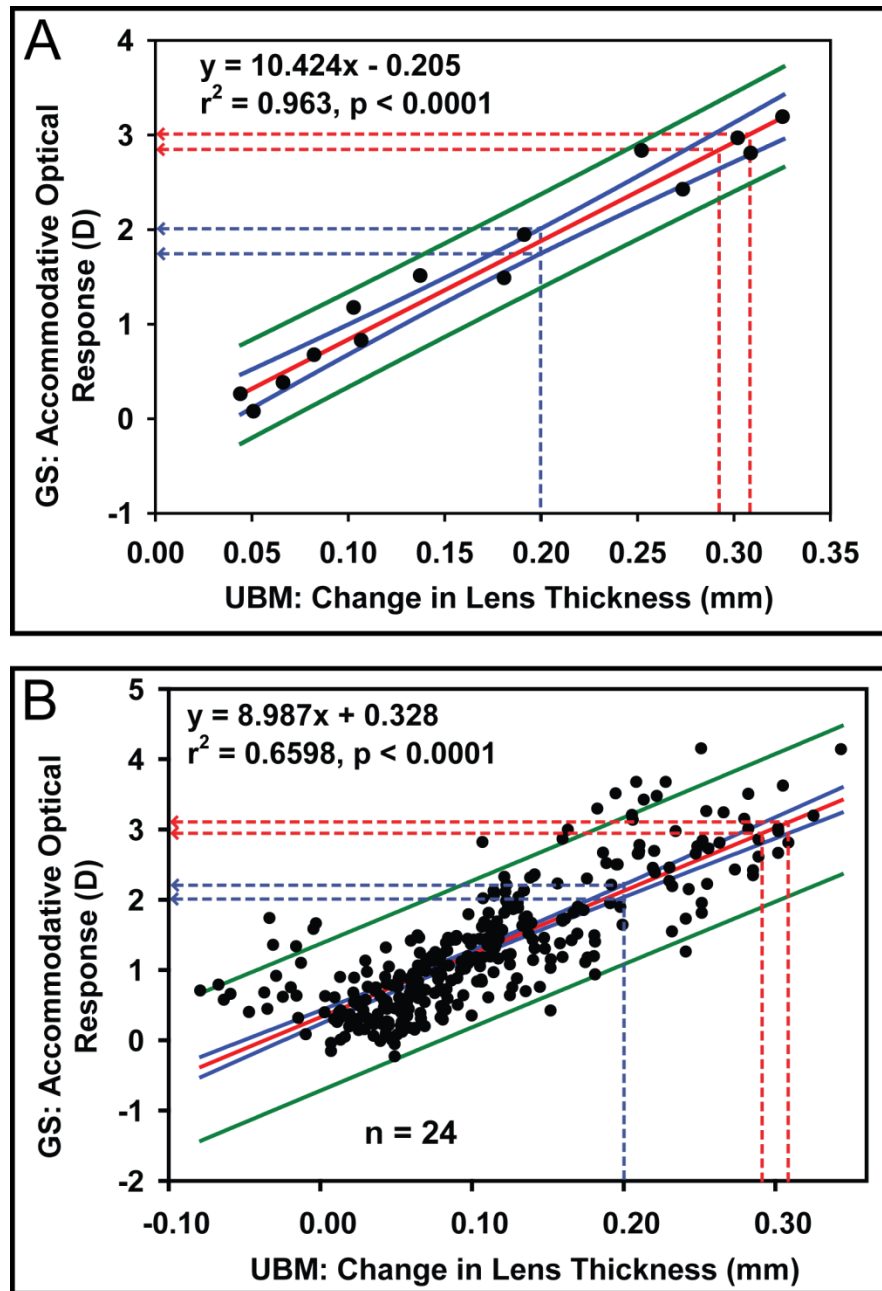
Table 4.4

Standard deviation of predicted accommodative optical response (AOR) from UBM measured biometry parameters using linear regression, the 95% confidence intervals and 95% prediction intervals in pre-presbyopic and young subject (Ramasubramanian & Glasser, 2014a) populations as a whole. ACD: anterior chamber depth, LT: lens thickness, ALRC: anterior lens radius of curvature, PLRC: posterior lens radius of curvature and ASL: anterior segment length.

Table 4.4

Biometry	Standard Deviation of Predicted AOR (D)					
	Pre-presbyopic Subjects			Young Subjects		
	Linear Regression	95% Confidence Interval	95% Prediction Interval	Linear Regression	95% Confidence Interval	95% Prediction Interval
ACD	0.15	0.28	2.68	0.24	0.37	3.05
LT	0.25	0.20	2.09	0.30	0.34	2.89
ALRC	0.09	0.30	2.60	0.24	0.46	3.66
PLRC	0.37	0.50	3.14	0.43	0.52	3.77
ASL	0.42	0.51	3.14	0.50	0.82	4.55

Table 4.5

Mean ± standard deviation (SD) of the standard deviations of predicted accommodative optical response (AOR) from individual subjects in the presbyopic and young populations (Ramasubramanian & Glasser, 2014a). ACD: anterior chamber depth, LT: lens thickness, ALRC: anterior lens radius of curvature, PLRC: posterior lens radius of curvature and ASL: anterior segment length.

Table 4.5

Biometry	Standard Deviation of Predicted AOR (D): Mean ± SD					
	Pre-presbyopic Subjects			Young Subjects		
	Linear Regression	95% Confidence Interval	95% Prediction Interval	Linear Regression	95% Confidence Interval	95% Prediction Interval
ACD	0.25 ± 0.08	0.58 ± 0.38	1.69 ± 1.12	0.29 ± 0.05	1.51 ± 0.75	3.20 ± 1.54
LT	0.32 ± 0.06	0.50 ± 0.13	1.43 ± 0.36	0.36 ± 0.10	1.06 ± 0.46	2.25 ± 0.94
ALRC	0.29 ± 0.15	0.53 ± 0.25	1.53 ± 0.69	0.37 ± 0.11	1.34 ± 0.58	2.85 ± 1.19
PLRC	0.49 ± 0.19	0.94 ± 0.34	2.71 ± 1.04	0.79 ± 0.49	1.45 ± 0.74	3.12 ± 1.57
ASL	0.64 ± 0.30	0.98 ± 0.43	2.77 ± 1.08	1.04 ± 0.43	2.15 ± 0.95	4.40 ± 1.77

Accommodative optical response was calculated independently from each of the UBM measured biometry parameters for each pre-presbyopic subject using the population linear regression equations (Table 4.6). The mean difference between the predicted and measured AOR from all the individual subjects from all stimulus demands is smaller in pre-presbyopes than in young subjects for all biometry parameters, with LT providing the best prediction of AOR in both age groups (Table 4.6).

Table 4.6

Comparison of accommodative optical response (AOR) predictions using linear regression equations from biometry for pre-presbyopic and young subjects. Absolute differences between measured and predicted AOR were calculated from all individual subjects for all stimulus demands. Δ: accommodative change in, ACD: anterior chamber depth, LT: lens thickness, ALRC: anterior lens radius of curvature, PLRC: posterior lens radius of curvature, ASL: anterior segment length, SD: standard deviation.

Table 4.6

Subjects	Biometry	Population Linear Regression Equations To Predict AOR from Biometry	Absolute Difference between Measured AOR and Predicted AOR (D)			
			Mean	**SD**	**Minimum**	**Maximum**
Pre-presbyopic Subjects	ACD	$AOR = -8.524 \times \Delta\,ACD + 0.627$	0.53	0.42	0.01	2.22
	LT	$AOR = +8.987 \times \Delta\,LT + 0.328$	0.41	0.33	0.00	1.70
	ALRC	$AOR = -0.511 \times \Delta\,ALRC + 0.586$	0.50	0.42	0.00	2.22
	PLRC	$AOR = -2.388 \times \Delta\,PLRC + 0.917$	0.62	0.47	0.01	2.75
	ASL	$AOR = +12.571 \times \Delta\,ASL + 0.807$	0.60	0.49	0.00	2.42
Young Subjects	ACD	$AOR = -13.405 \times \Delta\,ACD + 0.309$	0.62	0.44	0.02	1.87
	LT	$AOR = +10.121 \times \Delta\,LT + 0.219$	0.56	0.46	0.00	2.57
	ALRC	$AOR = -0.734 \times \Delta\,ALRC + 0.695$	0.74	0.54	0.00	3.08
	PLRC	$AOR = -2.726 \times \Delta\,PLRC + 0.991$	0.75	0.56	0.01	3.33
	ASL	$AOR = +14.678 \times \Delta\,ASL + 1.675$	0.91	0.65	0.00	3.29

In the pre-presbyopic subjects, there was a statistically significant linear correlation between A-scan and UBM measured ACD and LT measurements (Figure 4.6 A and Figure 4.6 B). Data from subjects who individually had statistically significant linear regressions are plotted. Data circled in red is from a single subject whose measured A-scan values differed markedly from the rest of the population. A-scan underestimated the UBM measured ACD by on average 63 μm and overestimated the UBM measured LT measurements by on average 193 μm as shown in the Bland-Altman plots (Figure 4.6 C and Figure 4.6 D).

Figure 4.6

(A & B) Linear correlation between A-scan ultrasound and ultrasound biomicroscopy (UBM) measured anterior chamber depth (ACD) and lens thickness (LT) respectively. (C & D) Bland-Altman comparison between A-scan ultrasound and UBM measured ACD and LT respectively. Data points circled in red are from a single subject who showed an unusual response. The data from this one subject is not included in the regression calculations/equations. Number of subjects with statistically significant linear fits is denoted by n.

Figure 4.6
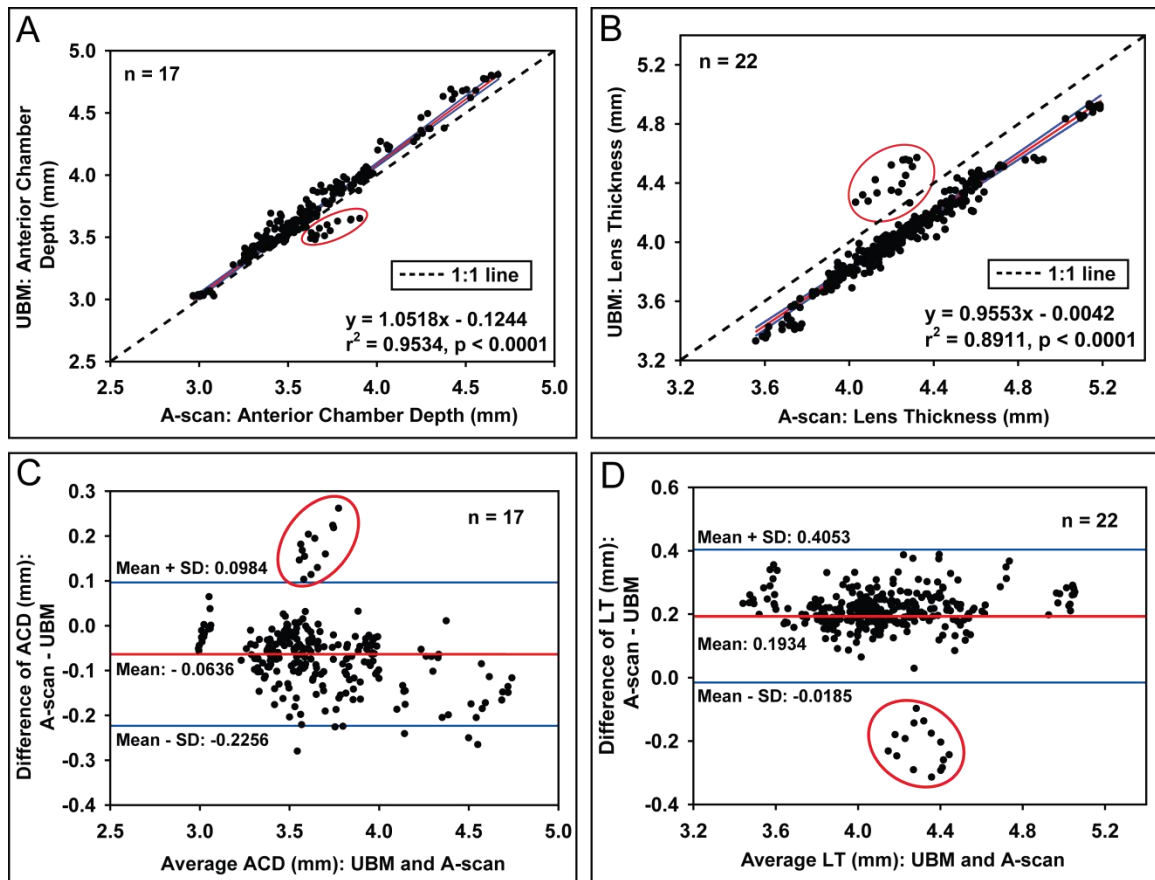
There was no statistically significant relationship between the SD of the A-scan measurements and stimulus demand in any individual pre-presbyopic subject. Therefore, the mean SD of A-scan measurements of ACD and LT were calculated as the average SD of five measurements for all stimulus demands, for all trials, from all subjects. The mean SD of the A-scan measured ACD and LT in the pre-presbyopic subjects were similar to the data from young subjects (Table 4.7). The mean SD of the UBM measurements is consistently smaller than the mean SD from the A-scan measurements in both age groups.

Table 4.7

Mean standard deviations (SD) of anterior chamber depth (ACD) and lens thickness (LT) during accommodation from ultrasound biomicroscopy (UBM) and A-scan ultrasound in pre-presbyopic and young subjects (Ramasubramanian & Glasser, 2014c).

Table 4.7

Biometry	Measured Biometry: Mean SD ± SD (mm)			
	Pre-presbyopic Subjects (n = 24)		Young Subjects (n = 24)	
	UBM	A-scan	UBM	A-scan
ACD	0.018 ± 0.004	0.047 ± 0.026	0.017 ± 0.003	0.041 ± 0.024
LT	0.028 ± 0.009	0.041 ± 0.027	0.029 ± 0.008	0.039 ± 0.022

The amplitudes of accommodation as determined objectively from the young subjects (Ramasubramanian & Glasser, 2014a) and the pre-presbyopes as a function of age were fit with a linear regression and when extrapolated to zero showed a complete loss of accommodation at age 54 years at the rate of -0.19 D/year (Figure 4.7 A). The mean accommodative amplitude was statistically significantly different between the two age groups (t = 13.476, p < 0.0001, independent sample t-test). With age, ACD decreases, LT increases, PLRC decreases and the posterior lens surface occupies more posterior position (Figure 4.7 B to Figure 4.7 F). Age-related changes (mm/year) in the UBM measured biometry parameters from the current study are comparable to values from prior studies (Kasthurirangan, Markwell, Atchison et al., 2008; Dubbelman et al., 2005; Koretz, Cook, & Kaufman, 2001; Koretz et al., 1997) (Table 4.8). There were statistically significant differences between mean LT (t = - 4.834, p < 0.0001), mean ASL (t = - 3.019, p = 0.004), mean PLRC (t = - 2.509, p = 0.016) and mean A-scan LT (t = - 4.339, p < 0.0001) between the two age groups based on independent sample t-test (Table 4.9).

Figure 4.7

(A) Age-related decline in the Grand Seiko measured accommodative amplitude in young (blue symbols) and pre-presbyopic subjects (black symbols). Linear regression lines from prior studies are plotted for comparison. Linear regression line (in green) is the fit to the accommodative amplitude data obtained from Anderson et al for subjects between 36 to 46 years of age. With age, anterior chamber depth decreases (B), lens thickness increases (C & F), anterior segment length increases (D), posterior lens surface radius decreases (E). Red triangles represent the mean values from both the age groups.

Figure 4.7
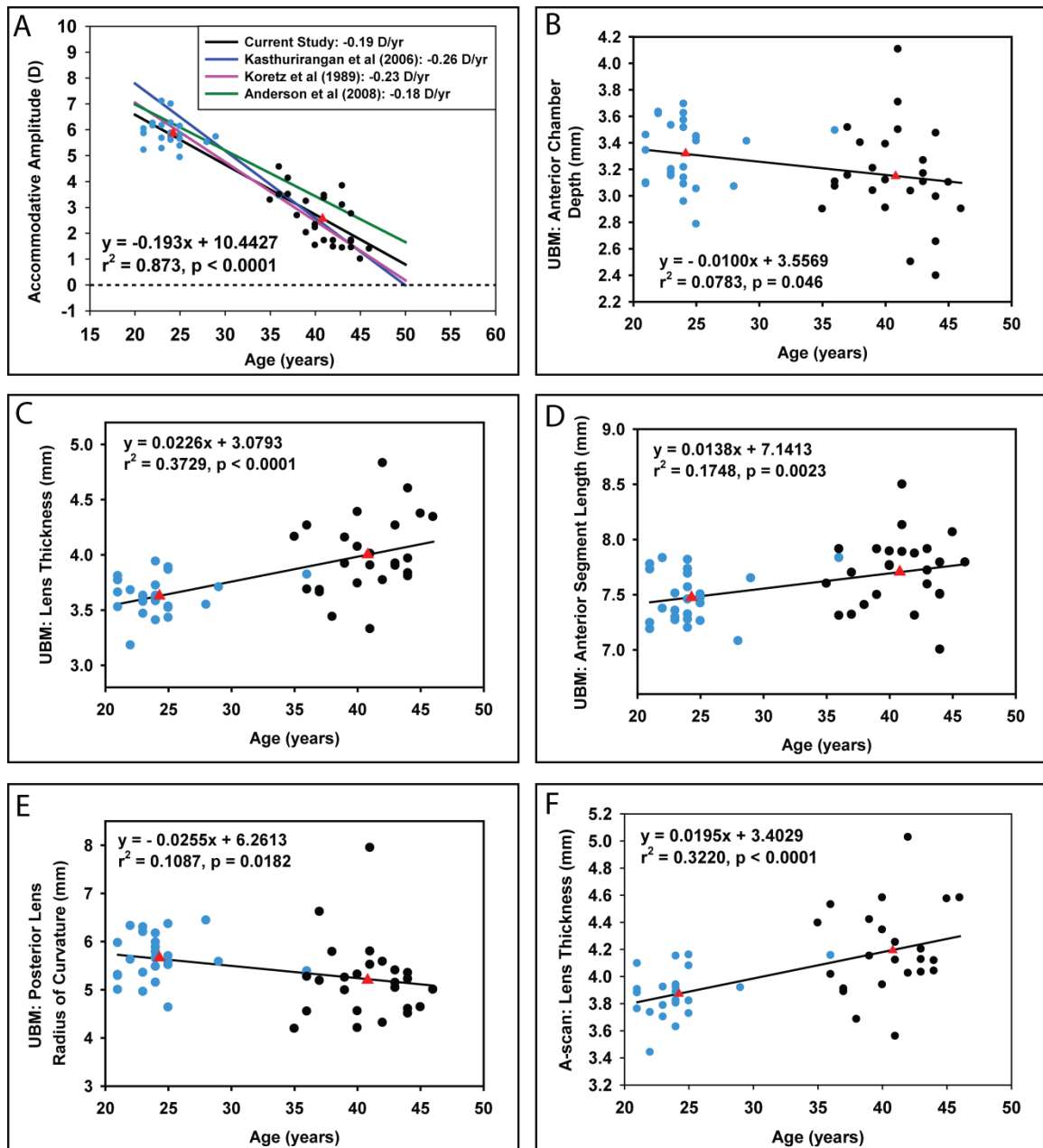
Table 4.8

Comparison of age-related changes (mm/year) in the ocular anterior segment biometry

parameters from prior human studies.

Table 4.8

Studies	Instrument	Age-related Changes in Anterior Segment Biometry (mm/year)				
		ACD	LT	ASL	ALRC	PLRC
Current Study	UBM	-0.010	+0.022	+0.014	No change	-0.026
(Richdale et al., 2013)	Ultrasound / Phakometry	-0.031	+0.031	No change	-0.110	No change
(Atchison et al., 2008)	MRI	-0.011	+0.024	+0.013	-0.044	No change
(Koretz, Strenk, Strenk et al., 2004)	Scheimpflug MRI	-0.0215 -0.0215	+0.0194 +0.0193	No change	-0.0759 -0.0828	No change
(Koretz et al., 2001)	Scheimpflug	NA	NA	NA	-0.020	-0.020
(Dubbelman, van der Heijde, & Weeber, 2001; Dubbelman & van der Heijde, 2001)	Scheimpflug	-0.010	+0.024	+0.015	-0.057	-0.012
(Koretz, Kaufman, Neider et al., 1989)	Ultrasonography	-0.011	+0.021	+0.009	NA	NA

Table 4.9

Comparison of demographics, optical and anterior segment biometric measurements between young and pre-presbyopic subjects. Except for accommodative amplitudes, all parameters are for the unaccommodated state. The symbol * indicates a statistically significant difference between young and pre-presbyopic subjects. Symbols † and ^ indicate statistically significant differences between UBM and A-scan measurements of lens thickness and anterior segment length, respectively. † $t = -4.965$, $p < 0.0001$; ^ $t = -2.389$, $p = 0.021$.

Table 4.9

Demographics and Measured Ocular Parameters at Baseline	Young Subjects Mean ± SD	Pre-presbyopic Subjects Mean ± SD	Significance
Sample size	26	25	
Age (years)	24.15 ± 3.03*	40.80 ± 3.08*	t = -19.444, p < 0.0001
Gender	males:8, females:18	males:8, females:17	
Refractive error (D)	-1.31 ± 2.03	-1.40 ± 1.98	
Grand Seiko autorefractor			
Accommodative amplitude (D)	5.86 ± 0.42*	2.56 ± 1.01*	t = 13.476, p < 0.0001
Infra-red photorefraction			
Accommodative amplitude (D)	5.62 ± 1.29*	2.67 ± 1.33*	t = 7.964, p < 0.0001
Pupil diameter (mm)	6.28 ± 0.84	6.14 ± 0.72	
A-scan ultrasound			
Anterior chamber depth + corneal thickness (mm)	3.75 ± 0.23	3.66 ± 0.35	
Lens thickness (mm)	3.87 ± 0.18*†	4.19 ± 0.32*	t = -4.339, p < 0.0001
Anterior segment length (mm)	7.62 ± 0.20*^	7.85 ± 0.32*	t = -3.041, p = 0.004
Vitreous chamber depth (mm)	16.28 ± 1.30	16.37 ± 1.07	
Axial length (mm)	23.90 ± 1.35	24.22 ± 1.12	

Table 4.9 (Continued)

Demographics and Measured Ocular Parameters at Baseline	Young Subjects Mean ± SD	Pre-presbyopic Subjects Mean ± SD	Significance
Ultrasound biomicroscopy			
Corneal thickness (mm)	0.53 ± 0.03	0.54 ± 0.04	
Anterior chamber depth (mm)	3.32 ± 0.24	3.15 ± 0.37	
Anterior chamber depth + corneal thickness (mm)	3.85 ± 0.24	3.69 ± 0.37	
Lens thickness (mm)	3.63 ± 0.17*†	4.00 ± 0.35*	t = -4.834, p < 0.0001
Anterior segment length (mm)	7.47 ± 0.22*^	7.71 ± 0.31*	t = -3.019, p = 0.004
Anterior lens radius of curvature (mm)	11.68 ± 1.44	11.00 ± 1.77	
Posterior lens radius of curvature (mm)	5.66 ± 0.47*	5.20 ± 0.80*	t = 2.509, p = 0.016
Angle-to-angle distance (mm)	10.81 ± 0.48	10.57 ± 0.39	
Left anterior chamber angle (deg)	38.83 ± 7.02	36.37 ± 9.02	
Right anterior chamber angle (deg)	40.59 ± 6.95	37.43 ± 9.62	

4.4   Discussion

As also described and discussed previously for young subjects (Ramasubramanian & Glasser, 2014a), infrared photorefraction overestimated the Grand Seiko measured accommodative optical response in the pre-presbyopes. The per-diopter accommodative change in pupil diameter was larger for the pre-presbyopic subjects compared to the young subjects as reported previously, suggesting a greater accommodative effort in the older subjects compared to the young subjects (Kasthurirangan & Glasser, 2006b; Schaeffel et al., 1993). Absolute pupil diameter at the baseline stimulus demand is smaller in the pre-presbyopic group due to age-related pupillary miosis (Table 4.9), however, when absolute pupil diameters are plotted as a function of age, there was no statistically significant age-related trend ($r^2 = 0.013$, p = 0.421) (data not shown). The GS autorefractor used did not measure pupil diameter, hence comparisons could not be made with photorefraction measured pupil diameters.

Per-diopter accommodative changes in the anterior segment biometry parameters in older subjects were similar to the values in young subjects (Figure 4.3). Prior studies have similarly shown that per diopter accommodative biometry changes do not change with age (Koretz et al., 1997; Dubbelman et al., 2005). In the current study, posterior movement of posterior lens surface with accommodation was observed in 9 eyes (36 % of the subjects). This is fewer than the 52% of subjects in which this was observed previously in young phakic eyes (Ramasubramanian & Glasser, 2014a). In the remaining

177

eyes, the posterior lens surface did not move significantly during accommodation. This might suggest age-related changes in accommodation in which there is a forward translation of the anterior lens surface with less movement of the posterior lens surface in older eyes. This finding also suggests that gravity does not influence lens accommodative movements in most pre-presbyopes since the lens does not sag posteriorly during accommodation while subjects are supine.

The age-related decline in the accommodative ability from the present study is comparable to rates from prior studies (Anderson, Hentz, Glasser et al., 2008; Kasthurirangan & Glasser, 2006a; Koretz et al., 1989) (Figure 4.7 A). Small differences between the studies might be due to differences in accommodation stimulation, noise and variability of the measurement technique and variability in subject population. Age-related changes in the UBM measured biometry parameters were observed except for ALRC. When ALRC was plotted with age, no statistically significant age-related trend (r^2 = 0.045, p = 0.131) was observed (data not shown). This is likely due to the limited number of lens surface pixels in the UBM images than can be used to fit a circle which is limited by the pupil diameter and indistinct edges of the anterior lens surface (Ramasubramanian & Glasser, 2014c). Since the anterior lens surface is relatively flat, more surface pixels are required to accurately fit the surface and to determine the radius of curvature.

Smaller standard deviations and good repeatability of the UBM measured anterior segment biometry parameters in the pre-presbyopic subjects compared to the young subjects demonstrate that UBM, despite having low axial resolution, can provide accurate measurements in pre-presbyopic subjects with lower accommodative amplitudes. Differences observed between A-scan and UBM measured ACD and LT in the current study were also observed in young subjects and have been discussed previously (Ramasubramanian & Glasser, 2014c). Ratios of A-scan measures and UBM measures of ACD and LT were calculated from subjects with statistically significant linear relationships, for all stimulus demands, to yield 244 UBM correction factors. The mean ± SD of all these ratios is 0.984 ± 0.02 and 1.049 ± 0.03 respectively for ACD and LT. The correction factors for ACD and LT from pre-presbyopes are similar to values reported previously in young subjects (Ramasubramanian & Glasser, 2014c). Multiplying the UBM measurements by the correction factors would, on average, get the UBM measurements in agreement with the A-scan measurements.

In the current study, the standard deviations of predicted AOR from the population as a whole is worse than predictions from individual subjects as reported in young subjects previously (Ramasubramanian & Glasser, 2014a). The standard deviations of predicted AOR from biometry using linear regression, 95% confidence and prediction intervals are smaller in older subjects than in younger subjects. This might be due to the smaller slope of the linear regression equations (Table 4.5) and relatively larger number of data points from the pre-presbyopic subjects due to having used more stimulus demands. In the current study, AOR was predicted independently from each

179

UBM measured biometry parameter. Due to the strong linear correlation among the UBM measured biometry parameters (Figure 4.4), a multiple linear regression model was unstable and therefore unsuitable to use.

One of the limitations of the current study is that the accommodative optical and biometric changes were not measured simultaneously; hence linear correlations between AOR and biometry might not be as strong as they actually are. Refraction measurements recorded simultaneous to the UBM biometry measurements in the contralateral eye could potentially be made using photorefraction. However, the refraction measurements from the Grand Seiko were considered more reliable than those from photorefraction due to the small pupil diameters. This meant the correlations were derived from sequential measurements of refraction and biometry in the same eye. Simultaneous measurements could provide better prediction of AOR. Based on the current study, if accommodative changes in anterior segment biometry are measured, the linear regression equations provided (Table 4.6) can be used to calculate AOR in pre-presbyopic subject population. On average, the prediction errors from the linear regressions are less than 0.65 D for all biometry parameters with LT being the best predictor for both age groups. Although only data from subjects who had statistically significant linear relationships between optical and biometric changes were used for AOR prediction, almost all of the subjects had statistically significant linear relationships for LT and ALRC. Hence it would be better to use LT and ALRC to estimate the AOR.

It might be of interest to see how the anterior segment parameters could collectively be used to predict the refraction and the AOR of the eye. One approach to doing this would be to put all the measured anterior segment biometry parameters into a schematic eye model to calculate the refractive state of the eye and the AOR. This might be useful to understand if a better prediction could be obtained from a schematic eye model than from the individual linear correlations. However, schematic eye calculations also require measurements of corneal curvature and axial length of the eye.

From the current study and the prior study in young subjects (Ramasubramanian & Glasser, 2014a), it can be seen that individual UBM measured anterior segment parameters are robust enough to predict the AOR in both young subjects with ample accommodation and in pre-presbyopic eyes with lower accommodative amplitudes. This method of predicting the AOR could be applied in clinical accommodation studies in young and pre-presbyopic phakic eyes. In addition, prediction of AOR as demonstrated here might be useful to observe and evaluate the accommodative ability of accommodation restoration concepts. However, for the purpose of evaluating pseudophakic eyes, the relationships between biometric movements and AOR in eyes with specific types of IOLs would have to be first established before predictions can be made.

This study has demonstrated the ability to predict the AOR from UBM measured anterior segment parameters in pre-presbyopic eyes with standard deviations of less than

0.55 D using the linear regressions and 95% confidence intervals. In general, the AOR predictions in pre-presbyopic subjects are better than in young subjects. Standard deviation and repeatability of UBM measured biometry parameters are similar in pre-presbyopic and young subjects. Further study would be required in eyes with accommodation restoration concepts to see if AOR could be predicted as described here.

Chapter 5 - Correction of Corneal Distortions from Visante Anterior Segment Optical Coherence Tomography Images

5.1   Introduction

Accurate measurement of corneal anterior and posterior radius of curvature and thickness is useful for contact lens fitting, refractive surgeries, diagnosis and management of corneal disorders and optical modeling. Various imaging modalities such as Scheimpflug photography (Dubbelman, Sicam, & van der Heijde, 2006; de Jong T., Sheehan, Dubbelman et al., 2013; Dubbelman, Weeber, van der Heijde et al., 2002), scanning slit topography (Liu, Huang, & Pflugfelder, 1999; Crawford, Patel, & McGhee, 2013; Zheng, Ying, Wang et al., 2013), ultrasound biomicroscopy (Al-Farhan & Al-Otaibi, 2012; Ogbuehi & Osuagwu, 2012) and anterior segment optical coherence tomography (AS-OCT) (Fishman, Pons, Seedor et al., 2005; Zhao, Wong, Wong et al., 2007; Sorbara, Maram, Fonn et al., 2010) have been used to measure corneal shape and thickness. The Visante is a commercial AS-OCT instrument that enables non-invasive measurement of anterior segment parameters with an axial resolution of 18 μm (*Visante OCT User Manual*, 2006).

Prior studies have reported spatial (geometric) and optical (refractive) distortions in custom built OCT systems (Westphal et al., 2002; Podoleanu, Charalambous, Plesea et al., 2004; Borja, Siedlecki, de Castro et al., 2010; Siedlecki et al., 2012). The spatial

distortions may be caused by the non-linear axial scanning and non-telecentric lateral scanning architecture (Westphal et al., 2002). Optical distortions of optical surfaces occur due to the refractive effects of a surface preceding the surface of interest. Spatial and optical distortions have been reported in Visante AS-OCT images (Dunne et al., 2007) although the exact source of the spatial distortion is unknown. Kao et al (Kao, Richdale, Sinnott et al., 2011) reported no spatial distortion in the Visante image of an optical flat captured using 'Enhanced High Resolution Corneal Mode'. However, that mode captures a magnified image of a small area which may not be enough to accurately determine the presence of distortion. The instrument manufacturer does not provide information about the correction applied to the images in various scan modes. The presence of residual errors in corneal and anterior segment parameters measured using the built-in Visante software (Dunne et al., 2007) suggests that the Visante software does not provide robust spatial and optical distortion correction.

Wolffsohn and colleagues (Dunne et al., 2007) previously described a distortion correction for the Visante AS-OCT (version 1.0.12.1896). When the anterior corneal surface distortion correction equation from that paper was used to try to correct contact lens surfaces imaged from the raw images from another Visante instrument (version 2.0.1.88), it did not yield correct values. There are a number of uncertainties in the description of that prior work. It is not clear whether raw or Visante distortion corrected images were used for their analysis. The Visante software described in that study appears to have capabilities that are not available in subsequent versions. There is some confusion over what is considered as the image x and y axes; for example, x coordinates are used in

a vertical line of pixels. Since the software versions are different, it is possible that the Visante software has been modified, so that the method described previously may not be applicable to later software versions. For these reasons, this current study was undertaken to develop spatial and optical distortion corrections for raw images captured from the Visante software version 2.0.1.88.

The goals of this study were to a) use contact lenses of known parameters to measure spatial and optical distortions and provide equations to obtain corrected corneal parameters from Visante AS-OCT images and b) to apply the distortion correction to corneal parameters measured from Visante AS-OCT images captured in 24 younger and 30 older human subjects. The purpose was to obtain corneal front and back surface radii of curvatures and central corneal thickness measurements from younger and older human subjects that are of sufficient accuracy to apply those values to future schematic eye calculations.

5.2   Methods

Visante AS-OCT (Carl Zeiss, Dublin, CA) (version 2.0.1.88) images were captured using the anterior segment single mode or the raw image mode. When a Visante image is captured and saved, the Visante software automatically stores a raw, unprocessed image in DICOM format in the folders created by the Visante software with 41 seemingly random character file names. These files can be located by exiting the Visante software and searching the hard drive for files created by time and date, or by searching for files with the extension '.EX.DCM'. These images were exported to a USB drive and converted to bitmap (.bmp) format using a custom developed Matlab (MathWorks, Natick, MA) program. Image subtraction showed that the raw images from the Visante 'anterior segment single' mode and the 'raw image' mode were identical. The Visante software applies no overlay or distortion correction to these images. All further processing described here was performed on these raw AS-OCT images.

Spatial Calibration

The horizontal spatial pixel to mm conversion factor was calculated by imaging a plastic millimeter scaled ruler. The ruler was positioned at 5 different axial distances along the instrument optical measurement axis. This resulted in the ruler being imaged at 5 different vertical (y-axis of the captured AS-OCT images) positions in the AS-OCT images in 5 separate images. The millimeter markings in each image were manually

marked using a custom developed Matlab program (Figure 5.1 A). The horizontal pixel to mm conversion factor was similar for all 5 vertical positions of the ruler on the image. The mean ± standard deviation (SD) of horizontal pixel to mm conversion factor from 15 measurements in 5 images was 31.80 ± 0.50 pixels/mm. This horizontal calibration is therefore applicable at any vertical position in the image.

To determine the vertical spatial pixel to mm conversion factor in the image, a microscope slide and independently a cover slip, were fixed to a micrometer translation stage on a goniometer (Figure 5.1 B). The goniometer was adjusted so that the surface of the microscopic slide/cover slip was perpendicular to the instrument optical measurement axis. The micrometer translation stage was used to move the slide/cover slip in 0.5 mm steps (a total of 15 positions) along the instrument measurement axis and images were captured at each position. The position of the front and back surface of the slide/cover slip on the image was manually marked at three different horizontal locations in the images (left, middle and right) (Figure 5.1 C). The difference in the vertical position between the corresponding red points in each successive image gave the number of pixels moved in the image for 0.5 mm movement in real space. The vertical pixel to mm conversion factors were similar for the 15 axial positions of the slide and the coverslip in the image. The mean ± SD of vertical spatial pixel to mm conversion factor from 168 measurements (6 locations on each image x 14 images x 2 (slide and the coverslip)) was 25.77 ± 1.09 pixels/mm.

Figure 5.1

(A) Visante image of a ruler with red points marked on the millimeter gradations to calculate the horizontal pixel to mm conversion factor. (B) Experimental setup to determine the vertical pixel to mm conversion factor. (C) Visante image of a microscope slide at one axial position with red points marked on the front and back slide surfaces. The third horizontal line is an artifact or 'shadow' resulting from the AS-OCT imaging of a glass slide. (D) Raw Visante image of a contact lens with circles fitted to the central 8 mm of the front (red) and back (green) surface. (E) Raw Visante image from a single subject showing circle fits to the central 8 mm of the anterior (red) and posterior (green) corneal surface.

Figure 5.1
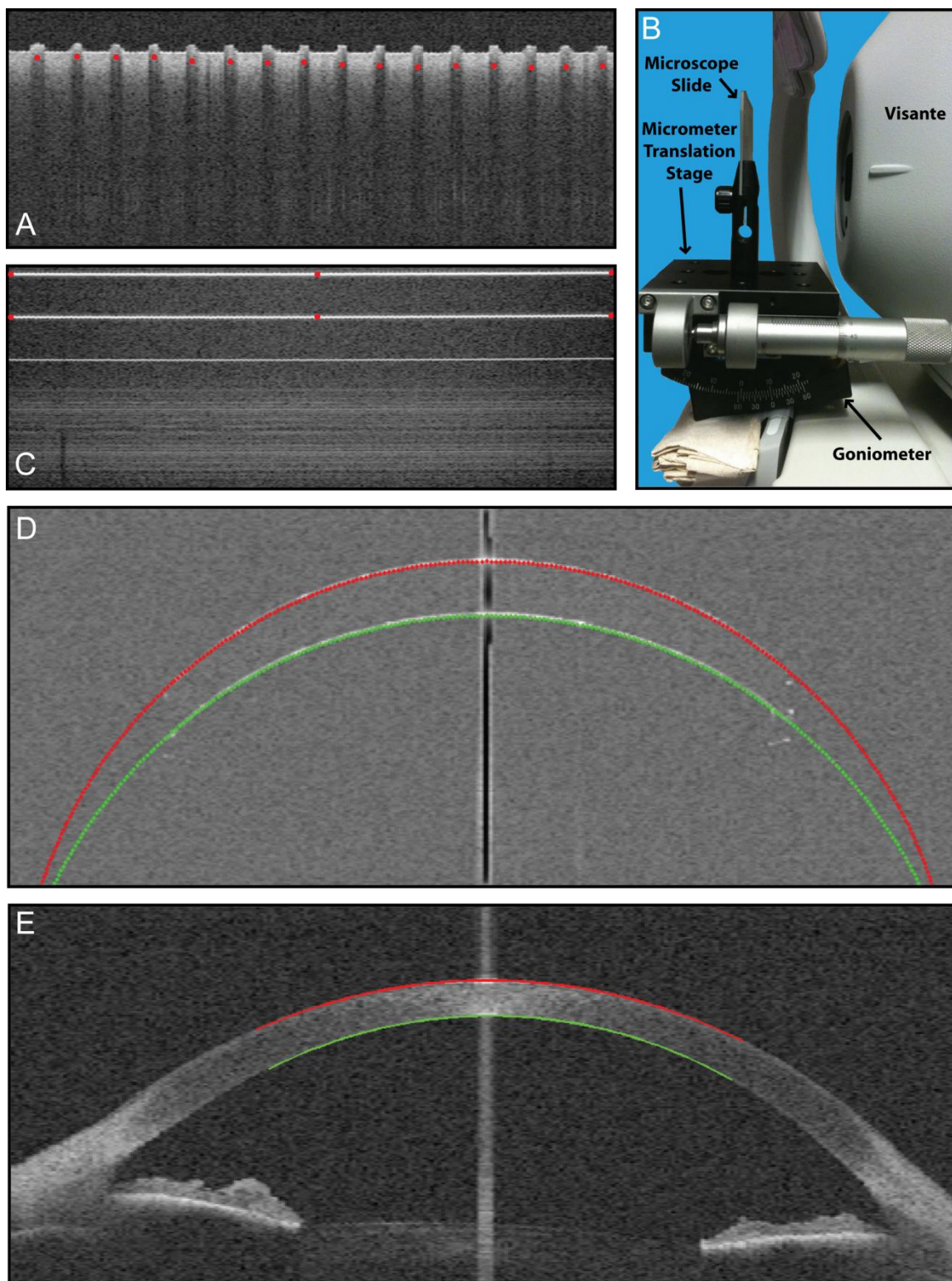
To calculate the spatial and optical distortion correction factors, 5 poly-methyl-methacrylate (PMMA) contact lenses (CLs) of known spherical surface curvatures and vertex thickness were imaged with the Visante. The parameters of the CL used are listed in Table 5.1. For the analysis of the Visante images, the front and back surface of the CL were identified in the images using a custom developed automated Matlab image analysis program. Both front and back surface points corresponding to a central 8 mm diameter were fit with circles (Figure 5.1 D). Later (see below), the same analysis methods were also applied to human corneas. Visante AS-OCT images of human eyes with the central 8 mm anterior and posterior corneal surfaces digitized were also well fitted with a circle (Figure 5.1 E). A circle provided acceptable fits to the central 8 mm of the CL and the corneal surface points as judged by examination of the residuals and was used for calculating distortion corrections.

Table 5.1

Parameters of the spherical calibration contact lenses used.

Table 5.1

Contact Lenses	Actual Parameters		
	Front Surface Radius of Curvature (mm)	Central Thickness (mm)	Back Surface Radius of Curvature (mm)
CL 01	6.60	0.80	6.30
CL 02	7.30	0.80	7.00
CL 03	7.55	0.80	7.25
CL 04	7.80	0.80	7.50
CL 05	8.30	0.80	8.00

Front Surface Distortion Correction

To correct the spatial distortion of the front CL surface, the identified surface coordinates and the fitted circle coordinates were converted from pixels to mm using the x and y spatial calibration factors described above. If necessary, the calibrated coordinates were rotated to achieve mirror symmetry about the vertex to correct for any tilt of the contact lens in the AS-OCT image. The coordinates of the fitted circle (the distorted circle) were scaled and cropped such that the vertex of the surface was set to x = 0, y = 0 and the range of x-data spanned from - 4 to + 4 mm (for the central 8 mm diameter). The radius of curvature of the circle fit to this data provided a spatially distorted front CL radius of curvature. Coordinates were then generated in Matlab for a circle with a radius that corresponded to the actual CL front surface radius of curvature (the actual circle). These generated coordinates used the same matching relative x-coordinates as were obtained from the CL surface in the distorted image. These two curves are shown in Figure 5.2 A. A two-step process was then used to correct the spatial distortions. In the first step the AS-OCT image spatial distortion was calculated by dividing each y-coordinate value of the actual circle by each corresponding y-coordinate value from the distorted circle. Figure 5.2 B shows a plot of the calculated spatial distortion as a function of x-coordinates from one CL. The calibration curve was then fitted with a 6th order polynomial which provided the spatial distortion correction equation for this CL. The coefficients for each term from five 6th order equations (Table 5.2) from the 5 separate CLs were averaged to generate a mean distortion correction equation. This mean distortion correction equation was applied to each front CL surface

y-coordinate value to correct the spatial distortion (step 1). Figure 5.2 C and Figure 5.2 D shows a comparison of actual and measured front CL surface radii of curvature for the 5 CLs before and after the initial distortion correction (step 1). As can be seen from the resulting curve (Figure 5.2 D), the data points did not lie exactly on the expected 1:1 line which would demonstrate complete correction. A second step in the distortion correction was then required. In the second step, the data points from all the calibration CL surfaces were then fitted with a 2nd order polynomial equation as shown in Figure 5.2 D. This polynomial equation was then applied (step 2) to the distortion corrected radius of each surface from step 1. Figure 5.2 E shows that after applying step 2, the distortion corrected radii fall on the 1:1 line with a slope close to 1. Bland - Altman plots show a maximum difference of less than 50 μm between the actual and final distortion corrected front surface radii of curvatures (Figure 5.2 F).

Figure 5.2

(A) Illustration showing the calculation of spatial distortion from the actual (green) and distorted (red) curves. (B) Calibration curve of the front surface of a contact lens (CL 05) with a 6th order polynomial fit. The equation of this polynomial is: $Spatial\ Distortion = -7.8086e^{-8} \times x^6 + 7.3596e^{-10} \times x^5 - 2.7542e^{-6} \times x^4 - 1.0987e^{-8} \times x^3 - 1.7667e^{-4} \times x^2 + 3.0205e^{-8} \times x + 1.00$ (C) Comparison of the actual and distorted front surface radii of curvature from all 5 contact lenses. (D) Step 1: Comparison of the actual and distortion corrected front surface radii of curvature after applying the average 6th order polynomial. (E) Step 2: Comparison of the distortion corrected front surface radii of curvature after applying the second polynomial correction. (F) Bland-Altman comparison between actual and distortion corrected front surface radii of curvature after step 2.

Figure 5.2
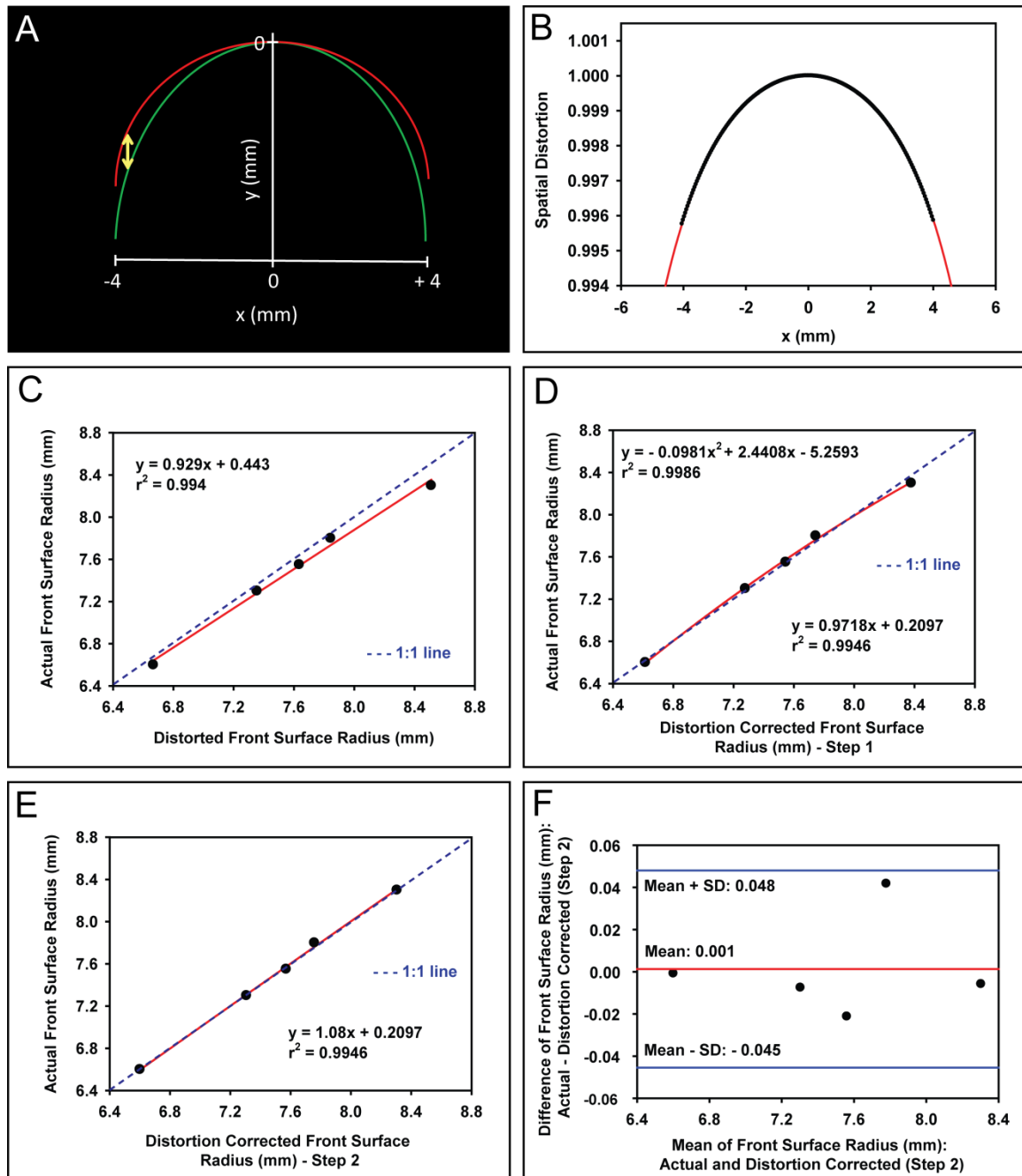
Table 5.2

Spatial distortion correction equations calculated for the front and back surfaces for all

contact lenses.

Table 5.2

Contact Lenses	Surfaces	Coefficients of the Spatial Distortion Correction Equation						
		x^6	x^5	x^4	x^3	x^2	x	constant
CL 01	Front	-1.9085E-07	-2.3894E-09	-2.0168E-06	3.5548E-08	-1.1906E-04	-9.7671E-08	1.000
CL 02		-6.5333E-08	7.1828E-10	-1.2742E-06	-1.0653E-08	-7.1063E-05	2.9139E-08	1.000
CL 03		-7.4584E-08	-4.1367E-19	-1.7218E-06	-2.3123E-18	-9.8337E-05	4.9935E-17	1.000
CL 04		-2.9999E-08	3.0496E-10	-7.8856E-07	-4.5272E-09	-4.6100E-05	1.2386E-08	1.000
CL 05		-7.8086E-08	7.3596E-10	-2.7542E-06	-1.0987E-08	-1.7667E-04	3.0205E-08	1.000
Mean		-8.7770E-08	-1.2605E-10	-1.7111E-06	1.8761E-09	-1.0224E-04	-5.1882E-09	1.000
SD		6.0691E-08	1.3020E-09	7.4559E-07	1.9370E-08	4.9902E-05	5.3197E-08	6.8719E-07
		x^6	x^5	x^4	x^3	x^2	x	constant
CL 01	Back	-1.8615E-06	-1.6229E-19	-1.8868E-05	1.1335E-17	-1.1326E-03	-1.4132E-16	1.000
CL 02		-7.8553E-07	-9.3164E-21	-1.5311E-05	1.0225E-17	-8.5766E-04	-1.1615E-16	1.000
CL 03		-5.8190E-07	6.4211E-09	-1.3176E-05	-9.5732E-08	-7.5250E-04	2.6305E-07	1.000
CL 04		-4.4478E-07	1.3909E-08	-1.1669E-05	-2.0696E-07	-6.8510E-04	5.6751E-07	1.000
CL 05		-2.9919E-07	1.8331E-18	-1.0472E-05	-2.5513E-17	-6.6796E-04	1.3157E-17	1.000
Mean		-7.9458E-07	4.0659E-09	-1.3899E-05	-6.0539E-08	-8.1917E-04	1.6611E-07	1.000
SD		6.2279E-07	6.1648E-09	3.3136E-06	9.1752E-08	1.9040E-04	2.5164E-07	7.1063E-06

Central Thickness Optical Correction

In the OCT image, the back surface of the CL is the *image* of the actual back surface as viewed after being refracted by the CL. The thickness of this central CL *image* was measured from the AS-OCT images as the distance between the front and back CL surfaces at the vertex. There is no spatial distortion to the CL thickness at the vertex because the CL vertex corresponds to the optical axis of the OCT instrument. The axial thickness observed in the AS-OCT image is the apparent thickness of the CL which is affected optically by refraction at the front surface and by the CL refractive index. The actual thickness of the CL can be calculated from the OCT image using simple paraxial optics. The refractive index of PMMA for the AS-OCT wavelength of 1310 nm was calculated to be 1.4738 (Kasarova, Sultanova, Ivanov et al., 2007). Equations 1 through 4 were used to correct the optical distortions for the central CL thickness. First the front CL surface power was calculated:

$$F = \frac{1000 \times (n_{PMMA} - n_{air})}{r_{fs}} \tag{1}$$

where F is surface power (D) of the front CL surface, n_{PMMA} is the refractive index of PMMA at a wavelength of 1310 nm, n_{air} is the refractive index of air (1.00) and r_{fs} is the actual front surface radius of curvature (mm) calculated as described above. Next, the vergence to the CL image posterior surface after refraction by the CL front surface was calculated:

$$L' = \frac{1000 \times n_{PMMA}}{l'} \qquad (2)$$

where L' is the image vergence (D), l' is the image distance in mm (measured CL image thickness from the OCT image). Next, the vergence before refraction by the CL front surface of the actual CL posterior surface was calculated:

$$L = L' - F \qquad (3)$$

where L is the object vergence (D). Finally, the distance before refraction by the CL front surface to the actual CL posterior surface was calculated:

$$l = \frac{1000 \times n_{air}}{L} \qquad (4)$$

where l is the object distance or the optically corrected (i.e., true) central CL thickness (mm).

Back Surface Spatial and Optical Correction

The CL back surface as seen in the AS-OCT image is the *image* of the actual CL back surface refracted by the front CL surface and has both the optical distortion from being refracted by the CL front surface and the CL thickness, and it has the spatial distortion from the AS-OCT instrument. The process for determining the spatial distortion of this surface is to a) generate the *image* of the actual CL back surface as though seen through the CL and b) to fit that image with a circle and then to compare that fitted circle with the CL back surface from the OCT image.

To generate the *image* of the actual CL back surface (i.e., the target back CL surface) as refracted through the CL front surface, the position of the center of curvature and the radius of the target CL back surface has to be calculated. The center of curvature of the actual CL back surface is the *object* for the CL front surface. Therefore the object distance is the CL thickness plus the distance to the back surface center of curvature. The object vergence (L_1) is then given by:

$$L_1 = \frac{1000 \times n_{PMMA}}{r_{bs} + CT_{actual}} \qquad (5)$$

where r_{bs} is the actual (i.e., true, known) CL back surface radius of curvature (mm) and CT_{actual} is the actual CL center thickness (mm). The denominator ($r_{bs} +$

CT_{actual}) represents the object distance (distance of the actual CL back surface center of curvature from the CL front surface).

After refraction by the CL front surface, the image vergence L'_1 to the center of curvature of the target CL back surface is:

$$L'_1 = L_1 + F \tag{6}$$

where F is the power of the front CL surface (D) from equation 1.

The image distance (l'_1) which is the distance of the target CL back surface center of curvature from the CL front surface is:

$$l'_1 = \frac{1000 \times n_{air}}{L'_1} \tag{7}$$

The target radius of curvature can then be obtained by subtracting the thickness of the CL OCT image as:

$$r_{tbs} = l'_1 - CT_{OCT} \tag{8}$$

where r_{tbs} is the target CL back surface radius of curvature (mm) and CT_{OCT} is the central CL thickness (mm) measured from the AS-OCT image.

Once the target back CL surface radius (r_{tbs}) is known, this can be directly compared with the back CL surface from the AS-OCT image and the spatial distortion can be calculated using the methods described above for the CL front surface. The CL back surface coordinates were extracted from the AS-OCT images for the central 8 mm diameter and fit with a circle (distorted circle). The radius of curvature calculated from the distorted circle is the spatially and optically distorted back CL radius. The target back CL surface radius was then used to generate a target circle x- and y-coordinates in Matlab using the same x-axis coordinates as were extracted from the AC-OCT image. The vertex of the target circle and the distorted circle were set to x = 0, y = 0 and the data was rotated, if necessary, and scaled and cropped from -4 to +4 mm as described above. The ratio of y-coordinate positions for each corresponding x-coordinate position was calculated to generate a 6th order distortion correction polynomial for each contact lens (Table 5.2). Five polynomials from the 5 CLs were averaged to generate a mean distortion correction equation for the CL back surface. This mean distortion correction equation was applied to each CL back surface y-coordinate value to correct the spatial distortion (step 1). Figure 5.3 A & Figure 5.3 B show a comparison of target back surface radii (r_{tbs}) and measured back surface radii of curvature for the 5 CLs before and after the distortion correction, respectively (step 1). The spatial distortion for the back surface also required a second correction step similar to the front surface. Data points for the individual CLs in Figure 5.3 B were fitted with a 2nd order polynomial. This polynomial was applied (step 2) to the distortion corrected radius for each CL surface calculated in step 1 to get the spatial distortion corrected back surface radius (r'_{tbs}) closer to target back

surface radius (r_{tbs}) (Figure 5.3 C). Bland - Altman plots show that the maximum difference between r_{tbs} and r'_{tbs} is less than 40 μm (Figure 5.3 D).

Figure 5.3

(A) Comparison of the target and distorted back surface radii of curvature from all 5 contact lenses. (B) Step 1: Comparison of the target and distortion corrected back surface radii of curvature after applying the average 6th order polynomial. (C) Step 2: Comparison of the distortion corrected back surface radii of curvature after applying the second polynomial correction. (D) Bland-Altman comparison between target and distortion corrected back surface radii of curvature after step 2.

Figure 5.3
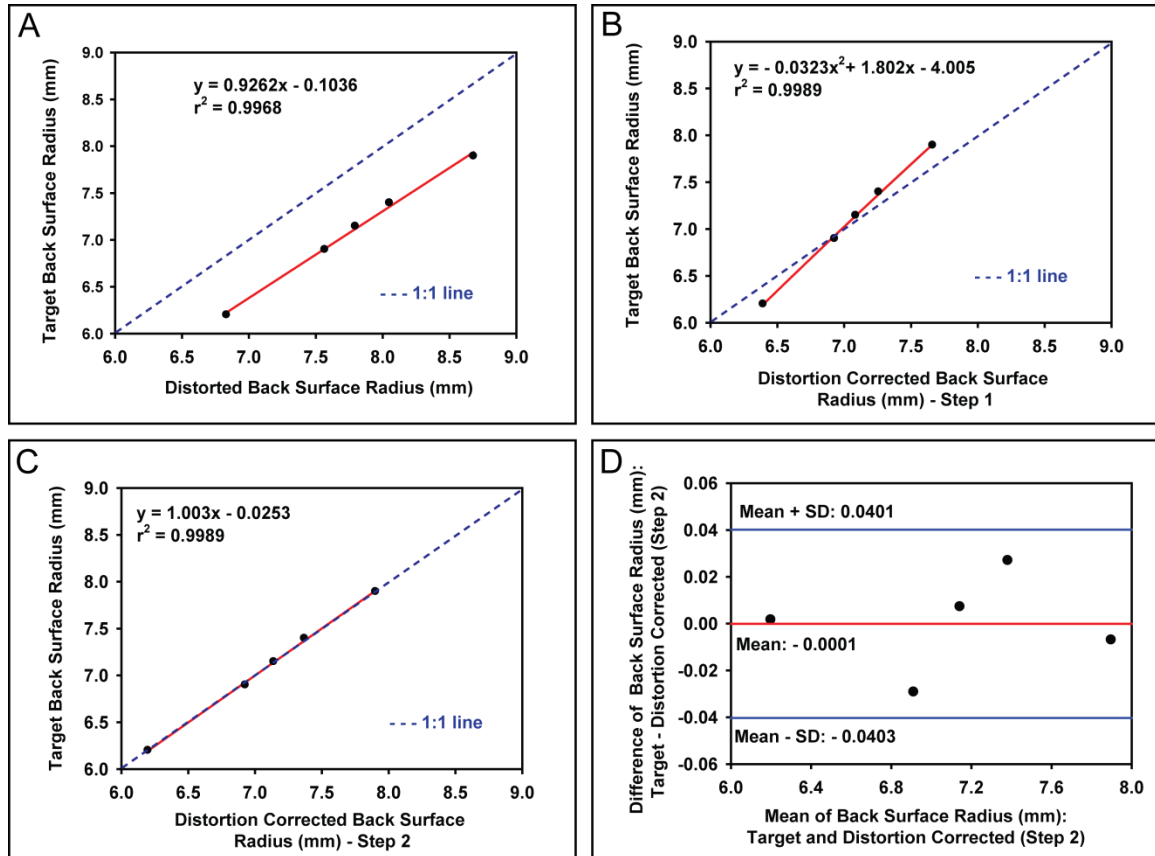
To get an optically corrected CL back surface radius (r_{cbs}) from the spatial distortion corrected CL back surface radius (r'_{tbs}), the position of the center of curvature of the corrected CL back surface has to be calculated. To do this, this spatially corrected surface must again be optically transformed by refraction through the CL front surface. The center of curvature of the spatially corrected surface serves as the object for the CL front surface and then the object vergence to the CL front surface can be calculated:

$$L_2 = \frac{1000 \times n_{air}}{r'_{tbs} + CT_{OCT}} \tag{9}$$

where L_2 is the object vergence for the center of curvature of the spatial distortion corrected back CL surface, ($r'_{tbs} + CT_{OCT}$) represents the object distance (distance of the spatial distortion corrected back CL surface center of curvature from the front CL surface).

The image vergence (L'_2) at the center of curvature of the optically corrected back CL surface is:

$$L'_2 = L_2 + F \tag{10}$$

where F is the power of the front CL surface (D) from equation 1.

The image distance (l_2') is the distance of the optically corrected back CL surface center of curvature from the front CL surface and is calculated from:

$$l_2' = \frac{1000 \times n_{PMMA}}{L_2'} \tag{11}$$

Finally, the optically corrected CL back surface radius of curvature can be calculated from:

$$r_{cbs} = l_2' - Corrected\ CT \tag{12}$$

where r_{cbs} is the optically corrected back CL surface radius of curvature (mm) and $Corrected\ CT$ is the optically corrected center CL thickness (l) calculated from equation 4.

Subjects

To use and test these optical and spatial corrections on corneal OCT images, two Visante images of the horizontal meridian of the anterior segment were captured from 24 younger subjects (7 males and 17 females), aged 21 to 36 years (mean ± standard deviation (SD): 24.04 ± 3.10 years) and 30 older subjects (10 males and 20 females), aged 36 to 48 years (mean ± SD: 40.83 ± 3.25 years) with normal visual and ocular histories. To assess the intra-session and inter-session repeatability, 15 younger subjects and 3 older subjects had AS-OCT scans repeated twice on a different day at least 5 days apart. Repeatability analysis was performed in SPSS software (version 20; SPSS Inc., Chicago, IL). Anterior and posterior corneal surface coordinates were identified and extracted using a custom Matlab image analysis program. The corneal surface coordinates were converted from pixels to mm using the calibration factors described previously. Central corneal thickness was measured as the vertical distance between the anterior and posterior corneal surfaces at the vertex. Optical and spatial distortions in the measured corneal parameters were corrected as described above using equations listed in Table 5.3.

Table 5.3

Summary of the distortion correction method. The corneal surface coordinates are converted from pixels to mm and scaled such that vertex is at x = 0, y = 0. Distortion correction equations are used in the order listed to correct distortions of corneal parameters. x_a, y_a and x_p, y_p: x and y coordinates of the circle fits to the anterior and posterior corneal surface, respectively; F: surface power of the anterior cornea; L and L' : object and image vergence at the actual and optically distorted posterior corneal surfaces, respectively; CT_{OCT} : corneal thickness measured from OCT image; $Corr\_CT$: optically corrected corneal thickness; L_2 and L'_2 : object and image vergence at the spatial and optical distortion corrected posterior corneal surface center of curvatures, respectively; $Corr\_r_{PC}$: optically corrected posterior corneal radius of curvature; n_{cornea}: refractive index of cornea for AS-OCT wavelength of 1310 nm was calculated to 1.4015 using the equation (Kasarova et al., 2007): $n_{cornea} = 1.376 + 0.0512 - (0.1455 \times 1.310) + 0.0961 \times 1.310^2$

Table 5.3

ANTERIOR CORNEAL SURFACE

Spatial distortion correction

a) $y_a = -8.77696399112472e^{-8} \times x_a^6 - 1.26047098634593e^{-10} \times x_a^5 - 1.7111029593407e^{-6} \times x_a^4 + 1.87608071693789e^{-9} \times x_a^3 - 1.0224453717464e^{-4} \times x_a^2 - 5.1881743271264e^{-9} \times x_a + 1.00000075090351$ ------ (1)

b) Calculate the anterior corneal radius of curvature (r_{AC}) from the coordinates x_a and y_a.

c) Apply a second step of correction to get spatial distortion corrected radius ($Corr\_r_{AC}$).

$Corr\_r_{AC} = -0.0904 \times (r_{AC})^2 + (2.3223 \times r_{AC}) - 4.8045$ ------ (2)

CENTRAL CORNEAL THICKNESS

Optical distortion correction

a) $F = \dfrac{1000 \times (n_{cornea} - 1)}{Corr\_r_{AC}}$ ------ (3)

b) $L' = \dfrac{1000 \times n_{cornea}}{CT_{OCT}}$ ------ (4)

c) $L = L' - F$ ------ (5)

d) $Corr\_CT = \dfrac{1000}{L}$ ------ (6)

Table 5.3 (Continued)

POSTERIOR CORNEAL SURFACE

Spatial distortion correction

a) $y_p = -7.94584588229656e^{-7} \times x_p^6 + 4.06594066225371e^{-9} \times x_p^5 - 1.3899072311646907e^{-5} \times x_p^4 -$

6.05389906276954e$^{-8} \times x_p^3 - 8.19165078653822e^{-4} \times x_p^2 + 1.66111950474094e^{-7} \times x_p +$

1.00000708889656 ------ (7)

b) Calculate the posterior corneal radius of curvature (r_{PC}) from the coordinates x_p and y_p.

c) Apply a second step of correction to get spatial distortion corrected radius ($SCorr\_r_{PC}$).

$SCorr\_r_{PC} = -0.0277 \times (r_{PC})^2 + (1.7321 \times r_{PC}) - 3.7429$ ------ (8)

Optical distortion correction

a) $L_2 = \dfrac{1000}{SCorr_{r_{PC}} + CT_{OCT}}$ ------ (9)

b) $L_2' = L_2 + F$ ------ (10)

c) $Corr\_r_{PC} = \dfrac{1000 \times n_{cornea}}{L_2'} - Corr\_CT$ ------ (11)

212

5.3   Results

Root mean square (RMS) error of the measured CL front and back surface radii of curvature (mm and D) and contact lens thickness (mm) at each step of distortion correction compared to the known values are shown in Table 5.4. The power of the front CL surface was calculated using the equation:

$$Front\ CL\ Power\ (D) = \frac{1000 \times (n_k - n_{air})}{Front\ CL\ radius\ of\ curvature\ (mm)} \qquad (13)$$

The power of the back CL surface was calculated using the equation:

$$Back\ CL\ Power\ (D) = \frac{1000 \times (n_{air} - n_k)}{Back\ CL\ radius\ of\ curvature\ (mm)} \qquad (14)$$

where n_k is the refractive index of PMMA at 555 nm (1.493). The RMS error of power for the CL front and back surfaces after full optical and spatial distortion corrections were 0.18 D and 0.11 D, respectively. The mean RMS error of central CL thickness after optical distortion correction was 0.004 mm. Figure 5.4 A shows the spatially distorted and corrected circle coordinates for the anterior and posterior corneal surface from a single subject.

Table 5.4

Root mean square error for the measured front and back contact lens radii and central contact lens thickness in units of millimeters (mm) and diopters (D) compared to the known values at various steps in the distortion correction process. NA: not applicable.

Table 5.4

Measured Parameters	Root Mean Square Error of Radius / Power		
	Before distortion correction (mm/D)	After spatial distortion correction (mm/D)	After optical distortion correction (mm/D)
Front contact lens surface radius	0.11 / 0.86	0.02 / 0.18	NA
Back contact lens surface radius	0.58 / 5.12	0.21 / 1.82	0.011 / 0.110
Central contact lens thickness	0.364 / NA	NA	0.004 / NA

Figure 5.4

(A) Comparison of the anterior and posterior corneal surface (central 8 mm diameter) before and after spatial distortion correction using equations listed in Table 5.3 for a single subject. (B) Graph of the optically corrected central corneal thickness as a function of age.

Figure 5.4
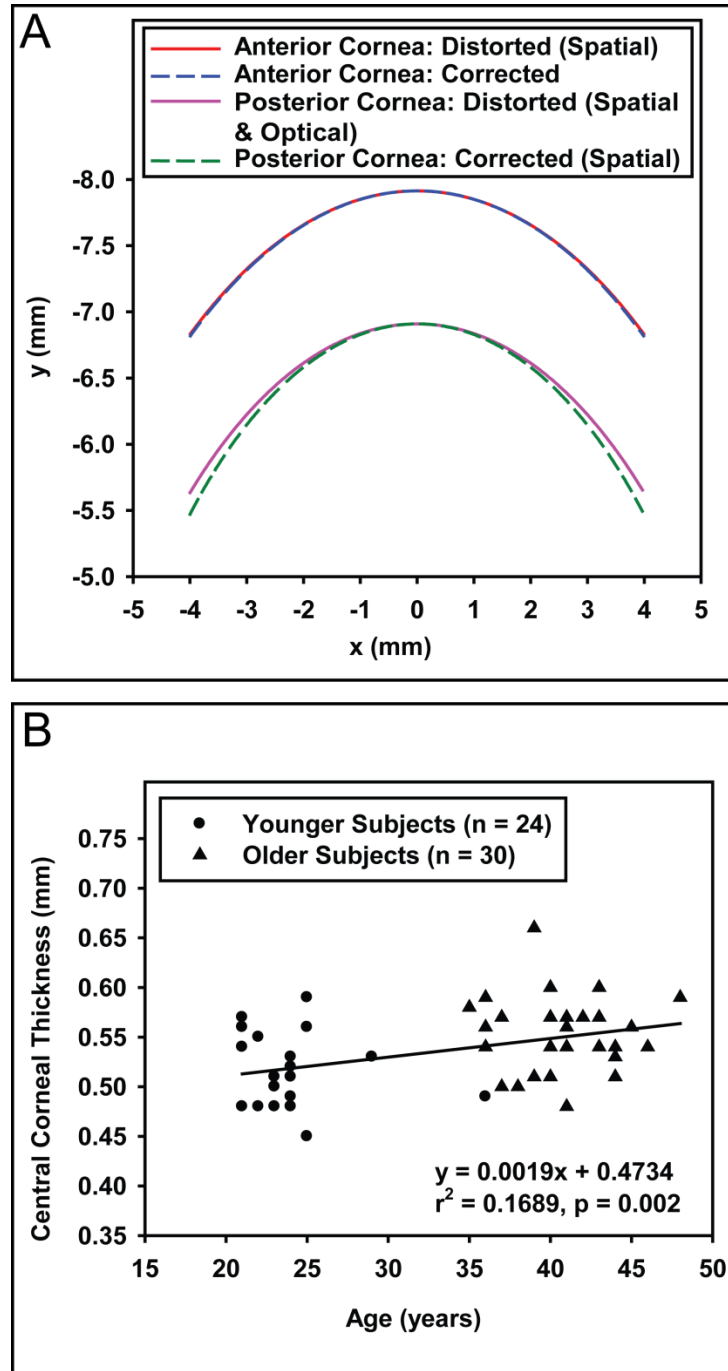
Mean, standard deviation, median, maximum and minimum values of the distortion corrected corneal radii and central thicknesses from the two subject groups are listed in Table 5.5. Corneal surface radii of curvature and central thickness values were normally distributed in both subject groups based on the Shapiro-Wilk test ($p > 0.05$). There was a statistically significant difference between mean posterior corneal radius of curvature ($t = -2.035$, $p = 0.048$, independent sample t-test) and mean central corneal thickness ($t = -3.863$, $p < 0.0001$, independent sample t-test) between the two subject groups. Figure 5.4 B shows the increase in central corneal thickness with age from this group of subjects. There were no statistically significant age-related relationships for either the anterior or posterior corneal radii of curvature (data not shown).

Table 5.5

Descriptive statistics of the distortion corrected corneal parameters for the younger and older subject groups. Symbols * and † indicate statistically significant difference between the means ($p < 0.05$, independent samples t-test). ARC: anterior corneal radius of curvature; PRC: posterior corneal radius of curvature; CT: central corneal thickness.

Table 5.5

Subjects	Measured Parameters	Descriptive Statistics (mm)				
		Mean	**SD**	**Median**	**Maximum**	**Minimum**
Young Subjects (n = 24)	ARC	7.701	0.275	7.666	8.296	7.218
	PRC	6.528*	0.304	6.486	7.260	6.053
	CT	0.514†	0.035	0.512	0.592	0.454
Older Subjects (n = 30)	ARC	7.761	0.213	7.782	8.162	7.234
	PRC	6.679*	0.221	6.708	7.132	6.187
	CT	0.552†	0.036	0.555	0.659	0.483

Intra-session repeatability analysis of the Visante AS-OCT measured anterior and posterior corneal radii of curvature and central corneal thickness was performed for all subjects who had at least two repeats of the AS-OCT scans. Repeatability (intra- and inter-session) was evaluated in terms of a) coefficient of variation, which is the ratio of the standard deviation of the measurements to the mean, b) mean ± SD of the difference between the measurements and c) Intraclass correlation coefficient (ICC). There is a good repeatability for all the three corneal parameters and the repeatability parameters for intra- and inter-session are comparable (Table 5.6).

Table 5.6

Intra-session and inter-session repeatability parameters for various Visante AS-OCT measured parameters. ARC: anterior corneal radius of curvature; PRC: posterior corneal radius of curvature; CT: central corneal thickness; CoV: coefficient of variation; ICC: Intraclass correlation coefficient.

Table 5.6

Repeatability parameters	Intra-session repeatability						Inter-session repeatability					
	Young subjects (n = 24)			Older subjects (n = 30)			Young subjects (n = 15)			Older subjects (n = 3)		
	ARC	PRC	CT	ARC	PRC	CT	ARC	PRC	CT	ARC	PRC	CT
CoV	0.008	0.008	0.019	0.010	0.011	0.020	0.008	0.009	0.023	0.008	0.008	0.035
Mean ± SD difference (mm)	0.093 ± 0.082	0.076 ± 0.063	0.014 ± 0.016	0.109 ± 0.084	0.107 ± 0.077	0.015 ± 0.018	0.090 ± 0.065	0.084 ± 0.045	0.017 ± 0.018	0.084 ± 0.058	0.071 ± 0.063	0.024 ± 0.022
ICC	0.952	0.976	0.915	0.899	0.918	0.910	0.964	0.980	0.886	0.933	0.969	0.921

5.4   Discussion

This study shows the importance of verifying that measurements from clinical instruments do provide accurate quantitative data and provides an example of the approach that can be undertaken to correct measurements if they are found to be inaccurate. Although prior corrections have been described for Visante OCT images (Dunne et al., 2007), application of those methods on the Visante OCT raw images failed to yield accurate corrections.

The RMS error for the measured power of the CL front and back surfaces corrected for optical and spatial distortions (Table 5.4) are not clinically significant and this shows the robustness of the corrections described. The distortion correction equations described are for the central 8 mm diameter only and will not translate to other diameters. These equations are only applicable to the Visante raw images, and for the software version 2.0.1.88 and later if no further changes have been made to the optical and distortion corrections by the manufacturer. If Visante 'raw images' are truly unprocessed images, then the distortion correction described here might work for raw images in later versions of the instrument that do not have hardware changes.

The population data for corneal parameters (mean and SD) from this study is comparable to data from prior population studies (Yuen, He, Aung et al., 2010; Tan, Chong, Tay et al., 2012; Chen, Liu, Tsai et al., 2009). In the current study, the central

corneal thickness was found to increase with age (1.9 µm/year). However, several studies report either no change (Rufer, Schroder, Bader et al., 2007; Hashemi, Yazdani, Mehravaran et al., 2009; Doughty & Zaman, 2000; Siu & Herse, 1993) or a decreasing (Galgauskas, Norvydaite, Krasauskaite et al., 2013; Aghaian, Choe, Lin et al., 2004) trend with age. The relationship between corneal thickness with age was reported to be weak (Galgauskas et al., 2013) or non-significant (Rufer et al., 2007; Doughty and Zaman, 2000). Sample size, ethnicity, age, gender, instrumentation, analysis methods might contribute to the differences between studies.

Intraclass correlation coefficients for all the measured corneal parameters (intra- and inter-session) were greater than 0.88 in both the age groups, which indicates good repeatability. Coefficient of variation and ICC values for corneal thickness were comparable with similar values from a prior AS-OCT study (Li, Leung, Wong et al., 2008).

Although the distortion correction applied to the corneal surfaces appears small, clearly from the CL calibrations (Figure 5.2 C & Figure 5.3 A) there is a systematic and not insignificant distortion introduced to both the anterior and posterior corneal surfaces that can be corrected to yield a higher degree of accuracy. Distorted corneal radii of curvature and thickness were flatter and thicker than after correction, respectively. If the uncorrected radii and thickness values were used for schematic eye optical calculations, they would make the eye relatively more hyperopic. To calculate the error these distorted

values would induce in schematic eye calculations, the refractive state of the normally emmetropic Bennetts & Rabbetts schematic eye (Bennett and Rabbetts, 2007) was calculated using the distorted corneal values. With a distorted anterior corneal radius, the schematic eye was hyperopic with a refractive error of + 1.09 D. With a distorted posterior corneal radius, the schematic eye was myopic with a refractive error of - 0.25 D. With a distorted corneal thickness, the schematic eye was myopic with a refractive error of - 0.04 D. With all the distorted radii and thickness values used together, the schematic eye was hyperopic with a refractive error of + 0.80 D. When compared to the parameters used in the Bennetts and Rabbetts schematic eye, a 0.1 mm error in anterior corneal radius of curvature caused 0.60 D error in refraction; a 0.1 mm error in posterior corneal radius of curvature caused 0.04 D error in refraction; a 0.1 mm error in corneal thickness caused 0.025 D error in refraction. These calculations show that if uncorrected corneal parameters from raw AS-OCT images are used for refractive surgeries, contact lens fitting or optical modeling, this would result in errors in refraction as high as 0.80 D. The corrected corneal radii of curvature and thickness values obtained from the subjects are of a sufficiently high degree of accuracy to allow their use in future schematic eye calculations.

The results from this chapter have demonstrated that spatial and optical distortions of the Visante AS-OCT measured front and back CL radii of curvatures can be corrected with a small residual error of 0.02 mm and 0.01 mm, respectively. Distorted and uncorrected corneal parameters can induce errors in ocular refraction as high as 0.80 D. The Visante AS-OCT measured corneal parameters showed good intra- and inter-

session repeatability. The distortion correction equations provided can be used to correct corneal biometry measurements from Visante AS-OCT images.

Chapter 6 – Predicting Accommodative Response in Young and Pre-presbyopic Eyes Using Schematic Eye Models

6.1   Introduction

Accommodation is measured clinically either as the optical change in power of the eye (accommodative optical response; AOR) or as biometric accommodative changes in the ocular anterior segment (such as changes in lens thickness or changes in lens surface curvatures). Measuring both the accommodative optical and biometric changes is important to fully evaluate the accommodative ability of an eye or of an accommodation restoration concept. However, currently, it is not possible to measure both the accommodative optical and biometric changes with a single clinical instrument.

Prior studies in young and pre-presbyopic subjects showed that ultrasound biomicroscopy (UBM) measured anterior segment parameters can be used to predict the AOR based on linear regressions between the individual biometric parameters and the AOR (Ramasubramanian & Glasser, 2014a; Ramasubramanian & Glasser, 2014d). On average, from population data, these predictions can be achieved with a standard deviation of less than 0.55 D in both subject populations. The limitation of using linear regressions from only a single biometric parameter is that this does not utilize all the other biometric changes that occur during accommodation. Accommodative changes in anterior chamber depth, lens thickness and anterior and posterior lens radii of curvature

occur simultaneously and are strongly linearly correlated with each other (Ramasubramanian & Glasser, 2014c; Ramasubramanian & Glasser, 2014d; Bolz et al., 2007; Ostrin et al., 2006). This might suggest that predictions could be strengthened if all the biometric parameters that change with accommodation could be used together. One approach might be to use a multiple regression model. However, because of the strong linear correlations among the individual biometry parameters (multicollinearity), a multiple regression model will have large prediction errors and therefore unsuitable to use.

Another approach to use all the anterior segment biometry parameters together might be to use paraxial schematic eye models. Schematic eyes provide information on the optical properties of the eye and are constructed using corneal surface radii of curvatures, corneal thickness, anterior chamber depth, lens surface radii of curvatures and thickness, axial length and the refractive indices of the various optical media. Schematic eye modeling generally includes calculations of surface and equivalent powers of the cornea, lens and the eye and other optical parameters such as cardinal points and entrance and exit pupil positions. Paraxial schematic eyes use simplified Gaussian optics equations, axial biometry parameters and radii of curvatures of the paraxial regions of the cornea and lens; therefore, paraxial schematic eyes are generally useful only for axial optical parameters such as refraction and accommodation, but not for spherical aberration or other aberrations, for example. These simplified paraxial calculations can be performed using four surface (anterior and posterior cornea and anterior and posterior lens) schematic eyes and using a single lens equivalent refractive index value. More

generally, schematic eyes can be useful for understanding optical image quality (Li et al., 2000), in the design of intraocular implants (Preussner et al., 2005) and for customized refractive surgery (MacRae et al., 1999).

Prior accommodation dependent schematic eye models have biometric and optical parameters for just a few accommodative states (Bennett and Rabbetts, 2007; Navarro et al., 1985). No prior accommodation dependent schematic eye models have been used to calculate refraction and AOR from measured accommodative biometric changes and to compare them with the measured refractions and AOR from the same subjects. Furthermore, there are no accommodation dependent schematic eye models for older eyes with low accommodative amplitudes.

The current study was undertaken; a) to construct schematic eye models for different accommodative states for each individual subject in the young and pre-presbyopic populations, b) to use the schematic eyes to calculate the refractive state and the accommodative optical response, c) to compare the calculated refraction and AOR with Grand Seiko autorefractor measured refraction and AOR from the subjects in these two populations, d) to construct individual schematic eyes using average accommodative changes in UBM biometry parameters calculated for the young and pre-presbyopic populations to calculate refraction and AOR , and e) to compare the prediction errors between schematic eyes and individual linear regressions in the two subject populations (Ramasubramanian & Glasser, 2014a; Ramasubramanian & Glasser, 2014d). A

statistically significant linear regression between schematic eye refraction and GS measured refraction or AOR with high r^2 values would indicate that the schematic eye might offer accurate predictions of refraction or AOR. Smaller r^2 values indicate variability in the data and impact the accuracy of schematic eye prediction. Higher r^2 values even with slopes different from one still permit linear regression equation to be used to predict actual measured refractions and AOR from calculated schematic eyes.

6.2   Methods

Biometric Data for Schematic Eye Modeling

Ocular biometric data from 24 young and 24 pre-presbyopic subjects from prior studies (Ramasubramanian & Glasser, 2014b; Ramasubramanian & Glasser, 2014c; Ramasubramanian & Glasser, 2014d) were used to construct accommodative schematic eye models. Briefly, corneal anterior and posterior radii of curvature and central corneal thickness were measured from Visante anterior segment optical coherence tomography (AS-OCT) images and were corrected for spatial and optical distortions (Ramasubramanian & Glasser, 2014b). Anterior chamber depth (ACD), lens thickness (LT) and anterior and posterior lens radii of curvature (ALRC & PLRC) were measured from distortion corrected UBM images as the eyes accommodated to various stimulus demands (Ramasubramanian & Glasser, 2014c; Ramasubramanian & Glasser, 2014d). Axial length was measured using A-scan ultrasound (Ramasubramanian & Glasser, 2014c; Ramasubramanian & Glasser, 2014d). Standard values for refractive indices for various ocular media were those used in the Bennett and Rabbetts schematic eye model (cornea: 1.376; aqueous/vitreous: 1.336 and lens: 1.422) (Bennett and Rabbetts, 2007). All the measured AS-OCT, UBM and A-scan data were stored in Matlab (MathWorks, Natick, MA) structures and saved as Matlab '.mat' files which were used for schematic eye calculations. Static AORs were measured in these subjects using a Grand Seiko (GS) autorefractor as the eyes accommodated to various stimulus demands (Ramasubramanian & Glasser, 2014a; Ramasubramanian & Glasser, 2014d). Subjects with refractive errors were corrected with soft contact lenses and GS measurements were recorded over the

232

contact lenses to achieve emmetropic refractions for the far target (baseline). Measurements from GS, UBM and A-scan were recorded from each eye for the same accommodative stimulus demands so that comparisons could be made between GS measured and schematic eye calculated refraction and AOR. For comparisons with the schematic eye, all the GS refraction measurements were adjusted for the contact lens prescription by adding the contact lens power to the GS measurements to get the uncorrected, underlying refractive error of the eyes. Henceforth, all GS measured refractions adjusted for contact lens prescription will be referred to as adjusted GS refractions.

Individual Paraxial Schematic Eye Model

Individual, four surface paraxial schematic eye models were constructed from the measured ocular biometry parameters for each subject in the young and pre-presbyopic subject populations. A Matlab program was written to read in the '.mat' files containing all the ocular biometry parameters and calculate schematic eye models using equations 1 to 22 (listed in the Appendix on page 300) for each accommodative stimulus demand for each subject in the young and pre-presbyopic subject populations. Absolute refractions and AORs relative to the baseline 0 D stimulus demand were calculated for each stimulus demand from the schematic eye models. Schematic eye calculated refractions and AORs were compared with adjusted GS refractions and AORs. All the calculated schematic eye parameters were stored as '.mat' files for further analysis.

The lens refractive index is one parameter required for the schematic eye calculations and it is potentially variable between subjects, but it cannot readily be measured. The natural lens has a gradient refractive index and the lens equivalent refractive index is the single refractive index value that achieves a lens of the same optical power as the lens of the same shape with a gradient refractive index. As mentioned above, the initial lens equivalent refractive index chosen for all the individual schematic eyes was a constant value of 1.422 (Bennett and Rabbetts, 2007). It is unlikely that every eye would have the same lens equivalent refractive index and, furthermore, there is a possibility that the lens equivalent refractive index could change systematically with age and accommodation (Jones et al., 2007). For these reasons, in addition to using the constant value of 1.422 described above, individual lens equivalent refractive index values were calculated for each subject, for each accommodative stimulus demand. To do this, the standard lens equivalent refractive index of 1.422 was used as the starting index for the baseline stimulus demand (0 D). Schematic eye calculations were performed using the custom developed Matlab program described above. The difference between the schematic eye calculated and adjusted GS refraction for the baseline 0 D stimulus was calculated and the starting lens equivalent refractive index was iterated in 0.00001 steps until the schematic eye calculated refraction matched the adjusted GS refraction. The calculated lens refractive index value that achieved the matching schematic eye and adjusted GS refraction at baseline was stored in a Matlab array. This calculated lens equivalent refractive index at baseline served as the starting index for the other stimulus demands and the refractive index was iterated to match the adjusted GS refraction as described above for each stimulus demand. The calculated lens equivalent refractive

indices for all stimulus demands for each subject were stored in '.mat files' for further analysis.

It is of interest to establish if the measured accommodative biometry changes can be used in conjunction with the calculated schematic eyes to try to predict the accommodative response from the younger and pre-presbyopic populations. The approach taken was to take the individual schematic eyes described above and to apply to each of them the average accommodative changes in UBM measured biometry parameters for each stimulus demand. Schematic eye refractions and AORs was recalculated and compared with the adjusted GS refraction and AORs from the two populations. In this method, UBM measured parameters (ACD, LT, ALRC & PLRC) for each accommodative stimulus demand were subtracted from the corresponding parameters at baseline (0 D) in each individual subject to calculate the accommodative change in these parameters. The resulting accommodative changes in UBM measured biometry parameters were averaged across all subjects for each stimulus demand in the young (Table 6.1) and pre-presbyopic populations (Table 6.2) separately. For the young and the pre-presbyopic populations, individual accommodative schematic eyes for each subject for each stimulus demand were then calculated. This was done using each subject's individual corneal thickness, corneal surface radii of curvatures and axial length and then the calculated average accommodative changes in UBM biometry parameters were added to each subjects' baseline biometry values. The iteratively calculated baseline lens equivalent refractive index for each subject as described above was used for these calculations. Individual schematic eye calculated refractions and AORs were compared

with adjusted GS refractions and AORs for both the young and pre-presbyopic populations.

Table 6.1

Average accommodative change in UBM measured biometry parameters from 24 young subjects. Corneal parameters from Visante and axial length from A-scan are average values from the baseline (0 D) stimulus demand. SD: standard deviation; AOR: accommodative optical response; ARC: anterior corneal radius of curvature; CT: corneal thickness; PRC: posterior corneal radius of curvature; ACD: anterior chamber depth; LT: lens thickness; ALRC: anterior lens radius of curvature; PLRC: posterior lens radius of curvature; AL: axial length.

Table 6.1

Stimulus Demand (D)	Average Accommodative Change in UBM Measured Biometry Parameters (mm) for Young Subjects							
	ACD	SD of ACD	LT	SD of LT	ALRC	SD of ALRC	PLRC	SD of PLRC
0	0.00	0.00	0.00	0.00	0.00	0.00	0.00	0.00
1	-0.04	0.03	0.07	0.05	-0.59	0.46	-0.11	0.14
2	-0.11	0.04	0.16	0.05	-1.82	0.70	-0.31	0.20
3	-0.18	0.05	0.24	0.07	-2.68	0.87	-0.57	0.25
4	-0.23	0.05	0.30	0.06	-3.42	1.01	-0.78	0.26
5	-0.26	0.06	0.36	0.07	-3.98	1.11	-0.91	0.36
6	-0.26	0.07	0.39	0.07	-4.26	1.20	-1.00	0.38

Table 6.2

Average accommodative change in UBM measured biometry parameters from 24 pre-presbyopic subjects. The number of subjects whose biometry parameters were averaged for each stimulus demand were: 0 D to 3 D: 24, 3.5 to 4 D: 23, 5 D: 19 and 6 D: 15. Corneal parameters from Visante and axial length from A-scan are average values from the baseline (0 D) stimulus demand. SD: standard deviation; AOR: accommodative optical response; ARC: anterior corneal radius of curvature; CT: corneal thickness; PRC: posterior corneal radius of curvature; ACD: anterior chamber depth; LT: lens thickness; ALRC: anterior lens radius of curvature; PLRC: posterior lens radius of curvature; AL: axial length.

Table 6.2

Stimulus Demand (D)	Average Accommodative Change in UBM Measured Biometry Parameters (mm) for Pre-presbyopic Subjects							
	ACD	SD of ACD	LT	SD of LT	ALRC	SD of ALRC	PLRC	SD of PLRC
0	0.00	0.00	0.00	0.00	0.00	0.00	0.00	0.00
0.25	0.00	0.02	0.02	0.03	-0.09	0.44	0.08	0.15
0.50	-0.01	0.03	0.03	0.03	-0.29	0.45	0.08	0.15
0.75	-0.02	0.03	0.04	0.02	-0.50	0.83	0.11	0.12
1.00	-0.04	0.04	0.06	0.03	-0.66	0.66	0.04	0.18
1.25	-0.05	0.04	0.07	0.03	-0.97	0.76	0.05	0.21
1.50	-0.06	0.05	0.09	0.04	-1.00	0.97	-0.03	0.18
1.75	-0.07	0.05	0.10	0.03	-1.27	1.02	-0.05	0.23
2.00	-0.09	0.06	0.11	0.04	-1.52	0.95	-0.08	0.24
2.50	-0.10	0.06	0.13	0.06	-1.62	1.01	-0.15	0.27
3.00	-0.11	0.06	0.15	0.06	-1.85	0.88	-0.10	0.32
3.50	-0.12	0.07	0.16	0.07	-2.17	1.21	-0.13	0.39
4.00	-0.12	0.07	0.17	0.07	-2.36	1.37	-0.12	0.38
5.00	-0.12	0.09	0.19	0.08	-2.39	1.20	-0.08	0.46
6.00	-0.13	0.09	0.21	0.09	-2.85	1.30	-0.18	0.40

6.3 Results

The mean ± standard deviation (SD), median age and age range of the young subjects was mean: 24.15 ± 3.03 years; median: 24 years; range: 21 to 36 years and for the pre-presbyopic subjects was mean: 40.80 ± 3.08; median: 41 years; range: 36 to 46 years.

Data from a young and a pre-presbyopic subject showing comparisons between individual schematic eye calculated and adjusted GS refraction and AOR is shown in Figure 6.1. The individual schematic eyes used the standard lens equivalent refractive index of 1.422. For the young subject, there is a linear change in GS measured refraction with increasing stimulus demand. However, the individual schematic eye calculated refraction is consistently more myopic than the adjusted GS measurements (Figure 6.1 A). The individual schematic eye AOR increasingly overestimates the GS measured AOR with increasing stimulus demands for this subject (Figure 6.1 B). In this young subject, each GS data point and the measured ocular biometry parameters used for the individual schematic eye are an average of 9 measurements from 3 different trials. For the pre-presbyopic subject, there is a reasonably systematic myopic change in adjusted GS refraction with increasing stimulus demand. The individual schematic eye calculated refraction is relatively less myopic than the adjusted GS measurements and asymptotes at higher stimulus demands (Figure 6.1 C). The individual schematic eye calculated AOR in the pre-presbyopic subject is initially higher than the GS measured AOR and saturates at

higher stimulus demands (Figure 6.1 D). In this pre-presbyopic subject, each GS data point and the ocular biometry parameters used for the individual schematic eye calculations is an average of 3 measurements from a single trial.

Figure 6.1

(A) Comparison of a calculated individual schematic eye and the Grand Seiko (GS) measured refraction from a 23 year old subject. (B) Comparison of the GS measured and the individual schematic eye calculated stimulus-response function. (C) Comparison of the individual schematic eye calculated and the GS measured refractions from a 36 year old pre-presbyopic subject. (D) Comparison of the GS measured and the individual schematic eye calculated stimulus-response function from the same pre-presbyopic subject. The schematic eye data shown here were calculated using the standard equivalent lens refractive index of 1.422. Grand Seiko data error bars represent standard deviations from 9 measurements from 3 different trials.
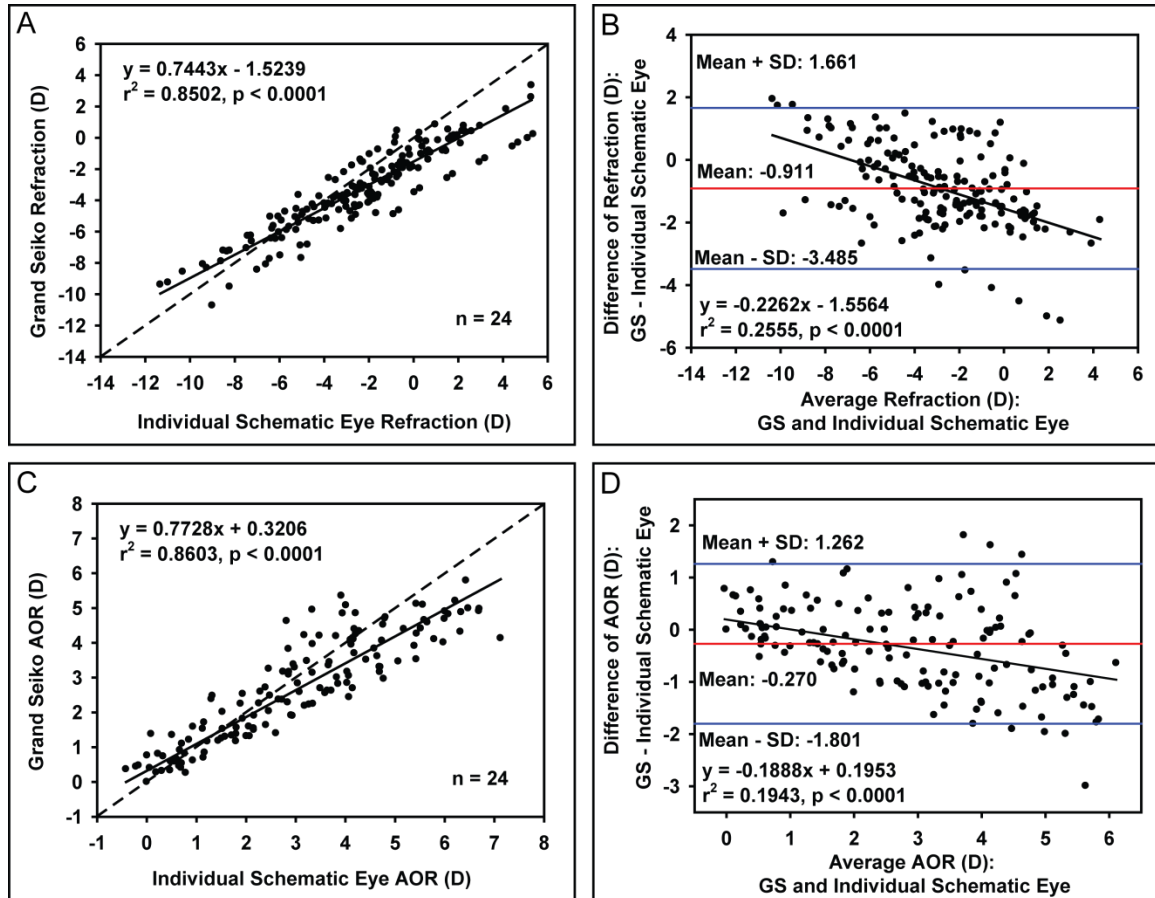
Figure 6.1
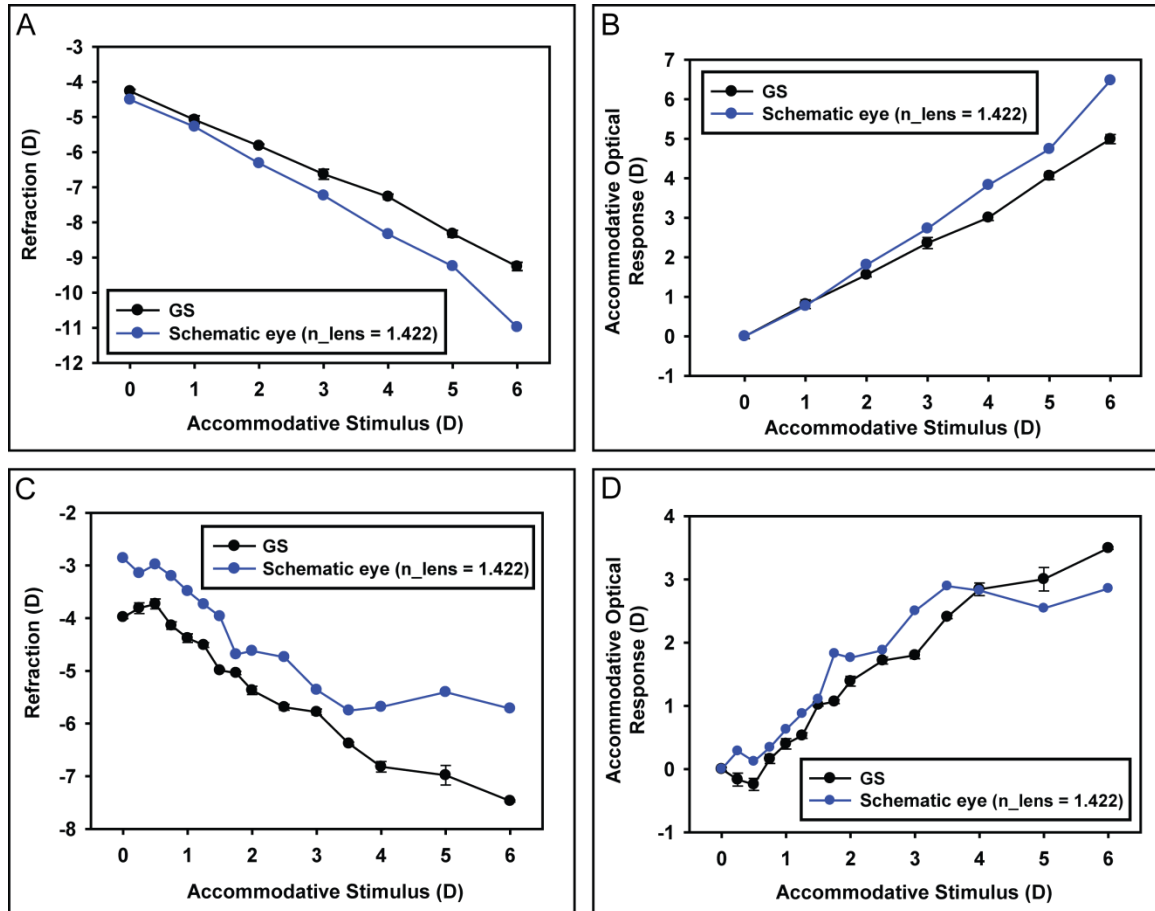
Comparison of individual schematic eye calculated and adjusted GS refractions from all stimulus demands from the 24 young subjects showed a linear relationship with an r^2 value of 0.85 indicating that the individual schematic eyes, in general, could provide reasonably good predictions of refraction (Figure 6.2 A). Bland-Altman analysis showed that individual schematic eye refractions were on average hyperopic by 0.91 D than adjusted GS refractions with a statistically significant linear relationship (Figure 6.2 B). The schematic eye calculated accommodative optical response was underestimated at lower response levels and overestimated at higher response levels compared to GS measured accommodation (Figure 6.2 C) and this overestimation showed a linear increase as a function of increasing AOR (Figure 6.2 D).

Figure 6.2

(A) Comparison of individual schematic eye calculated and Grand Seiko (GS) measured refractions from 24 young subjects. (B) Bland-Altman comparison of refractions between GS and individual schematic eyes showing a statistically significant linear trend. (C) Comparison of accommodative optical response (AOR) between GS and individual schematic eyes. (D) Bland-Altman comparison of AOR between GS and individual schematic eyes showing a systematic linear overestimation at higher AORs.
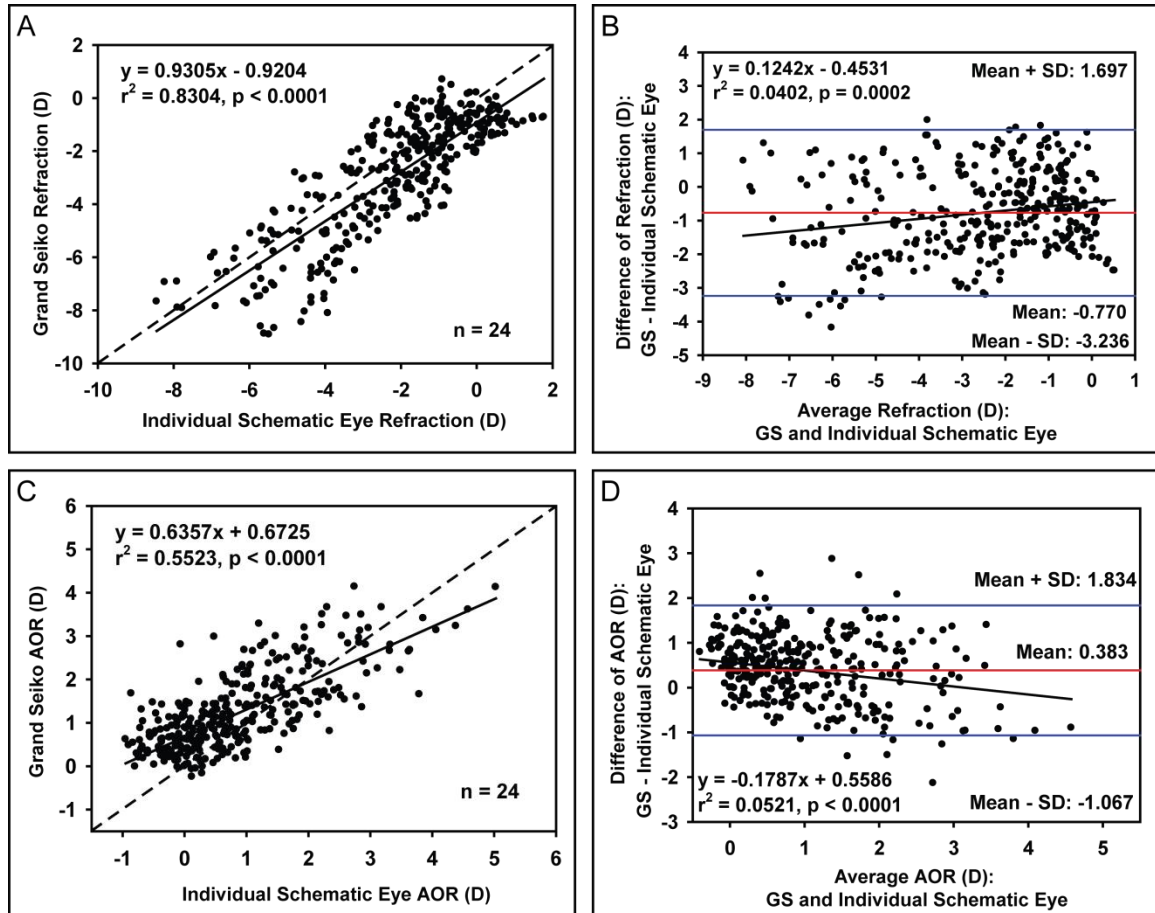
Figure 6.2

In the 24 pre-presbyopic subjects, there was a linear relationship between individual schematic eye refractions and GS refractions with an r^2 value of 0.83 (Figure 6.3 A). The r^2 values for refractions were comparable between the young and pre-presbyopic subjects. Most of the schematic eye measured refractions were more hyperopic than adjusted GS refractions and the Bland-Altman analysis showed a mean difference of -0.77 D with a statistically significant linear trend (Figure 6.3 B). The individual schematic eye models underestimated the AOR at lower response levels and overestimated the AOR at higher response levels compared to GS measured AOR (Figure 6.3 C). The r^2 values for AOR were smaller than for refraction which means that the predictions of AOR are worse than for refraction. Bland-Altman analysis showed that the individual schematic eye underestimated the AOR, on average, by 0.38 D or more with a statistically significant linear trend (Figure 6.3 D).

Figure 6.3

(A) Comparison of individual schematic eye calculated and Grand Seiko (GS) measured refractions from 24 pre-presbyopic subjects. (B) Bland-Altman comparison of refractions between GS and individual schematic eyes showing a statistically significant linear trend. (C) Comparison of accommodative optical response (AOR) between GS and individual schematic eyes. (D) Bland-Altman comparison of AOR between GS and individual schematic eyes showing a systematic linear overestimation by the individual schematic eyes for higher accommodative responses.
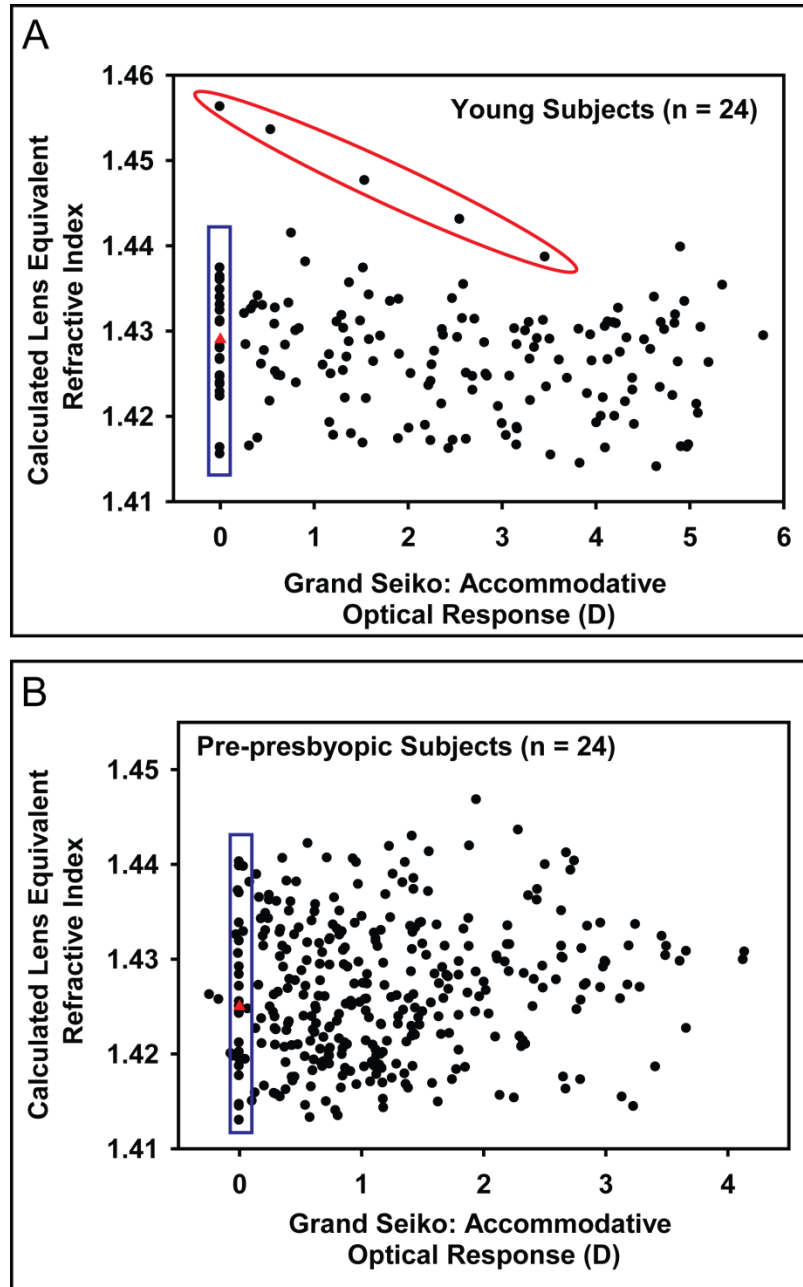
Figure 6.3

The iteratively calculated lens equivalent refractive index values when plotted as a function of the GS measured AOR showed no trend as a function of the AOR for either the young (Figure 6.4 A) or the pre-presbyopic subjects (Figure 6.4 B). The mean ± SD of the calculated baseline lens refractive index values in the young and pre-presbyopic subject populations was 1.428 ± 0.006 and 1.425 ± 0.008, respectively. The mean ± SD of the calculated lens refractive index values from all stimulus demands was 1.427 ± 0.007 in both the young and pre-presbyopic subject populations. So, to determine if altering the schematic eye lens equivalent refractive index improved the predictive ability of the individual schematic eye models, in addition to using the fixed standard lens equivalent refractive index value of 1.422 as described above, schematic eye calculations were also performed using two additional lens equivalent refractive index methods: i) using the lens equivalent refractive index calculated from each individual subject's baseline refraction for each individual subject and ii) using the average lens equivalent refractive index calculated from all subject's baseline refraction for all subjects (young: 1.428; pre-presbyopic: 1.425).

Figure 6.4

Calculated lens equivalent refractive index plotted as a function of GS measured AOR in young (A) and pre-presbyopic subjects (B). Data points circled in red are from the same subject shown in Figure 6.4 and are not included in the calculation of the average refractive index. Data points within the blue box represent the lens refractive index values for baseline. Red triangles represent the average calculated refractive index at baseline.

Figure 6.4

Comparison of adjusted GS refractions and AOR and individual schematic eye calculated refraction and AOR for the different lens equivalent refractive index calculations for a young and a pre-presbyopic subject are shown in Figure 6.5. Data from the same subjects shown in Figure 6.1 are plotted here for comparison. For the young subject, the refraction for the subject's calculated baseline lens refractive index of 1.420 is closer to the adjusted GS curves than for other refractive index values (Figure 6.5 A). The AOR curves for the standard lens equivalent refractive index of 1.422 is closer to the adjusted GS curves (Figure 6.5 B). For the mean baseline lens refractive index of 1.428, refraction is more myopic and produces a relatively larger AOR. For the pre-presbyopic subject, the mean baseline lens equivalent refractive index of 1.425, in general, brought the refraction and AOR curves closer to adjusted GS curves than for the other lens refractive index values (Figure 6.5 C and Figure 6.5 D).

Figure 6.5

Comparison of Grand Seiko (GS) measured and individual schematic eye calculated refractions (A) and AORs (B) for three lens refractive index values from a 23 year old subject. Comparison of GS measured and individual schematic eye calculated refractions (C) and AORs (D) from a 36 year old pre-presbyopic subject for three lens refractive index values. Blue, red and green curves represent the data from the standard, individual baseline and averaged population baseline lens equivalent refractive index values respectively.

Figure 6.5
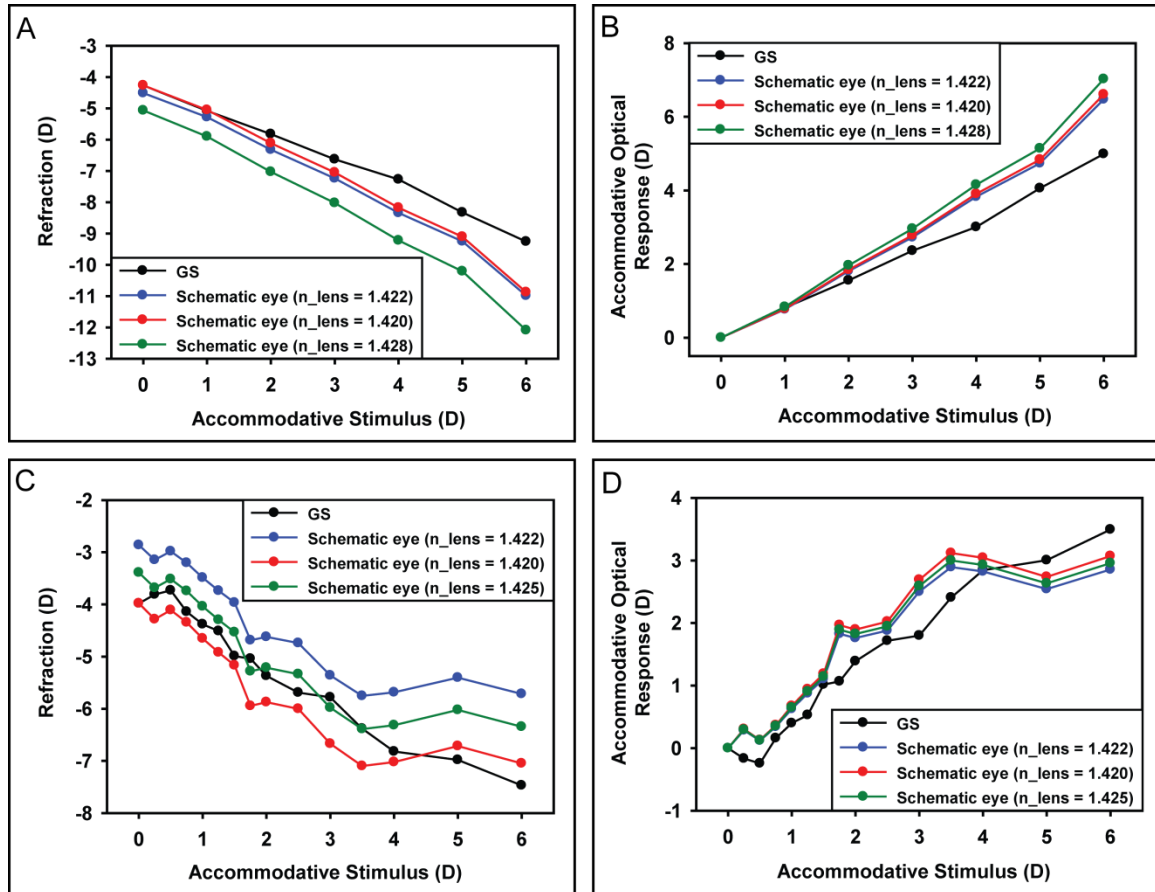
Linear regression parameters and Bland-Altman analyses for comparisons between adjusted GS refractions and AORs and individual schematic eye refractions and AORs calculated using three different lens equivalent index methods for young subjects are shown in Table 6.3. The r^2 values for the linear regressions ranged from 0.85 to 0.89 for refraction. Root mean square (RMS) errors of refraction calculated relative to the 1:1 line were, on average, 1 D or more. For AOR, the mean RMS errors calculated relative to the 1:1 line ranged from 0.77 to 1.04 D. The RMS errors show that predictions for AOR are, on average, better than for refraction. In pre-presbyopic subjects, the RMS error of refraction calculated relative to the 1:1 line was smaller when the individual subject's calculated baseline lens equivalent refractive index was used than for other refractive index methods (Table 6.4). For AOR, all three lens refractive index methods had comparable RMS errors. Overall, in pre-presbyopic subjects, using the individual subject's calculated baseline lens refractive index offered good predictions of refraction and AOR. The purpose of constructing individual schematic eye models using three different lens equivalent refractive index values was to see if better predictions of refraction and AOR could be achieved. However, no single lens equivalent refractive index method could provide better predictions of both refraction and AOR for young subjects.

Individual schematic eye calculated refractions and AORs in individual subjects were corrected using linear regression parameters (slopes and intercepts) for refraction and AOR, respectively, for each of the three lens equivalent refractive index methods in young (Table 6.3) and pre-presbyopic subjects (Table 6.4). Root mean square (RMS)

257

errors relative to the 1:1 line after the linear regression correction were calculated for refraction and AOR. For both the young and the pre-presbyopic subjects, the RMS errors after linear regression correction, were in general, smaller than before correction for refraction and AOR using all three lens equivalent refractive index methods.

Table 6.3

Parameters from linear regressions and Bland-Altman analyses comparing Grand Seiko measured and individual schematic eye calculated refractions and accommodative optical responses (AORs) using the three different lens equivalent refractive index methods for the young subject population. RMS: root mean square relative to 1:1 line; n_{lens} = lens equivalent refractive index.

Table 6.3

Parameters			Grand Seiko vs. Individual Schematic Eye (Young Subjects, n = 24)					
			Refraction (D)			AOR (D)		
			$n_{lens} =$ 1.422	$n_{lens} =$ subject's baseline index	$n_{lens} =$ 1.428	$n_{lens} =$ 1.422	$n_{lens} =$ subject's baseline index	$n_{lens} =$ 1.428
Linear Regression		Slope	0.744	0.803	0.698	0.771	0.655	0.688
		Intercept	-1.524	-0.212	-0.653	0.326	0.446	0.367
		r^2	0.858	0.886	0.847	0.859	0.810	0.843
		p value	< 0.0001	< 0.0001	< 0.0001	< 0.0001	< 0.0001	< 0.0001
Bland - Altman Analysis		Mean Difference (D)	-0.912	0.544	0.493	-0.270	-0.544	-0.529
		Upper limit (D)	1.662	2.674	3.403	1.262	1.587	1.356
		Lower limit (D)	-3.485	-1.587	-2.417	-1.801	-2.675	-2.414
Mean RMS error before correction (D)			1.42	1.04	1.28	0.77	1.04	0.98
Mean RMS error after linear regression correction (D)			0.84	0.79	0.87	0.58	0.66	0.61

Table 6.4

Parameters from linear regressions and Bland-Altman analyses comparing Grand Seiko measured and individual schematic eye calculated refractions and accommodative optical responses (AORs) using the three different lens equivalent refractive index methods for the pre-presbyopic subject population. RMS: root mean square relative to 1:1 line; n_{lens} = lens equivalent refractive index.

Table 6.4

Parameters			Grand Seiko vs. Individual Schematic Eye (Pre-presbyopic Subjects, n = 24)					
			Refraction (D)			Accommodative Optical Response (D)		
			$n_{lens} = 1.422$	$n_{lens} =$ subject's baseline index	$n_{lens} = 1.425$	$n_{lens} = 1.422$	$n_{lens} =$ subject's baseline index	$n_{lens} = 1.425$
Linear Regression		Slope	0.931	0.854	0.911	0.635	0.585	0.611
		Intercept	-0.920	-0.707	-0.456	0.673	0.679	0.676
		r^2	0.689	0.899	0.673	0.552	0.539	0.551
		p value	< 0.0001	< 0.0001	< 0.0001	< 0.0001	< 0.0001	< 0.0001
Bland - Altman Analysis		Mean Difference (D)	-0.770	-0.326	-0.215	0.383	0.328	0.353
		Upper limit (D)	1.697	1.238	2.324	1.834	1.894	1.848
		Lower limit (D)	-3.236	-1.891	-2.755	-1.068	-1.239	-1.141
Mean RMS error before correction (D)			1.31	0.80	1.20	0.78	0.80	0.79
Mean RMS error after linear regression correction (D)			1.13	0.66	1.16	0.60	0.60	0.60

Mean absolute differences between GS measured and individual schematic eye calculated AORs after linear regression correction for the three different lens equivalent index methods in young subjects are listed in Table 6.5. Prediction results from individual linear regressions of UBM measured biometry parameters from a prior study are shown for comparison. The mean difference between measured and predicted AOR was smaller from the schematic eyes than from individual biometry parameters, indicating better prediction with schematic eyes in young subjects. For pre-presbyopic eyes, AOR predictions with schematic eyes were comparable to those from individual biometry parameters (Table 6.6).

Table 6.5

Comparison of absolute differences between Grand Seiko (GS) measured accommodative optical response (AOR) and predicted AOR from schematic eyes and using individual linear regressions of UBM biometry parameters in young subjects from Chapter 3. ACD: anterior chamber depth; LT: lens thickness; ALRC: anterior lens radius of curvature; PLRC: posterior lens radius of curvature; ASL: anterior segment length; SD: standard deviation; n_{lens}: lens equivalent refractive index.

Table 6.5

Prediction Method	Biometry Parameters Used	Absolute Difference between GS Measured AOR and Predicted AOR (D) in Young Subjects			
		Mean	SD	Minimum	Maximum
Linear Regression	ACD	0.62	0.44	0.02	1.87
	LT	0.56	0.46	0.00	2.57
	ALRC	0.74	0.54	0.00	3.08
	PLRC	0.75	0.56	0.01	3.33
	ASL	0.91	0.65	0.00	3.29
Schematic Eyes	All parameters $n_{lens} = 1.422$	0.50	0.39	0.00	2.13
	All parameters $n_{lens} =$ subject's baseline index	0.57	0.46	0.00	3.01
	All parameters $n_{lens} = 1.428$	0.52	0.41	0.00	2.15

Table 6.6

Comparison of absolute differences between Grand Seiko (GS) measured accommodative optical response (AOR) and predicted AOR from schematic eyes and using individual linear regressions of UBM biometry parameters in pre-presbyopic subjects from Chapter 4. ACD: anterior chamber depth; LT: lens thickness; ALRC: anterior lens radius of curvature; PLRC: posterior lens radius of curvature; ASL: anterior segment length; SD: standard deviation; n_{lens}: lens equivalent refractive index.

Table 6.6

| Prediction Method	Biometry Parameters Used	Absolute Difference between GS Measured AOR and Predicted AOR (D) in Pre-presbyopic Subjects			
		Mean	**SD**	**Minimum**	**Maximum**
Linear Regression	ACD	0.53	0.42	0.01	2.22
	LT	0.41	0.33	0.00	1.70
	ALRC	0.50	0.42	0.00	2.22
	PLRC	0.62	0.47	0.01	2.75
	ASL	0.60	0.49	0.00	2.42
Schematic Eyes	All parameters $n_{lens} = 1.422$	0.50	0.37	0.00	2.17
	All parameters n_{lens} = subject's baseline index	0.51	0.38	0.00	2.16
	All parameters $n_{lens} = 1.425$	0.50	0.37	0.00	2.17

Comparisons of refraction and AOR between individual schematic eyes constructed using the average change in UBM biometry parameters and the GS measurements in young subjects is shown in Figure 6.6. The individual schematic eye refractions and adjusted GS refractions had a statistically significant linear relationship with an r^2 value of 0.90 (Figure 6.6 A). Bland-Altman analysis showed a mean difference of 0.646 D with a statistically significant linear trend (Figure 6.6 B). The schematic eye calculated AOR was underestimated at lower response levels and overestimated at higher response levels compared to GS measured AOR (Figure 6.6 C) and this overestimation showed a linear increase as a function of increasing AOR (Figure 6.6 D). The RMS errors of refraction and AOR relative to the 1:1 line for the young subjects were 0.95 D and 0.96 D, respectively.

Figure 6.6

(A) Comparison of refraction between Grand Seiko (GS) measurements and individual schematic eyes calculated from the average change in UBM biometry measurements from 24 young subjects. (B) Bland-Altman comparison of refraction between GS and individual schematic eyes showing a statistically significant linear trend. (C) Comparison of accommodative optical response (AOR) between GS and individual schematic eyes. (D) Bland-Altman comparison of AOR between GS and individual schematic eyes showing a systematic linear overestimation.

Figure 6.6
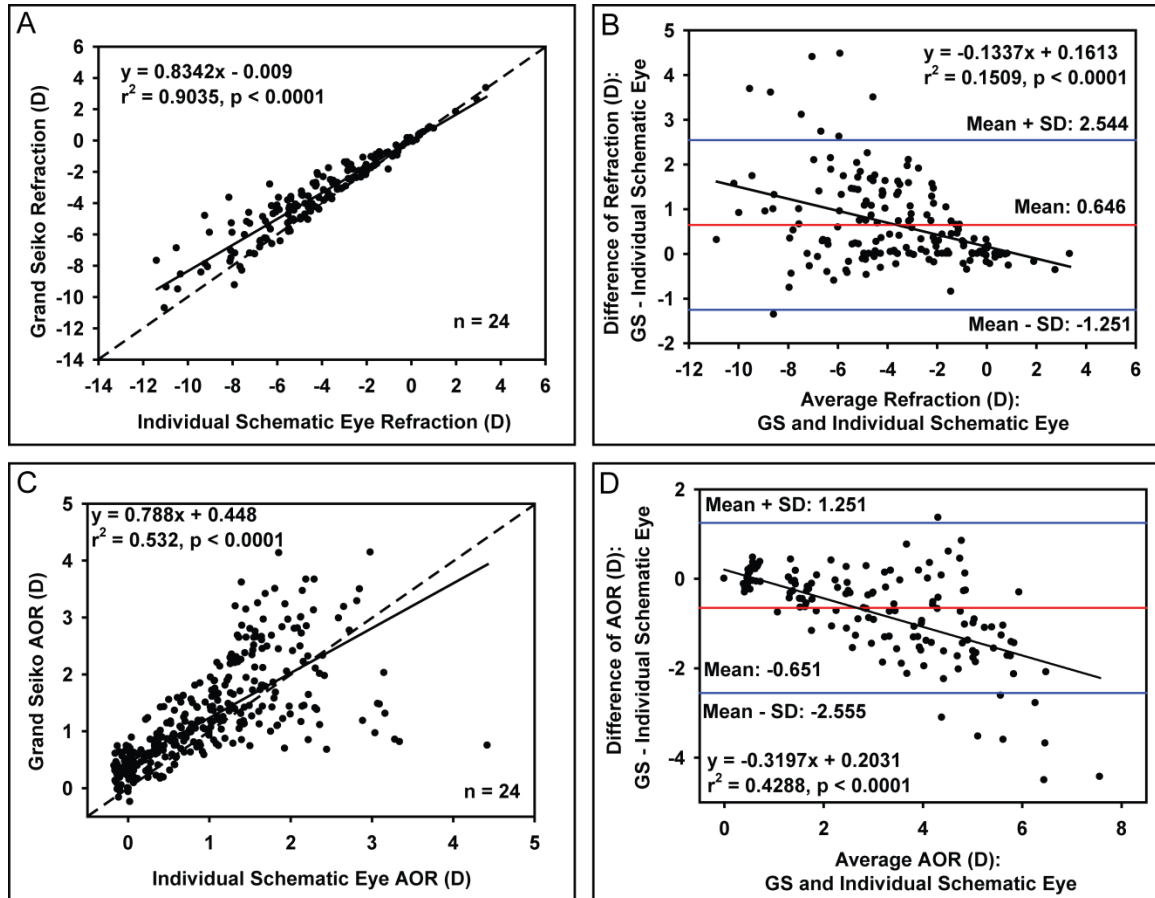
270

Comparisons of refraction and AOR between individual schematic eyes constructed using the average change in UBM biometry parameters and the GS in pre-presbyopic subjects is shown in Figure 6.7. The individual schematic eye refractions were linearly correlated with the adjusted GS refractions with a slope 1.02 (Figure 6.7 A). Bland-Altman analysis showed a mean difference of -0.188 D between schematic eye and adjusted GS refractions (Figure 6.7 B). As observed in young subjects, the schematic eye calculated AOR was underestimated at lower response levels and overestimated at higher response levels compared to GS measured AOR (Figure 6.7 C). Bland-Altman analysis showed a mean difference of 0.252 D between schematic eye and GS AORs (Figure 6.7 D). The RMS errors of refraction and AOR relative to the 1:1 line for the pre-presbyopic subjects were 0.69 D and 0.63 D, respectively.

Figure 6.7

(A) Comparison of refraction between Grand Seiko (GS) and individual schematic eyes calculated from the average change in UBM biometry measurements from 24 pre-presbyopic subjects. (B) Bland-Altman comparison of refraction between GS and individual schematic eyes showing a statistically significant linear trend. (C) Comparison of accommodative optical response (AOR) between GS and individual schematic eyes. (D) Bland-Altman comparison of AOR between GS and individual schematic eyes.

Figure 6.7
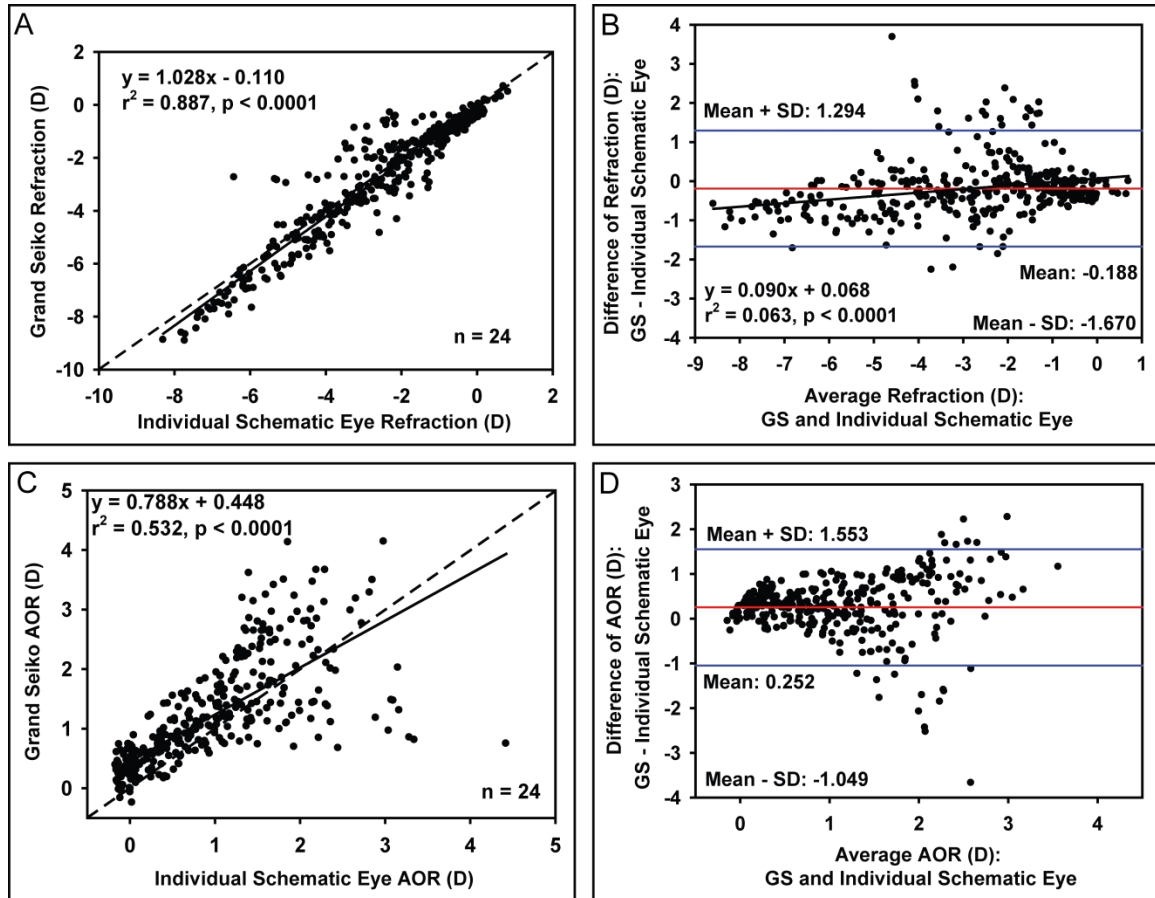
6.4   Discussion

In the current study, the RMS errors relative to the 1:1 line for AOR from individual schematic eyes were in general larger than RMS errors from individual linear regressions of UBM measured biometry parameters for both young and pre-presbyopic subjects (Ramasubramanian & Glasser, 2014a; Ramasubramanian & Glasser, 2014d). However, when the individual schematic eye AORs were corrected using linear regression equations (Table 6.3 and Table 6.4), the RMS errors after correction were comparable to the RMS errors from individual linear regressions of UBM measured biometry parameters in both young and pre-presbyopic subjects. For refraction, the RMS errors after linear regression corrections were smaller in young subjects than in pre-presbyopes as demonstrated by the higher r^2 values. For young subjects, the individual schematic eye offers marginally better AOR predictions than from individual linear regressions of UBM biometry parameters (Ramasubramanian & Glasser, 2014a). For pre-presbyopic subjects, both individual schematic eyes and individual linear regressions of UBM biometry parameters offer comparable AOR predictions (Ramasubramanian & Glasser, 2014d). Overall, linear regression corrections can be applied to the individual schematic eye AORs calculated using either of the three lens equivalent refractive index methods to predict the AOR.

One of the limitations of the current study is that the Grand Seiko, UBM and A-scan measurements were performed sequentially and not simultaneously. Hence, there is

a possibility of subjects accommodating to different amplitudes during each procedure. UBM and A-scan are both instruments with relatively low axial resolution and this could have resulted in inaccuracies in obtaining the true measurements of the ocular accommodative biometric changes, thereby contributing to variation in the refraction and AOR predictions. The relatively small number of lens surface pixels from UBM images that were used to calculate radius of curvature and indistinct edges of the lens surface in the UBM images could have resulted in variable lens curvatures which could have affected the individual schematic eye calculations.

Inaccuracies in the schematic eye calculations could come from inaccuracies in one, several or all of the individual measured parameters used for the schematic eye calculations. In an effort to try to improve the accuracy of individual schematic eyes, individual schematic eye parameters such as ACD, LT, ALRC and PLRC can be arbitrarily changed to achieve a matching GS refraction. An attempt was made to do this by iteratively calculating each of the individual schematic eye biometry parameters independently while using all the other parameters as measured using a standard lens equivalent refractive index of 1.422. This was done in a similar manner to the calculations described above for the lens equivalent refractive index to obtain schematic eye refractions that matched the adjusted GS refractions for each stimulus demands in all subjects. When the iteratively re-calculated ALRC and PLRC values were plotted as function of GS measured AOR, they tended to show flattening of lens surface curvatures with increasing accommodation. Since this is contrary to what actually happens with accommodation (Rosales et al., 2006), neither of these parameters alone could account

for the inaccuracies in the schematic eyes. Similarly, the iteratively calculated ACD and LT values were impossibly small or showed no change with increasing accommodation. These impossible outcomes for individual parameters demonstrate that the lens surface curvatures, ACD or LT per-se could not be the sole independent cause of the discrepancies between the schematic eye and measure refractions and AOR. Further, a prior UBM study identified a discrepancy between A-scan and UBM measured LT and reported correction factors (Ramasubramanian & Glasser, 2014c). However, these discrepancies are small and small changes to ACD and LT do not impact the schematic eye calculations markedly. With these corrections applied, although there was the expected systematic shift in calculated refractions, this had no influence on accommodation which was calculated by subtracting out the baseline refraction.

Lens equivalent refractive index is one parameter that provides a significant contribution to the lens power and to the overall power of the eye. It is unlikely that every eye has the same lens equivalent refractive index, therefore this warrants the calculations of individual values. The averaged iterated baseline lens equivalent refractive index values (young: 1.428, pre-presbyopes: 1.425) were close to the standard lens equivalent index of 1.422 used in Bennetts and Rabbetts schematic eye model (Bennett and Rabbetts, 2007). This suggests that the UBM measured lens biometry parameters are reasonably accurate. However, using the individual baseline lens equivalent refractive index improved the overall accuracy of the refraction and accommodation predictions in pre-presbyopic subjects and not in young subjects. Small changes in lens equivalent refractive index can result in large changes in ocular refraction and although the average

276

lens equivalent refractive index values come out close to the standard value, there is still considerable variation in the individual iteratively calculated values at different stimulus demands. The average calculated lens refractive index for all stimulus demands from both the young and pre-presbyopic subjects was 1.427. This means that a single lens equivalent refractive index value can be justifiably used for baseline and for various accommodative demands to construct accommodative schematic eyes. Calculating this lens equivalent refractive index, requires the refractive and biometric parameters to be measured only for the baseline (0 D stimulus) condition. Prior studies on human eyes have reported that the lens equivalent refractive index and the gradient refractive index do not change with accommodation (de Castro et al., 2013; Kasthurirangan et al., 2008) and this is in agreement with the findings of the current study. However, trends from individual subjects in the current study showed that the iteratively calculated lens equivalent refractive index decreased with accommodation in 18 out of 24 young subjects and showed no change with accommodation in most presbyopic subjects. Using a lens gradient refractive index for schematic eye calculations would not increase the accuracy of predictions because an appropriate lens equivalent refractive index achieves the same paraxial lens power.

Individual accommodative schematic eyes constructed using the average accommodative change in UBM measured parameters applies the average accommodative changes in UBM parameters to each individual subjects' measured baseline biometry parameters. This means that the refractions and AOR calculated using this approach don't actually require measuring the accommodative biometric changes in

each individual subject in order to calculate their accommodative responses. This approach would not yield accurate predictions when an individual subjects' per-diopter accommodative biometric changes are different from the average per-diopter biometric changes in the population. The ideal approach to use for trying to predict the accommodative optical response from an individual subject would be to measure the baseline biometry parameters and the refraction of the eye and to then construct a schematic eye from those measured and to then measure the accommodative changes in the ocular biometry for a variety of stimulus demands and to then apply those measured changes to the schematic eye to then calculate the accommodative optical response for each stimulus demand.

The results from this chapter have demonstrated that individual schematic eyes offer marginally better AOR predictions than with individual linear regressions of UBM measured biometry parameters in young subjects. For pre-presbyopic subjects, AOR prediction from individual linear regression and individual schematic eyes were comparable.

Chapter 7 – Summary and Conclusions

The overall goal of the work in this dissertation was to try to predict the accommodative optical response (AOR) in young eyes with ample accommodation and in pre-presbyopic eyes with lower accommodative amplitudes using anterior segment accommodative biometric changes measured objectively via ultrasound biomicroscopy (UBM) . The results presented have shown that UBM, despite having a low axial resolution, can be used to predict the AOR in young and pre-presbyopic subjects to within 0.50 D.

One of the outcomes of this work is the demonstrated utility of objective automated measurements of accommodative biometry parameters from UBM images. Automated objective analysis allows rapid, unbiased and repeatable measurements on a large number of images. Prior studies have performed measurements on single UBM images manually using software calipers (Modesti et al., 2011; Marchini et al., 2004; Marchini, Pedrotti, Modesti et al., 2008). Standard deviations of UBM measurements from these prior studies were larger than reported here. The presence of spatial distortion in UBM images as described in Chapter 2 has not been reported previously. Based on these findings, distortion correction as described in Chapter 2 should be applied to UBM instruments to get accurate, quantitative measurements. Results from Chapters 2 and 4 showed that the accommodative anterior segment biometric changes in young and pre-presbyopic subjects were comparable with prior studies and that the standard deviations

from the automated UBM analysis were smaller than prior measures from high resolution optical coherence tomography (OCT) and partial coherence interferometry (PCI) systems (Bolz et al., 2007; Sun et al., 2013). The UBM image analysis as developed and used here performs automated offline analysis of UBM images. Automated image analysis software as described here could potentially be developed to perform real-time anterior segment biometric measurements in a commercially available UBM or in other anterior segment imaging systems.

This work has established the standard deviation of AOR prediction in young and pre-presbyopic subjects using each of the UBM measured biometry parameters. The average predictive standard deviation of 0.60 D or less in both age-groups is small, despite using sequential refraction and biometry measurements and despite the fact that the biometry measurements are from a low resolution instrument such as UBM. The linear regression equations listed in Chapters 3 and 4 can be used to estimate the AOR from a single individual biometry parameter. However, it has to be realized that the error associated with predicting AOR from linear regression equations can range from 0.56 D to 0.91 D and 0.41 D to 0.62 D for various biometry parameters in the young and pre-presbyopic subjects, respectively. The error associated with AOR predictions using the linear regressions depends on the strength of the linear relationships between the accommodative optical and biometric changes and how closely an individual's linear regression compares to the population linear regression. In general, lens thickness predicts the AOR with the smallest standard deviation in both young and pre-presbyopic subjects compared to other parameters; hence it is a recommended parameter to use.

Another outcome from this work is the demonstration that spatial and optical distortion corrections described for the Visante AS-OCT (Chapter 5) provided robust correction for corneal parameters. The Visante software allows only corneal thickness to be measured using the software calipers and although the software fits curves to the front and back corneal surfaces, it does not provide the radii of curvatures. Corneal biometric parameters from uncorrected Visante images are inaccurate and should not be used without distortion correction applied. The distortion correction equations described in Chapter 5 can be used to obtain accurate corneal biometry measurements and the errors after correction are clinically insignificant. Accurate corneal parameters from Visante images after distortion correction allowed the use of these parameters to construct accommodative schematic eye models to calculate refraction and AOR as described in Chapter 6.

Individual schematic eyes calculated using the three lens equivalent refractive index methods after applying the linear regression correction provides good prediction of the AORs (Chapter 6). Before correcting the schematic eye AORs with linear regression equations, the prediction errors were in general worse than predictions from individual regressions of UBM biometry parameters (Chapters 3 and 4). However, prediction errors of AORs from individual schematic eyes after linear regression correction were on average 0.50 D, which is smaller than prediction errors from linear regressions of UBM biometry parameters. Predictions of AOR independently from linear regressions and from individual schematic eyes could be even further improved by: i) performing simultaneous

measures of accommodative optical and biometric changes, ii) using higher resolution imaging modalities (such as OCT) with automated image analysis methods.

The results described in this work have demonstrated: 1) the utility of automated image analysis to get accurate, rapid and objective measurements of anterior segment biometry from UBM images; 2) how spatial distortions in UBM images can be corrected to get accurate measurements and the ability of each UBM measured biometry parameter to predict the AOR; 3) how UBM, despite having low axial resolution, can predict AOR in pre-presbyopic eyes with low accommodative amplitudes; 4) how spatial and optical distortions in Visante images can be corrected to get accurate corneal biometry that can be used for schematic eye modeling; and 5) how predictions of the AOR from individual schematic eyes are better than predictions using linear regressions from individual UBM measured biometry parameters.

Prediction methods described in this work could eventually be applied to evaluate the accommodative ability of accommodation restoration concepts in clinical studies. However, the specific relationships between accommodative optical and biometric changes in pseudophakic eyes would have to be established for individual intraocular lens designs before predictions can be made.

References

Visante OCT User Manual. Dublin, CA: Carl Zeiss Meditec, Inc. 2006.

Aghaian, E., Choe, J.E., Lin, S., & Stamper, R.L. (2004). Central corneal thickness of Caucasians, Chinese, Hispanics, Filipinos, African Americans, and Japanese in a glaucoma clinic. *Ophthalmology,* 111, 2211-2219.

Al-Farhan, H.M. & Al-Otaibi, W.M. (2012). Comparison of central corneal thickness measurements using ultrasound pachymetry, ultrasound biomicroscopy, and the Artemis-2 VHF scanner in normal eyes. *Clinical Ophthalmology,* 6, 1037-1043.

Anderson, H.A., Hentz, G., Glasser, A., Stuebing, K.K., & Manny, R.E. (2008). Minus-lens-stimulated accommodative amplitude decreases sigmoidally with age: a study of objectively measured accommodative amplitudes from age 3. *Invest Ophthalmol Vis Sci,* 49, 2919-2926.

Atchison, D.A., Markwell, E.L., Kasthurirangan, S., Pope, J.M., Smith, G., & Swann, P.G. (2008). Age-related changes in optical and biometric characteristics of emmetropic eyes. *Journal of Vision,* 8, 29-20.

Beauchamp, R. & Mitchell, B. (1985). Ultrasound measures of vitreous chamber depth during ocular accommodation. *American Journal of Optometry and Physiological Optics,* 62, 523-532.

Bennett, A.G., Rabbetts, R.B. (2007). The Schematic Eye. In R.B.Rabbetts (Eds.), *Clinical Visual Optics* (pp. 221-243). Philadephia: Elsevier/Butterworth Heinemann.

Bolz, M., Prinz, A., Drexler, W., & Findl, O. (2007). Linear relationship of refractive and biometric lenticular changes during accommodation in emmetropic and myopic eyes. *The British Journal of Ophthalmology,* 91, 360-365.

Borja, D., Siedlecki, D., de Castro, A., et al. (2010). Distortions of the posterior surface in optical coherence tomography images of the isolated crystalline lens: effect of the lens index gradient. *Biomedical Optics Express,* 1, 1331-1340.

Brown, N. (1973). The change in shape and internal form of the lens of the eye on accommodation. *Experimental Eye Research,* 15, 441-459.

Chen, M.J., Liu, Y.T., Tsai, C.C., Chen, Y.C., Chou, C.K., & Lee, S.M. (2009). Relationship between central corneal thickness, refractive error, corneal curvature, anterior chamber depth and axial length. *Journal of the Chinese Medical Association,* 72, 133-137.

Crawford, A.Z., Patel, D.V., & McGhee, C.N. (2013). Comparison and repeatability of keratometric and corneal power measurements obtained by Orbscan II, Pentacam, and Galilei corneal tomography systems. *American Journal of Ophthalmology,* 156, 53-60.

de Castro, A., Birkenfeld, J., Maceo, B., et al. (2013). Influence of shape and gradient refractive index in the accommodative changes of spherical aberration in

nonhuman primate crystalline lenses. *Investigative Ophthalmology and Visual Science,* 54, 6197-6207.

de Jong T., Sheehan, M.T., Dubbelman, M., Koopmans, S.A., & Jansonius, N.M. (2013). Shape of the anterior cornea: comparison of height data from 4 corneal topographers. *Journal of Cataract and Refractive Surgery,* 39, 1570-1580.

Dick, H.B. (2005). Accommodative intraocular lenses: current status. *Current Opinion in Ophthalmology,* 16, 8-26.

Dick, H.B. & Dell, S. (2006). Single optic accommodative intraocular lenses. *Ophthalmology Clinics of North America,* 19, 107-24, vi.

Doughty, M.J. & Zaman, M.L. (2000). Human corneal thickness and its impact on intraocular pressure measures: a review and meta-analysis approach. *Survey of Ophthalmology,* 44, 367-408.

Drexler, W., Baumgartner, A., Findl, O., Hitzenberger, C.K., & Fercher, A.F. (1997). Biometric investigation of changes in the anterior eye segment during accommodation. *Vision Research,* 37, 2789-2800.

Dubbelman, M., Sicam, V.A., & van der Heijde, G.L. (2006). The shape of the anterior and posterior surface of the aging human cornea. *Vision Research,* 46, 993-1001.

Dubbelman, M. & van der Heijde, G.L. (2001). The shape of the aging human lens: curvature, equivalent refractive index and the lens paradox. *Vision Research,* 41, 1867-1877.

Dubbelman, M., van der Heijde, G.L., & Weeber, H.A. (2001). The thickness of the aging human lens obtained from corrected Scheimpflug images. *Optometry and Vision Science,* 78, 411-416.

Dubbelman, M., van der Heijde, G.L., & Weeber, H.A. (2005). Change in shape of the aging human crystalline lens with accommodation. *Vision Research,* 45, 117-132.

Dubbelman, M., Weeber, H.A., van der Heijde, R.G.L., & Volker-Dieben, H.J. (2002). Radius and asphericity of the posterior corneal surface determined by corrected Scheimpflug photography. *Acta Ophthalmologica Scandinavica,* 80, 379-383.

Dunne, M.C., Davies, L.N., & Wolffsohn, J.S. (2007). Accuracy of cornea and lens biometry using anterior segment optical coherence tomography. *Journal of Biomedical Optics,* 12, 064023

Fishman, G.R., Pons, M.E., Seedor, J.A., Liebmann, J.M., & Ritch, R. (2005). Assessment of central corneal thickness using optical coherence tomography. *Journal of Cataract and Refractive Surgery,* 31, 707-711.

Galgauskas, S., Norvydaite, D., Krasauskaite, D., Stech, S., & Asoklis, R.S. (2013). Age-related changes in corneal thickness and endothelial characteristics. *Clinical Interventions in Aging,* 8, 1445-1450.

Gambra, E., Ortiz, S., Perez-Merino, P., Gora, M., Wojtkowski, M., & Marcos, S. (2013). Static and dynamic crystalline lens accommodation evaluated using quantitative 3-D OCT. *Biomedical Optics Express,* 4, 1595-1609.

Garner, L.F. & Yap, M.K.H. (1997). Changes in ocular dimensions and refraction with accommodation. *Ophthalmic and Physiological Optics,* 17, 12-17.

Glasser, A. (2008). Restoration of accommodation: surgical options for correction of presbyopia. *Clinical and Experimental Optometry,* 91, 279-295.

Glasser, A. & Campbell, M.C.W. (1999). Biometric, optical and physical changes in the isolated human crystalline lens with age in relation to presbyopia. *Vision Research,* 39, 1991-2015.

Glasser, A. & Kaufman, P.L. (1999). The mechanism of accommodation in primates. *Ophthalmology,* 106, 863-872.

Glasser, A., Wendt, M., & Ostrin, L. (2006). Accommodative changes in lens diameter in rhesus monkeys. *Investigative Ophthalmology and Visual Science,* 47, 278-286.

Gullstrand, A. (1909). The mechanism of accommodation. In J.P.C.Southall (Eds.), *Helmholtz's Treatise on Physiological Optics* (pp. 382-415). New York: Dover.

Hashemi, H., Yazdani, K., Mehravaran, S., et al. (2009). Corneal thickness in a population-based, cross-sectional study: the Tehran Eye Study. *Cornea,* 28, 395-400.

He, L., Donnelly, W.J., III, Stevenson, S.B., & Glasser, A. (2010). Saccadic lens instability increases with accommodative stimulus in presbyopes. *Journal of Vision,* 10, 14-16.

Helmholtz von, H.H. (1962). Mechanism of accommodation. In J.P.C.Southall (Eds.), *Helmholtz's Treatise on Physiological Optics, translation edited by Southall in 1924 - original German in 1909* (pp. 143-173). New York, NY: Dover.

Hermans, E.A., Pouwels, P.J., Dubbelman, M., Kuijer, J.P., van der Heijde, R.G., & Heethaar, R.M. (2009). Constant volume of the human lens and decrease in surface area of the capsular bag during accommodation: an MRI and Scheimpflug study. *Investigative Ophthalmology and Visual Science,* 50, 281-289.

Heys, K.R., Cram, S.L., & Truscott, R.J. (2004). Massive increase in the stiffness of the human lens nucleus with age: the basis for presbyopia? *Molecular Vision,* 10, 956-963.

Ishikawa, H., Liebmann, J.M., & Ritch, R. (2000). Quantitative assessment of the anterior segment using ultrasound biomicroscopy. *Current Opinion in Ophthalmology,* 11, 133-139.

Jansson, F. & Sundmark, E. (1961). Determination of the velocity of ultrasound in ocular tissues at different temperatures. *Acta Ophthalmologica,* 39, 899-910.

Jones, C.E., Atchison, D.A., & Pope, J.M. (2007). Changes in lens dimensions and refractive index with age and accommodation. *Optometry and Vision Science,* 84, 990-995.

Kao, C.Y., Richdale, K., Sinnott, L.T., Grillott, L.E., & Bailey, M.D. (2011). Semiautomatic extraction algorithm for images of the ciliary muscle. *Optometry and Vision Science,* 88, 275-289.

Kasarova, S.N., Sultanova, N.G., Ivanov, C.D., & Nikolov, I.D. (2007). Analysis of the dispersion of optical plastic materials. *Optical Materials,* 29, 1481-1490.

Kasthurirangan, S. & Glasser, A. (2005). Influence of amplitude and starting point on accommodative dynamics in humans. *Investigative Ophthalmology and Visual Science,* 46, 3463-3472.

Kasthurirangan, S. & Glasser, A. (2006a). Age related changes in accommodative dynamics in humans. *Vision Research,* 46, 1507-1519.

Kasthurirangan, S. & Glasser, A. (2006b). Age related changes in the characteristics of the near pupil response. *Vision Research,* 46, 1393-1403.

Kasthurirangan, S., Markwell, E.L., Atchison, D.A., & Pope, J.M. (2008). In vivo study of changes in refractive index distribution in the human crystalline lens with age and accommodation. *Investigative Ophthalmology and Visual Science,* 49, 2531-2540.

Kasthurirangan, S., Markwell, E.L., Atchison, D.A., & Pope, J.M. (2011). MRI study of the changes in crystalline lens shape with accommodation and aging in humans. *Journal of Vision,* 11, 1-16.

Koeppl, C., Findl, O., Kriechbaum, K., & Drexler, W. (2005). Comparison of pilocarpine-induced and stimulus-driven accommodation in phakic eyes. *Experimental Eye Research,* 80, 795-800.

Koretz, J.F., Bertasso, A.M., Neider, M.W., True-Gabelt, B., & Kaufman, P.L. (1987). Slit-lamp studies of the rhesus monkey eye. II Changes in crystalline lens shape, thickness and position during accommodation and aging. *Experimental Eye Research,* 45, 317-326.

Koretz, J.F., Cook, C.A., & Kaufman, P.L. (1997). Accommodation and presbyopia in the human eye. Changes in the anterior segment and crystalline lens with focus. *Investigative Ophthalmology and Visual Science,* 38, 569-578.

Koretz, J.F., Cook, C.A., & Kaufman, P.L. (2001). Aging of the human lens: changes in lens shape at zero-diopter accommodation. *Journal of the Optical Society of America A, Optics, Image Science, and Vision,* 18, 265-272.

Koretz, J.F., Kaufman, P.L., Neider, M.W., & Goeckner, P.A. (1989). Accommodation and presbyopia in the human eye - aging of the anterior segment. *Vision Research,* 29, 1685-1692.

Koretz, J.F., Strenk, S.A., Strenk, L.M., & Semmlow, J.L. (2004). Scheimpflug and high-resolution magnetic resonance imaging of the anterior segment: a comparative study. *Journal of the Optical Society of America A, Optics, Image Science, and Vision,* 21, 346-354.

Li, G., Zwick, H., Stuck, B., & Lund, D.J. (2000). On the use of schematic eye models to estimate retinal image quality. *Journal of Biomedical Optics,* 5, 307-314.

Li, H., Leung, C.K., Wong, L., et al. (2008). Comparative study of central corneal thickness measurement with slit-lamp optical coherence tomography and visante optical coherence tomography. *Ophthalmology,* 115, 796-801.

Liu, Z., Huang, A.J., & Pflugfelder, S.C. (1999). Evaluation of corneal thickness and topography in normal eyes using the Orbscan corneal topography system. *The British Journal of Ophthalmology,* 83, 774-778.

Lopez-Gil, N., Fernandez-Sanchez, V., Legras, R., Montes-Mico, R., Lara, F., & Nguyen-Khoa, J.L. (2008). Accommodation-related changes in monochromatic aberrations of the human eye as a function of age. *Investigative Ophthalmology and Visual Science,* 49, 1736-1743.

Maceo, B.M., Manns, F., Borja, D., et al. (2011). Contribution of the crystalline lens gradient refractive index to the accommodation amplitude in non-human primates: in vitro studies. *Journal of Vision,* 11, 1-13.

MacRae, S., Schwiegerling, J., & Snyder, R.W. (1999). Customized and low spherical aberration corneal ablation design. *Journal of Refractive Surgery,* 15, S246-S248

Marchini, G., Pedrotti, E., Modesti, M., Visentin, S., & Tosi, R. (2008). Anterior segment changes during accommodation in eyes with a monofocal intraocular lens: high-frequency ultrasound study. *Journal of Cataract and Refractive Surgery,* 34, 949-956.

Marchini, G., Pedrotti, E., Sartori, P., & Tosi, R. (2004). Ultrasound biomicroscopic changes during accommodation in eyes with accommodating intraocular lenses:

291

pilot study and hypothesis for the mechanism of accommodation. *Journal of Cataract and Refractive Surgery,* 30, 2476-2482.

Marcos, S., Ortiz, S., Perez-Merino, P., Birkenfeld, J., Duran, S., & Jimenez-Alfaro, I. (2014). Three-dimensional evaluation of accommodating intraocular lens shift and alignment in vivo. *Ophthalmology,* 121, 45-55.

McLeod, S.D., Vargas, L.G., Portney, V., & Ting, A. (2007). Synchrony dual-optic accommodating intraocular lens. Part 1: optical and biomechanical principles and design considerations. *Journal of Cataract and Refractive Surgery,* 33, 37-46.

Modesti, M., Pasqualitto, G., Appolloni, R., Pecorella, I., & Sourdille, P. (2011). Preoperative and postoperative size and movements of the lens capsular bag: ultrasound biomicroscopy analysis. *Journal of Cataract and Refractive Surgery,* 37, 1775-1784.

Nakatsuka, C., Hasebe, S., Nonaka, F., & Ohtsuki, H. (2004). Accommodative lag under habitual seeing conditions: comparison between adult myopes and emmetropes. *Japanese Journal of Ophthalmology,* 47, 291-298.

Navarro, R., Santamaria, J., & Bescos, J. (1985). Accommodation-dependent model of the human eye with aspherics. *Journal of the Optical Society of America A, Optics and Image Science,* 2, 1273-1281.

Nichamin, L.D., Scholl, J.A. (2008). Shape-changing IOLs: PowerVision. In Chang DF (Eds.), *Mastering Refractive IOLs. The Art and Science* (pp. 220-222). Thorofare, NJ: Slack, Inc.

Ogbuehi, K.C. & Osuagwu, U.L. (2012). Repeatability and interobserver reproducibility of Artemis-2 high-frequency ultrasound in determination of human corneal thickness. *Clinical Ophthalmology,* 6, 761-769.

Ossma, I.L., Galvis, A., Vargas, L.G., Trager, M.J., Vagefi, M.R., & McLeod, S.D. (2007). Synchrony dual-optic accommodating intraocular lens. Part 2: pilot clinical evaluation. *Journal of Cataract and Refractive Surgery,* 33, 47-52.

Ostrin, L., Kasthurirangan, S., Win-Hall, D., & Glasser, A. (2006). Simultaneous measurements of refraction and A-scan biometry during accommodation in humans. *Optometry and Vision Science,* 83, 657-665.

Podoleanu, A., Charalambous, I., Plesea, L., Dogariu, A., & Rosen, R. (2004). Correction of distortions in optical coherence tomography imaging of the eye. *Physics in Medicine and Biology,* 49, 1277-1294.

Preussner, P.R., Wahl, J., & Weitzel, D. (2005). Topography-based intraocular lens power selection. *J Cataract Refract Surg,* 31, 525-533.

Ramasubramanian, V. & Glasser, A. (2014a). Can Ultrasound Biomicroscopy (UBM) be Used to Predict Accommodation Accurately? *Submitted.*

Ramasubramanian, V. & Glasser, A. (2014b). Correction of Corneal Distortions from Visante Anterior Segment Optical Coherence Tomography Images. *Submitted.*

Ramasubramanian, V. & Glasser, A. (in press). Objective Measurement of Accommodative Biometric Changes Using Ultrasound Biomicroscopy. *Journal of Cataract and Refractive Surgery.*

Ramasubramanian, V. & Glasser, A. (2014d). Prediction of Accommodative Optical Response in Pre-presbyopes using Ultrasound Biomicroscopy (UBM). *Submitted.*

Richdale, K., Bailey, M.D., Sinnott, L.T., Kao, C.Y., Zadnik, K., & Bullimore, M.A. (2012). The effect of phenylephrine on the ciliary muscle and accommodation. *Optometry and Vision Science,* 89, 1507-1511.

Richdale, K., Bullimore, M.A., & Zadnik, K. (2008). Lens thickness with age and accommodation by optical coherence tomography. *Ophthalmic and Physiological Optics,* 28, 441-447.

Richdale, K., Sinnott, L.T., Bullimore, M.A., et al. (2013). Quantification of age-related and per diopter accommodative changes of the lens and ciliary muscle in the emmetropic human eye. *Investigative Ophthalmology and Visual Science,* 54, 1095-1105.

Roorda, A., Campbell, M.C., & Bobier, W.R. (1997). Slope-based eccentric photorefraction: theoretical analysis of different light source configurations and effects of ocular aberrations. *Journal of Optical Society of America A,* 14, 2547-2556.

Rosales, P., Dubbelman, M., Marcos, S., & van der Heijde, R. (2006). Crystalline lens radii of curvature from Purkinje and Scheimpflug imaging. *Journal of Vision,* 6, 1057-1067.

Rufer, F., Schroder, A., Bader, C., & Erb, C. (2007). Age-related changes in central and peripheral corneal thickness: determination of normal values with the Orbscan II topography system. *Cornea,* 26, 1-5.

Schaeffel, F., Wilhelm, H., & Zrenner, E. (1993). Inter-individual variability in the dynamics of natural accommodation in humans: relation to age and refractive errors. *The Journal of Physiology,* 461, 301-320.

Sheppard, A.L., Bashir, A., Wolffsohn, J.S., & Davies, L.N. (2010). Accommodating intraocular lenses: a review of design concepts, usage and assessment methods. *Clinical and Experimental Optometry,* 93, 441-452.

Sheppard, A.L., Evans, C.J., Singh, K.D., Wolffsohn, J.S., Dunne, M.C., & Davies, L.N. (2011). Three-Dimensional Magnetic Resonance Imaging of the Phakic Crystalline Lens during Accommodation. *Investigative Ophthalmology and Visual Science,* 52, 3689-3697.

Shum, P.J., Ko, L.S., Ng, C.L., & Lin, S.L. (1993). A biometric study of ocular changes during accommodation. *American Journal of Ophthalmology,* 115, 76-81.

Siedlecki, D., de Castro, A., Gambra, E., et al. (2012). Distortion correction of OCT images of the crystalline lens: gradient index approach. *Optometry and Vision Science,* 89, E709-E718

Siu, A. & Herse, P. (1993). The effect of age on human corneal thickness. Statistical implications of power analysis. *Acta Ophthalmologica,* 71, 51-56.

Sorbara, L., Maram, J., Fonn, D., Woods, C., & Simpson, T. (2010). Metrics of the normal cornea: anterior segment imaging with the Visante OCT. *Clinical and Experimental Optometry,* 93, 150-156.

Sun, Y., Fan, S., Zheng, H., Dai, C., Ren, Q., & Zhou, C. (2013). Noninvasive Imaging and Measurement of Accommodation Using Dual-Channel SD-OCT. *Current Eye Research,*

Tabernero, J. & Schaeffel, F. (2009). More irregular eye shape in low myopia than in emmetropia. *Investigative Ophthalmology and Visual Science,* 50, 4516-4522.

Tan, D.K., Chong, W., Tay, W.T., et al. (2012). Anterior chamber dimensions and posterior corneal arc length in Malay eyes: an anterior segment optical coherence tomography study. *Investigative Ophthalmology and Visual Science,* 53, 4860-4867.

Tromans, C. & Storey, J.K. (1990). Biometric investigation of the effect of gravity on the crystalline lens during accommodation. *Documenta Ophthalmologica Proceedings Series,* 12, 125-129.

Tsorbatzoglou, A., Nemeth, G., Szell, N., Biro, Z., & Berta, A. (2007). Anterior segment changes with age and during accommodation measured with partial coherence interferometry. *Journal of Cataract and Refractive Surgery,* 33, 1597-1601.

van der Heijde, G.L., Beers, A.P.A., & Dubbelman, M. (1996). Microfluctuations of steady-state accommodation measured with ultrasonography. *Ophthalmic and Physiological Optics,* 16, 216-221.

Vilupuru, A.S. & Glasser, A. (2003). Dynamic accommodative changes in Rhesus monkey eyes assessed with A-scan ultrasound biometry. *Optometry and Vision Science,* 80, 383-394.

Vilupuru, A.S. & Glasser, A. (2005). The relationship between refractive and biometric changes during Edinger-Westphal stimulated accommodation in rhesus monkeys. *Experimental Eye Research,* 80, 349-360.

Wendt, M, Croft, M.A., McDonald, J., Kaufman, P.L., & Glasser, A. (2008). Lens diameter and thickness as a function of age and pharmacologically stimulated accommodation in rhesus monkeys. *Experimental Eye Research,* 86, 746-752.

Westphal, V., Rollins, A., Radhakrishnan, S., & Izatt, J. (2002). Correction of geometric and refractive image distortions in optical coherence tomography applying Fermat's principle. *Optics Express,* 10, 397-404.

Win-Hall, D.M. & Glasser, A. (2008). Objective accommodation measurements in prepresbyopic eyes using an autorefractor and an aberrometer. *J Cataract Refract Surg,* 34, 774-784.

Win-Hall, D.M. & Glasser, A. (2009). Objective accommodation measurements in pseudophakic subjects using an autorefractor and an aberrometer. *Journal of Cataract and Refractive Surgery,* 35, 282-290.

Win-Hall, D.M., Houser, J., & Glasser, A. (2010). Static and Dynamic Accommodation Measured Using the WAM-5500 Autorefractor. *Optom Vis Sci,* 87, 873-882.

Win-Hall, D.M., Ostrin, L.A., Kasthurirangan, S., & Glasser, A. (2007). Objective accommodation measurement with the Grand Seiko and Hartinger coincidence refractometer. *Optometry and Vision Science,* 84, 879-887.

Wold, J.E., Hu, A., Chen, S., & Glasser, A. (2003). Subjective and objective measurement of human accommodative amplitude. *Journal of Cataract and Refractive Surgery,* 29, 1878-1888.

Wolffsohn, J.S., O'Donnell, C., Charman, W.N., & Gilmartin, B. (2004). Simultaneous continuous recording of accommodation and pupil size using the modified Shin-Nippon SRW-5000 autorefractor. *Ophthalmic and Physiological Optics,* 24, 142-147.

Yuen, L.H., He, M., Aung, T., Htoon, H.M., Tan, D.T., & Mehta, J.S. (2010). Biometry of the cornea and anterior chamber in chinese eyes: an anterior segment optical coherence tomography study. *Investigative Ophthalmology and Visual Science,* 51, 3433-3440.

Zhao, P.S., Wong, T.Y., Wong, W.L., Saw, S.M., & Aung, T. (2007). Comparison of central corneal thickness measurements by visante anterior segment optical coherence tomography with ultrasound pachymetry. *American Journal of Ophthalmology,* 143, 1047-1049.

Zheng, S., Ying, J., Wang, B., Xie, Z., Huang, X., & Shi, M. (2013). Three-dimensional model for human anterior corneal surface. *Journal of Biomedical Optics,* 18, 065002

Appendix

In a four surface paraxial schematic eye, A_1, A_2, A_3 and A_4 represent the anterior and posterior surfaces of the cornea and the lens, respectively. All distances are measured from the anterior corneal vertex (A_1).

Surface powers and equivalent power of the cornea were calculated using equations 1, 2 and 3.

$$F_{AC} = \frac{(n_{cornea} - n_{air}) \times 1000}{r_{AC}} \tag{1}$$

$$F_{PC} = \frac{(n_{aqueous} - n_{cornea}) \times 1000}{r_{PC}} \tag{2}$$

$$F_{Cornea} = F_{AC} + F_{PC} - \left(\left(\frac{CT}{n_{cornea} \times 1000} \right) \times F_{AC} \times F_{PC} \right) \tag{3}$$

where F_{AC} and F_{PC} are the surface powers (D) of the anterior and posterior corneal surfaces, respectively, F_{Cornea} is the equivalent power of cornea (D), r_{AC} and r_{PC} are the Visante OCT measured radii of curvature (mm) of the anterior and posterior corneal surfaces after distortion correction, respectively, n_{cornea} is the refractive index of cornea (1.376), n_{air} is the refractive index of air (1.0), $n_{aqueous}$ is the refractive index of

aqueous (1.336) and CT is the Visante OCT measured corneal thickness (mm) after distortion correction.

Distances of the first (A_1P_1) and second (A_1P_1') principal points of the cornea from the anterior corneal vertex was calculated using equations 4 and 5.

$$A_1P_1 = \frac{n_{air} \times CT \times F_{PC}}{n_{cornea} \times F_{Cornea}} \tag{4}$$

$$A_1P_1' = \frac{-CT \times n_{aqueous} \times F_{AC}}{(n_{cornea} \times F_{Cornea})} + CT \tag{5}$$

Surface powers and equivalent powers of the crystalline lens were calculated using equations 6, 7 and 8.

$$F_{AL} = \frac{(n_{lens} - n_{aqueous}) \times 1000}{r_{ALRC}} \tag{6}$$

$$F_{PL} = \frac{(n_{vitreous} - n_{lens}) \times 1000}{r_{PLRC}} \tag{7}$$

$$F_{Lens} = F_{AL} + F_{PL} - \left(\left(\frac{LT}{n_{lens} \times 1000} \right) \times F_{AL} \times F_{PL} \right) \tag{8}$$

where F_{AL} and F_{PL} are the surface powers (D) of the anterior and posterior lens surfaces, respectively, F_{Lens} is the equivalent power of lens (D), r_{ALRC} and r_{PLRC} are the UBM measured radii of curvature (mm) of the anterior and posterior lens surfaces, respectively, n_{lens} is the equivalent refractive index of the lens (1.422), $n_{vitreous}$ is the refractive index of vitreous (1.336) and LT is the UBM measured lens thickness (mm).

Distances of the first (A_1P_2) and second (A_1P_2') principal points of the lens from the anterior corneal vertex was calculated using equations 9 and 10.

$$A_1P_2 \ = \frac{n_{aqueous} \times LT \times F_{PL}}{n_{lens} \times F_{Lens}} + CT + ACD \tag{9}$$

$$A_1P_2' \ = \frac{-LT \times n_{vitreous} \times F_{AL}}{(n_{lens} \times F_{Lens})} + CT + ACD + LT \tag{10}$$

where ACD is the UBM measured anterior chamber depth (mm).

Equivalent power of the eye (F_{Eye}) was calculated using equation 11. Distances of the first and second principal points $(A_1P \ \& A_1P')$, first and second focal points $(A_1F \ \& A_1F')$, first and second nodal points $(A_1N \ \& A_1N')$, entrance pupil (A_1E) and exit pupil (A_1E') of the eye from the corneal vertex were calculated using equations 12 through 21.

$$F_{Eye} = F_{Cornea} + F_{Lens} - \left(\frac{(A_1P_2 - A_1P_1') \times F_{Cornea} \times F_{Lens}}{n_{aqueous} \times 1000}\right) \tag{11}$$

$$A_1P = \frac{n_{air} \times (A_1P_2 - A_1P_1') \times F_{Lens}}{n_{aqueous} \times F_{Eye}} + A_1P_1 \tag{12}$$

$$A_1P' = A_1P_2' + \frac{-n_{vitreous} \times (A_1P_2 - A_1P_1') \times F_{Cornea}}{n_{aqueous} \times F_{Eye}} \tag{13}$$

$$f_o = -1000 \times \left(\frac{n_{air}}{F_{Eye}}\right) \tag{14}$$

$$f_o' = 1000 \times \left(\frac{n_{vitreous}}{F_{Eye}}\right) \tag{15}$$

where f_o & f_o' are the primary and secondary equivalent focal lengths (mm) of the

eye.

$$A_1F = f_o + A_1P \tag{16}$$

$$A_1F' = f_o' + A_1P' \tag{17}$$

$$A_1N = A_1P + f_o + f_o' \tag{18}$$

$$A_1N' = A_1P' + f_o + f_o' \tag{19}$$

$$A_1E = A_1P_1 + \frac{\frac{CT + ACD - A_1P_1'}{1000}}{n_{aqueous} + \left(F_{Cornea} \times -\left(\frac{CT + ACD - A_1P_1'}{1000}\right)\right)} \times 1000 \tag{20}$$

$$A_1E' = A_1P_2' + \frac{n_{vitreous} \times \left(-\frac{A_1P_2 - CT - ACD}{1000}\right)}{n_{aqueous} + \left(F_{Lens} \times -\left(\frac{A_1P_2 - CT - ACD}{1000}\right)\right)} \times 1000 \tag{21}$$

303

Refractive state of the eye was calculated using equation 22 for each accommodative demand.

$$Refraction\ (D) = \left(\frac{1000 \times n_{vitreous}}{Axial\ Length - A_1P'}\right) - F_{Eye} \qquad (22)$$

Accommodative optical response was calculated as the difference in refraction between each accommodative state and the baseline.